Performance of a combined LCC and VSC Bipole HVDC link

AALBORG UNIVERSITET

Electrical Energy Engineering

EPSH, 2. Semester, Spring 2010

The Faculty of Engineering, Science and Medicine

Department of Energy Technology, Aalborg University

The Faculty of Engineering, Science and Medicine
Department of Energy Technology
Pontoppidanstræde 101
Telefon: 96 35 92 40
Fax: 98 15 14 11
http://iet.aau.dk

Title:

Performance of a combined LCC and VSC Bipole HVDC link

Project period: E10, Fall 2010

Participant: Alemayo Tadese

Supervisor:

Associate Professor Claus Leth Bak

co-supervisor:

Filipe Miguel Faria da Silva

Circulation:3

Pages: 130

Appendices: 3

Additional material: 1 CD-ROM

Finished: 02-05-2010

Keywords: HVDC, LCC, VSC, PSCAD, control, Commutation failure

Synopsis:

This paper presents a performance of a bipole HVDC link based on line commutated converter (LCC) with a Voltage Source Converter (VSC). Connecting a VSC based link in a bipole fashion with an LCC based link has never been practically implemented yet.
In implementing such a system, as the commutation process is different for the two. Therefore, study of issues such as the control of the links, commutation failures and harmonics are important for the proper operation of the system.
The control strategy for both the LCC and VSC links has been presented. The VSC control is based on PWM techniques which enables it to have full control of the active and reactive power exchanged with the ac grid. However the LCC is controlled by adjusting the firing angle of the converter and can only control the active power exchanged with the ac grid.
The LCC link has a higher probability to commutation failures than the VSC. Hence, the performance of the bipole link has been studied during normal operation and faulty conditions. The faults which have been simulated deal with both ac and dc side faults. For ac side faults, single phase to ground, reduction in the amplitude and distortion of the voltages and three phase to ground have been simulated. For dc side, line to ground and sudden rapid increase in the dc current have been simulated.
The results obtained by using the simulation program, PSCAD are presented at the end. The results show that the link operates satisfactorily during normal operation. During faulty conditions, depending on the type of fault, the results show that the link either operates through one line or is completely down in worst fault case, three phase to ground.

Preface

This report is made as documentation of a 10th. semester project in the Institute of Energy Technology at Aalborg University in the period 1. February to 2 June 2010.

The report comprises of two main parts - the main project and an Appendix part. The main report contains 9 chapters and 3 appendix chapters.

A CD is included containing the PDF version of the report, the literature referenced materials, commutation failure measurement data and used PSCAD programs.

Citations are given in square brackets like shown next [10, p. 1]. The author and book refereing to the reference number can be found in the Bibliography after the main report.

Designations:
Unless other is stated, voltages and currents are always given by their rms values. Voltages are given as their line value and currents in their phase values unless other is specified.

Alemayo Tadese

Acknowledgement

At this stage, I would like to express my gratitude to those without whose help this thesis would not have been possible.

Allow me to start by thanking Aalborg University for giving me the opportunity to study by providing financial support. I am really indebted.

I would like to express my gratitude to Professor Claus Leth Bak, my supervisor and examiner, for his guidance and feedback throughout this thesis project. He has patiently commented and gave me the necessary feedback timely.

I would also like to thank my co-supervisor Filipe Miguel Faria da Silva for his useful suggestions and encouragement throughout the time.

I am also grateful for the valuable information and support provided by Kim Søøgard from Energinet.dk, starting from the initial stage of the project till the end.

Finally, I would like to thank the staff and friends at the Department of Energy Technology for making such a productive working environment and who supported me in any respect during the completion of the project and my study.

Contents

List of Figures

Chapter 1

Introduction

This chapter discusses about the background of the project, a brief overview description of the system, the goals of the project, its limitation and overview of the thesis.

1.1 Back Ground

Transmission of electrical power can be accomplished in two different ways, by using alternating or direct current, both via overhead lines or underground cables. Nowadays, a majority of the transmission systems use HVAC however for long underground or submarine transmissions, HVDC connections are preferred. This is the case in this project. The project is concerned with the transmission of power between Denmark and Norway using an HVDC link. At the moment, the existing HVDC links between the two countries are Skagerrak(SK)1, SK2 and SK3. SK1 and SK2 operate in bipole mode with SK3.

A new HVDC transmission link, SK4 is planned between the two for the near future and feasibility studies are being conducted by Energinet.dk and Statne. It is assumed that the new link will work in bipole mode with the existing SK3 HVDC link. The SK4 link is at 500KV DC and with a power rating of 715MW. The bipole link is based on Voltage Source Converters (VSC) at Skagerrak 4 (SK4) and line commutated current source converters (LCC) at SK3.

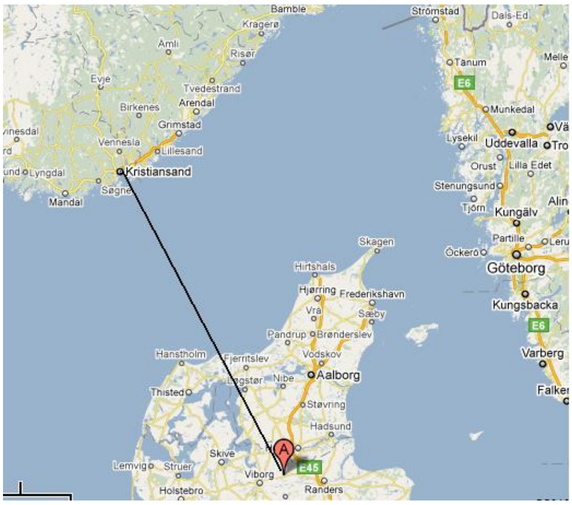

Figure 1.1: Denmark to Norway HVDC link.

1.2 System overview

For the transmission of large amount of power through undersea cable, HVDC transmission is preferred to HVAC [3] as it is more economical. The system under consideration is an HVDC link between Denmark and Norway. At present, there are a large number of HVDC links in the scandinavian countries. Example of this type of link is the Skagerrak HVDC link, which was first established in 1977 with a capacity of 500MW. The Skagerrak was implemented in a bipole fashion, where SK1 and SK2 were in bipole with SK3. The bipole mode of connections.

The connections SK1,SK2, and SK3 were made in view of strengthening the network of both countries and for mutual benefits. The benefits gained from the interconnection may arise [3], due to the differences in means of generation, where production in Norway is from hydropower and Denmark is with coal fired plants. Denmark may use the power from Norway for peaking capacity and Norway can take power from Denmark during dry years. But with the deregularization of the electricity market, links which have been implemented recently are based on business decisions where there may be an advantage in power exchange between markets with different price structures [3].

To extend the power exchange between the countries, the transmission system operators Energinet.dk from Denmark and Statnet from Norway, are working in a new project. The project extends the Skagerrak link with SK4 link, which has a capacity of 715MW at 500KV DC. SK4 may be implemented in three different possible ways,

- SK4 based on conventional thyristor based converter in bipole mode with SK3

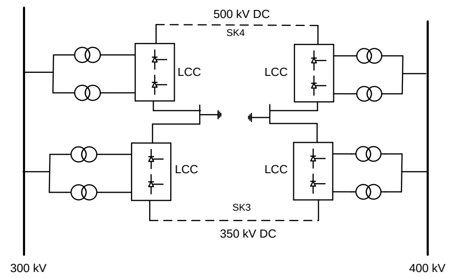

Figure 1.2: SK4 based on conventional thyristor.

- SK4 based on VSC converter on a monopolar mode

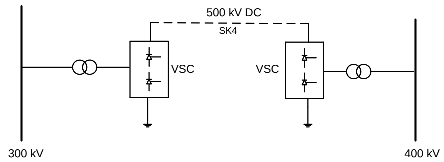

Figure 1.3: SK4 monopolar mode.

- SK4 based on VSC converter in balanced bipole with SK3

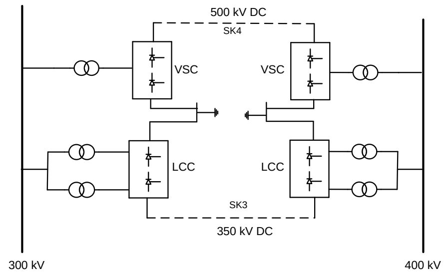

Figure 1.4: SK4 based on VSC in balanced bipole with SK3.

The option that is analysed in the project is, SK4 based on VSC converter in balance bipole mode with SK3. Moreover, SK1 and SK2 will be made to operate as a bipole. The converter to be used for SK4 may be a multilevel converter or a modular multilevel converter.

Figure 1.5, illustrates the layout of SK4 in bipole with SK3.

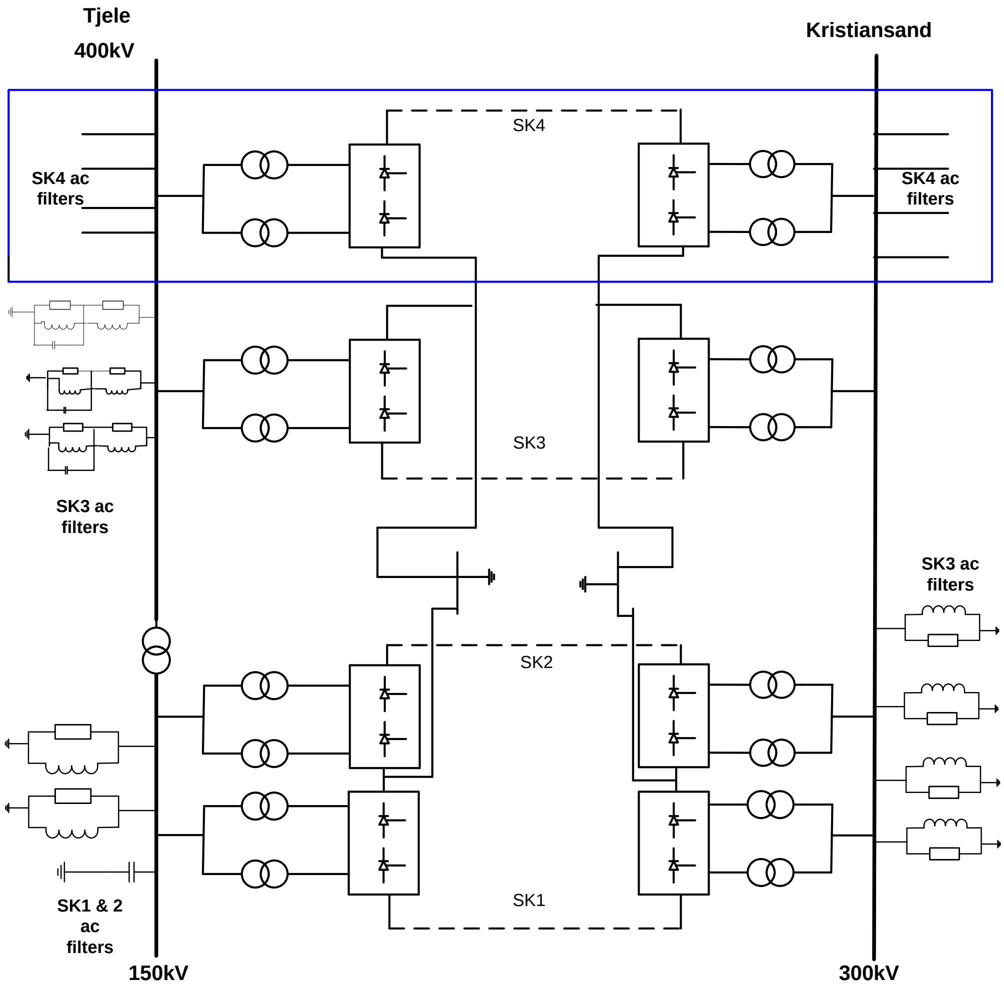

Figure 1.5: Sk4 and SK3 layout.

The HVDC Skagerak links are connected at Tjele in Denmark and Kristiansand in Norway, a distance of 240Km apart. SK4 will be using underground sea cable for a distance of 127Km and the rest on land.

1.3 Problem statement

The main objectives of this thesis are concerned with the performance study of the SK3 HVDC link working in bipole mode with SK4. The SK3 link is based on LCC converter which is prone to commutation failures. SK4 is based on VSC technology and is assumed to operate in bipole mode with SK3. These configurations, where an LCC based link and VSC based link are operated in bipole, has never been implemented practically before.

The implementation of the system in such an arrangement raises questions that have to be answered. The project attempts to answer the following questions:

- The power flow control for an LCC and VSC based converters are accomplished in different manner. The power flow direction control mechanisms in both cases is done in different ways and this raises the problem of how to control the transmission of power between the link ?
- In case of faults such as commutation failure occur in the LCC, How will the bipole link perform ? Faults occurring could be on the ac side as well as on the dc side.
- A commutation failure measurement on SK3 has been done by the transmission system operator energinet and validation of SK3 model is made in regards to the measurement data.
- The harmonics that is created by the two systems, that is LCC and VSC are different. How will the harmonics created by the two converters influence the system and can be managed?

An attempt has been made to analyse the above situations for the system discussed.

1.4 Delimitation

1.5 Thesis overview

chapter two : presents the background of HVDC consisting of the historical background, starting with indicating the main milestones in HVDC history. The commonly used HVDC configurations are discussed, and the main technologies used for conversion purposes, line commutated converters (LCC) and voltage source converters (VSC) are introduced. At the end a comparison between the two is made.

chapter three : discusses about multilevel converters, the main multilevel circuit configurations are presented. The pulse width modulation technique, (PWM) that are commonly used for the multilevel converter are also discussed. Then the principle of operation of an LCC converter and VSC converter is presented in the end.

Chapter four : discusses about the latest type of converter, the modular multilevel converter. The chapter covers the structure of the converter and it principle of operation and finally it modulation method.

Chapter five : explains the control methods that are applicable for the LCC converter as well as the VSC. The control methods employed in the SK3 LCC converter are explained. Then the control methods used for the SK4 VSC converter are explained.

Chapter six : presents the validation of the SK3 model commutation failures. First a description of the SK3 system model is given, then the measurement data given for the validation of the model are presented. Next, the results from the simulation model are discussed and finally a comparison between the measured data and the simulated results is made.

Chapter seven : presents the description of the layout for the SK4 model in bipole with SK3 model. Then different cases of faults, such as single phase to ground, three phase to ground and on dc side, rapid increase of the current have been presented. And finally a conclusion for the behaviour of the system under those conditions is given.

Chapter 2

High Voltage Direct Current

This chapter is an introductory chapter to HVDC, discussing about the milestones in the history of HVDC, a comparison between HVAC and HVDC, also the basic HVDC configurations are discussed. The main technologies used for the conversion of AC to DC and vice versa are the line commutated converter and voltage source converter, and this are introduced and a comparison is made between the two.

2.1 Introduction

2.1.1 History of DC transmission

The first generated power is claimed to be in the DC form by Thomas Edison. At the same time, the first transmission system was also direct current operated at 110V by Edison in 1882 [15, p. 1]. However for long distance transmission, HVDC was not competitive with HVAC at the time. This is because, HVAC has the advantage of being transformable from one level to another, and this led to the domination of HVAC transmission systems. But now a days with advances in converter technology, HVDC transmission system is being preferred in certain applications. This section points out which evolutions made feasible the use of the HVDC technology today :

- Experiments with thyratrons in America and mercury arc valves in Europe before 1940 [26, p. 1].
- First commercial under sea cable HVDC connection was established between the island of Gotland and the Sweedish mainland in 1954 using mercury arc valve [31, p. 5].

- The appearance of first solid state semiconductor valves, thyristors in 1970. The technology was used for the first time in 1972, the first back to back asynchronous interconnection between Quebec and New Brunswick, Canada [26, p. 1].

- Micro-computer control of HVDC equipment from 1979.

- Highest DC transmission voltage link at +/- 600kV established in Itaipu, Brazil, 1984.

- First connection using voltage source controlled (VSC) in Gotland in 1997.

2.1.2 Comparison of HVAC and HVDC

To make a decision on which system to select for transmitting power, a number of factors can be taken in to consideration. The main factors that may be taken are such as: transmission costs, technical considerations and the reliability/availability of the transmission system.

Transmission costs

The comparison may be made depending on infrastructure and operational costs [18, p. 5]. A bipole HVDC using two conductors of opposite polarity can transmit the same amount of power as three AC cables of the same size. This implies for transmitting the same amount of power, HVDC requires less number of conductors, less number of towers and smaller right of way.

Since HVDC uses two conductors, the conductor losses are also decreased by two-third. Moreover the absence of skin effect, the lower amount of dielectric losses and less significant corona effect contribute to the better efficiency of DC transmissions. There is no need of reactive power compensation in DC lines, however, it should be noted that CSC-HVDC stations require reactive power. For an HVDC transmission, the costly parts are the converters and the associated filters.

Figure 2.1, shows the variation of transmission cost with the distance for an AC and DC transmission system.

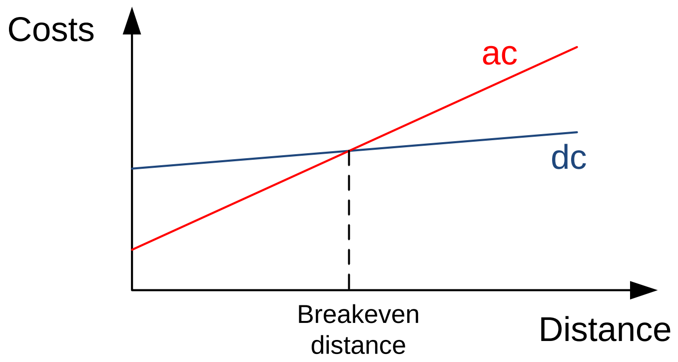

Figure 2.1: Break even distance.

From figure 2.1, it can be seen that AC system tend to be more economical for distances below the breakeven distance and DC system become economical above the break even distance. The breakeven distance depends on factors such as the transmission medium and local factors. For over head transmission, the breakeven distance is around 400 - 600km, where as for a cable, it is much less, around 50Km. The local factors could be permits, cost of laborers, and so on.

Technical considerations

HVDC systems have the advantage of being able to fully control the power flow, improving the dynamic and transient stability of the AC networks connected to it and can limit fault currents in the DC line [18, p. 7].

Some limitation of HVAC systems are:

- Distance limitation: The power carrying capability of an AC line is inversely proportional to the transmission distance where as DC is not affected by the distance[15, p. 2].
- Line compensation: AC transmission lines require compensators which reduce the problem of charging currents
- Asynchronous connection: HVDC controllability allows to connect AC grids of different frequencies.
- Frequent tripping : large power oscillations in the AC grid can lead to frequent tripping and disturbances can be transmitted from one system to another.

All of the above problems can be overcome with an HVDC link. However, HVDC has it's disadvantages also. These disadvantages are high cost of converters at the moment, harmonic production due to the converters, inability of voltage level transformation, and complexity of controls.

However, advances in HVDC technologies, such as increased ratings of IGBTs and GTOs, application of multilevel converters, and digital electronics for control purposes, have reduced the importance of these problems except for the level transformation. The use of HVDC transmission has been in the rise and this trend is expected to increase significantly in the future, creating HVDC grids with multiterminal systems which are integrated in HVAC grids.

Reliability and availability

For reliability comparison of HVDC and HVAC, the bipole HVDC and double three phase AC line are assumed for comparison. The criteria used to asses the availability and reliability is related with the cost of the system. This criteria takes in to account, tower structure and right of way, insulators and losses. Datas for the availability of each system at different power levels and their frequency of departing from their specified levels is documented by CIGRE and IEEE. The datas indicate that both systems are comparable. For an HVDC, the availability is above 90 percent [18, p. 10][4, p. 260].

2.2 HVDC Configurations

The basic configurations which are employed in HVDC transmission systems are the monopole, bi-pole, back to back and multi terminal [28].

Back-to-back configuration : is the simplest one as the converters on both sides are located at the same place. There is no need for long distance cables. This type is used where there is asynchronous power systems. The basic set up of these system can be seen in figure 2.2.

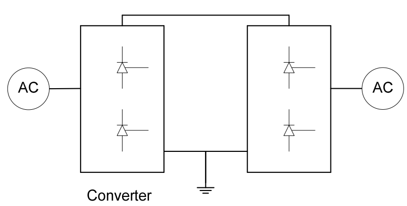

Figure 2.2: Configuration of a back to back system.

Monopole system : contains a single DC line connecting two AC grids. Here the return path is provided by the earth but in applications such as HVDC light, a cable return is used. This system operates in negative polarity as harmonics and the corona effect is less [18, p. 12]. The system configuration can be seen in figure 2.3.

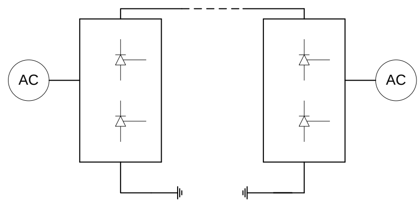

Figure 2.3: Configuration of a monopolar system.

Bi-pole connection : uses a double DC line with voltages of opposite polarity. Each line has a converter of the same rating connected in series. The junction between the two converters is grounded on both sides of the link. This is the commonly used configuration in HVDC transmission [28, p. 40]. It has the advantage that when one line has a fault then power can still be transferred through the other line. Moreover the currents flowing in both poles are equal during normal operation resulting in a zero ground current. The HVDC link considered for this project is of this type and is further discussed in the second chapter. Figure 2.4, illustrates the set up of this system.

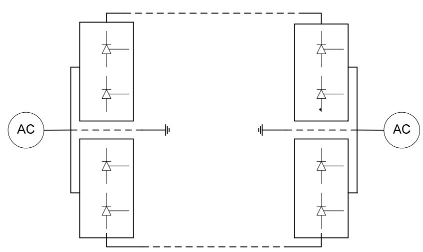

Figure 2.4: Configuration of a bi-polar system.

Multi-terminal connection : consists of multiple converters which makes possible the connection of a number of AC grids through an HVDC link. The connections between converters could be in a parallel or in series. Figure 2.5 shows the series and parallel configuration of multi terminal system.

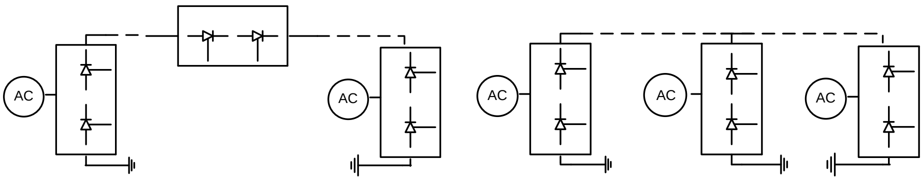

(a) (b)

Figure 2.5: Configuration of a multi-terminal system for (a) series and (b) parallel.

The serial configuration is used for small power tappings, and one converter is made to control that the current flowing across the converters is the same. The parallel configuration is the commonly applied where at least one of the converters is made to control the DC voltage. A combination of series and parallel connection results in a hybrid multi-terminal system. For multiterminal links, the parallel configuration with three terminals has been implemented in a number of projects, terminals more than that have not been implemented yet. [23, p. 160].

2.2.1 Applications of HVDC transmission

HVDC transmission has been applied in many countries and with specific justification for its use. Some of the reasons which made it applicable are discussed below .

- Long distance transmission : For transmission systems above the breakeven distance, HVDC is more economical. This is applicable for overhead and cable medium of transmission. Examples of such projects include, Itaipu in brazil with the highest HVDC transmission level of 600KV, other applications with similar reason can be found in India and China [26, p. 10].

- Asynchronous connection : to connect two AC systems of different frequencies, HVDC is the best solution. The back to back connection is widely used for this application and has been implemented in many countries [26, p. 2,3].

- Stability purposes : due to the fast controllability of HVDC power, HVDC links improve the overall stability of an HVAC system which may be prone to disturbances. Examples of such applications include IPP link in the USA and others.

- Environmental reasons : Using cable, HVDC is more attractive than HVAC. This may be, because of less visual impact, less effect on sensitive wildlife environment, and no relevant electromagnetic fields. An example is the Gotland HVDC link in Sweden [31, p. 7].

2.3 LCC

Line commutated current source converters (LCC) employ thyristors to convert AC to DC and vice versa. LCC converters can be in their basic form as a six pulse bridge or Graetz bridge and twelve pulse bridge which is made up of two six pulse bridges connected in series.

The six pulse bridge is comprised of six thyristor valves which results in six switching operations per period. The twelve pulse bridge has the advantage of handling an increased voltage level and decreased harmonics levels both on the AC and DC side of the system. The harmonics which appear on the AC side are of $nP+/-1$, where P is the pulse number and n = 1,2,3...,. On the DC side, the harmonics that may appear are of the order nP. The twelve pulse bridge has the advantage of reduced harmonics, where the 5th and 7th harmonics don't appear on the ac side and 6th on the dc side. This is accomplished by feeding the two six pulse bridges with two converter transformers, where one of the transformers is in Y/Y arrangement and the other one is in Y/Δ arrangement to make the three phase AC source to be displaced by 30 degrees [28, p. 33]. This can be seen in figure 2.6.

Both six pulse and twelve pulse LCCs require a synchronous voltage source, which is a set of three phase, sinusoidal waveforms at the fundamental frequency and with controllable phase angle for their normal operation. LCC operate with the current lagging the voltage and this demands for reactive power supply to the converters. The reactive power required is supplied by the ac filters, shunt banks or series capacitors which are part of the system.

The common set up of an HVDC station with a LCC for a twelve pulse converter can be seen in figure 2.6.

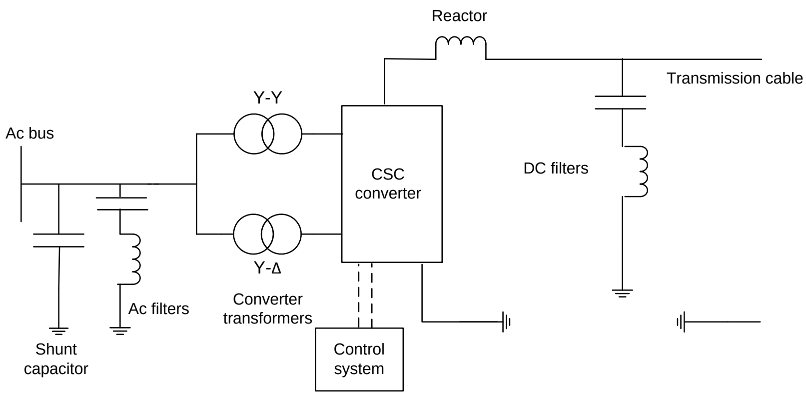

Figure 2.6: Set up of an HVDC CSC.

The figure shows in general the converter station and the transmission line. The converter station consists of : shunt banks, AC filters, converter transformers, LCC, reactor and DC filters.

Converter station

The LCC is the main part which converts the AC to DC and vice versa and is made with thyristor valves. A single thyristor has the ability to carry currents up to 4KA and can also block voltages up to 10KV [26, p. 2]. The thyristors can be arranged in series or parallel manner to increase their current and voltage handling capability. Thyristors arranged in such a manner are known as thyristor valves. Thyristors once switched on require a negative voltage at their terminals to switch off.

Converter transformers are used for adapting the voltage level to that of the converter and for galvanic isolation. They also contribute to the commutation reactance.

AC and DC filters, are used to filter out harmonics on the AC and DC side respectively which are created by the converter. The AC filters together with the shunt bank are also used to supply reactive power to the converter for its normal operation and to improve the power factor.

The reactor on the DC side is used to smooth the ripples. Moreover, it is used to prevent commutation failures, limit DC fault currents and prevent resonance of the DC circuit.

Transmission line

Transmission medium used may be overhead lines or DC cables. For an overhead transmission line, the bipolar arrangement is usually used with opposite polarities. HVDC cables commonly used are of the type, solid cable, self contained fluid filled cable and extruded XLPE(cross linked polyethylene) cables.

2.4 VSC

Self commutated voltage source converter (VSC) was introduced in the 1990s and the first VSC-HVDC was implemented in Sweden in 1997, transmitting power between Hellsjon and Grøngesberg [5, p. 1]. The VSC HVDC is known as HVDC light for ABB trademark and HVDC plus for the siemens trademark, which are large companies involved in HVDC business. It is made of either IGBTs (Insulated Gate Bipolar Transistors) or GTOs (Gate Turn Off thyristor) and uses PWM in the control of its operation. The IGBTs and GTOs have the ability to turn on and off at will and have switching frequency up to 2KHz.

The VSC maybe a single level or multilevel. The single level VSC is made with the basic Graetz bridge consisting of six IGBTs. This arrangement can be seen in figure 2.7. The multilevel VSC is made of a serial combination of the single level to meet the desired performance of the converter.

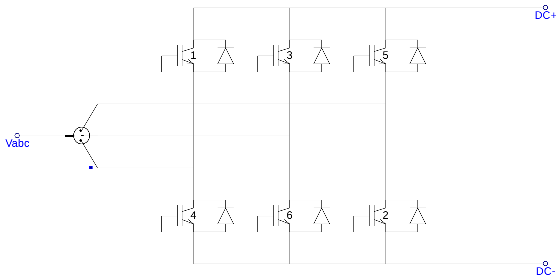

Figure 2.7: Six pulse converter.

The common set up of the VSC station is illustrated in figure 2.8.

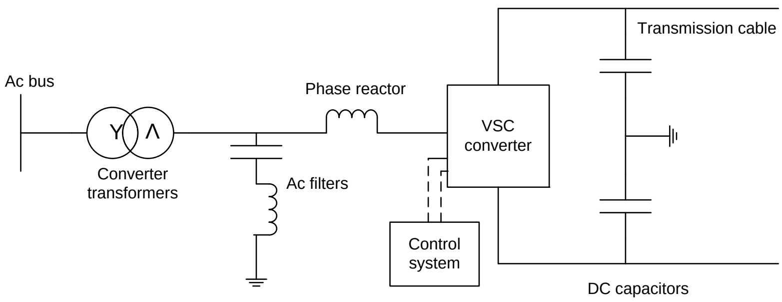

Figure 2.8: Set up of an HVDC VSC.

The converter station consists of ac filters, converter transformers, reactor, VSC, dc capacitors, dc filters and dc cables. The ac and dc filters are used to remove harmonics created by the converter[31, p. 41]. The converter transformer is used for adapting the voltage level to that of the converter rating, galvanic isolation and contributes to the commutation reactance. The reactor is used to limit short circuit currents, provide active and reactive power control, and to provide low pass filtering. The Dc capacitor is used for reducing the harmonics ripple on the dc voltage, provide low inductance path for the turned off current and to store energy. The VSC as mentioned is the main part which converts the ac to dc and vice versa. The multilevel VSC is further explained in the next chapter.

2.5 Comparison of LCC and VSC

HVDC transmission uses either LCC or VSC for the conversion process. Both systems are being used at the present time and selection of which to use is usually determined by economical and technical considerations. Some points are listed below for a comparison of the two converter technologies:

Active and reactive power control - VSC has the capacity to control active and reactive power independently as its control is based on PWM. Using PWM, it is possible to control the magnitude and phase of the ac voltages to the desired level thereby controlling the active and reactive power independently. This is not possible with LCC [18, p. 7].

Power reversal - LCC uses voltage polarity reversal to change the direction of power, which may require switching devices for a multiterminal configuration. However VSC uses current direction reversal[28, p. 39].

Black start - VSC permits black start, where if there is a total system shut down, the VSC could be used to restart the system. whereas LCC needs external power supply to restart the system[14, p. 1].

Converter placement in HVAC network - For VSC, the converter can be placed anywhere in the network, be it in a strong or weak grid. However, LCC are placed in strong networks, where, in the possibility of complete shutdown, there is a power supply which could enable the system to restart [18, p. 26].

Filters - VSC uses less filters compared to LCC, this is also related to the use of the PWM, which is used to generate a signal very close to sinusoidal. Moreover, VSC needs only one converter transformer which makes the VSC station much smaller [26, p. 4].

Reactive power supply - LCC requires a reactive power supply for power factor correction where as VSC does not require as it can be operated in any of the four quadrants[28, p. 39].

Losses - switching in VSC occurs at high frequency, frequencies up to 2KHz, which results in higher switching losses compared to LCC, which switches in the line frequency of 50Hz [18, p. 16].

Cost - as they use IGBT's or GTO's which are expensive semiconductor devices at the present, VSC is much more expensive than LCC.

Maturity - LCC is a mature converter technology which has been in business since the 1970's, where as the VSC has come to the industry a few decades ago, starting in 1990's.

Taking in to consideration the many advantages mentioned for VSC, a lot of research and development is being undertaken to bring the technology to a mature stage and to make it economical. LCC has been used for the last three decades and VSC is expected to be the future converter technology.

The above introductory sections on LCC and VSC are further discussed in chapter three.

Chapter 3

Multilevel converters

In this chapter, the different topologies of the multilevel converter are presented. Then discussion on PWM techniques employed for multilevel converters is presented. The principles of operation of an LCC and VSC are also presented at the end.

3.1 Introduction

The converter that is assumed to be used for SK4 is a VSC based multilevel converter. The two level converter has been widely used in the past, but with advances in semiconductors and requirement for higher power handling and quality, the multilevel power converter (MPCs) has come to play a major role in HVDC transmission system. A MPC, basically starts from a three level converter and produces as an inverter, a staircase voltage waveform. In this section a comparative discussion of MPCs with respect to two level converter, the commonly used circuit configurations and pulse width modulation(PWM) techniques used for MPCs are presented.

3.1.1 Comparison of MPC to two level converter

In comparison to two level converters, the advantages gained from using MPCs in high voltage HVDC transmission are:

- For MPC's, switching losses are less. This is because, the switching frequency for multilevel power converters can be lower than that of a two level. The higher the switching frequency, the higher switching losses for the converter. This results in an overall power loss which is less than in two level converter [13, p. 1].

- The multilevel produces the AC output in three or above levels as a staircase waveform and this results in less harmonics. A comparison of the two level and three level converters, voltage and current output for an inverter operation can be seen in figure 3.1 [13, p. 3].

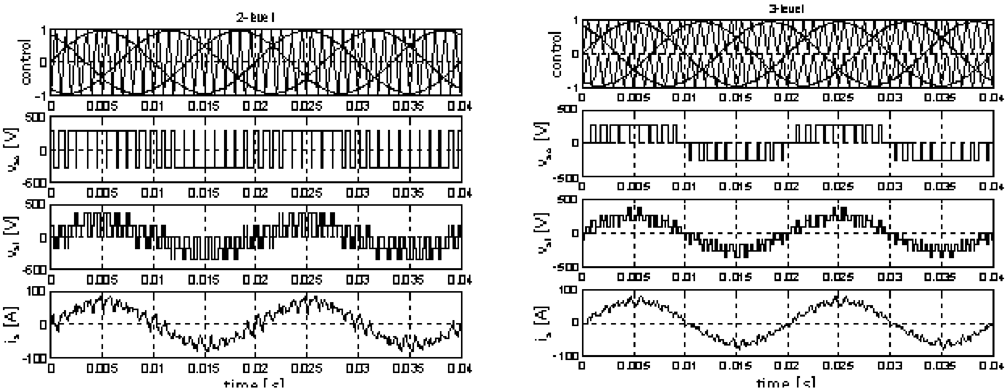

(a) (b)

Figure 3.1: Comparison of two and three level converters (a) two level (b) three level.

It can be seen that, the voltage and current output from the three level converter are much better in quality with respect to harmonics.

- As the MPC has higher number of levels, the dV/dt is decreased, hence less stress on cables and electromagnetic compatibility (EMC) problems are reduced [17, p. 1]. Common mode voltages can cause premature insulation failures and this problem is reduced as the voltage is produced in smaller steps with low dV/dt [1, p. 2].

- As the number of levels increases in MPCs, the voltage handling capability also increases and this reduces the need of transformers which are used with the two level in high voltage applications [1, p. 2]. For an MPC's, the number of voltage handling capacity is limited by the voltage unbalance problems, circuit layout and packaging requirements. The highest MPC's implemented is for a back to back intertie application with six levels [27, p. 1].

The disadvantages that may be faced in using of MPC's are:

- as the number of levels increases, MPC's are more complex to control

- MPC's are more expensive as it requires more number of diodes and semiconductor switches (thyristors or IGBTs) [17, p. 1]

Regarding the control of MPC's, as mentioned above, MPC's with six levels has been successfully controlled and implemented for a back to back connection. Levels above six have been discussed theoretically in a number of literatures but have not found practical application. Hence considering the above mentioned advantages of MPCs over the two level, MPCs are becoming the attractive choice for an HVDC transmissions and is a good choice for this project.

3.1.2 Classification of MPCs

MPC's can be classified according to their power flow direction capability, number of phases and circuit configurations. Figure 3.2 shows the different MPC's available in the market.

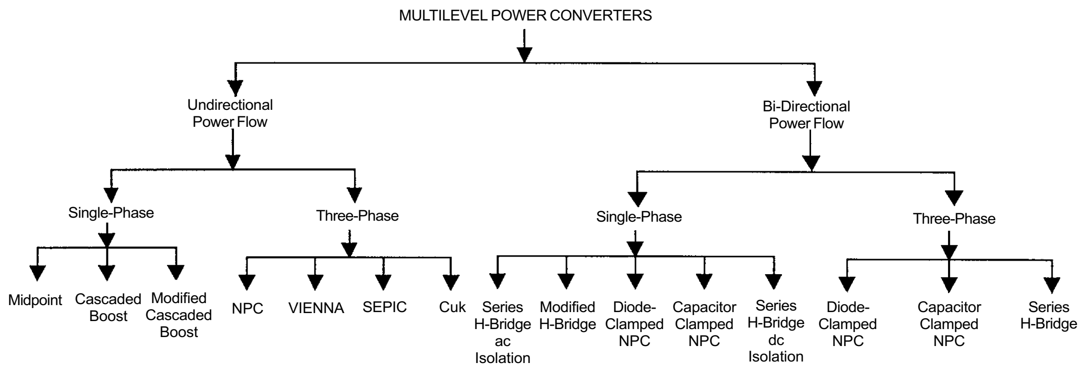

Figure 3.2: MPC classification.

Discussions on the unidirectional, single phase and three phase and bidirectional, single phase MPC's can be found in the literatures [1, p. 2]. The possible MPC configurations that may be suitable for this project are the bidirectional, three phase diode clamped, flying capacitor (FCC), and cascaded H-bridge (CHB) MPC's. These three configurations are discussed taking in to account their circuit behavior, advantages and disadvantages.

Diode clamped (neutral point clamped converter - NPC)

NPC requires one DC bus, and voltage levels are produced by summation of the voltage across several capacitors. The capacitors can be seen in figure 3.3, which illustrates the circuit configuration of a three level diode clamped MPC. In comparison to the other types of MPC, the advantages and disadvantages of this configuration are presented:

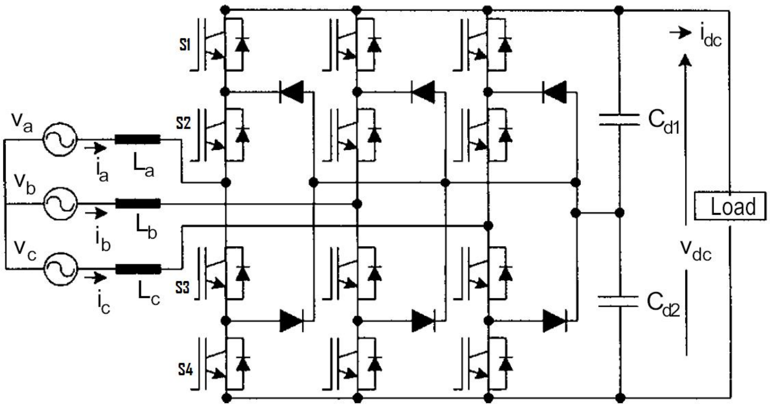

Figure 3.3: Three phase three level diode clamped MPC.

Advantages :

- requirement of one DC bus results in less capacitance requirements of the converter and capacitors can be precharged as a group [17, p. 8]

- has become a mature solution, with high performance in terms of harmonics spectrum, low switching losses and is economical. [9, p. 1]

- provides excellent control over power flow and is the topology of choice in most HVDC transmission applications [1, p. 2].

Disadvantages :

- large number of diodes are required when the number of levels increases [27, p. 3]

- balancing capacitors is a challenge for high number of levels [27, p. 3]

Operating principle: An m level converter consists of $m - 1$ capacitors on the dc bus and produces m levels of the phase voltage. The number of diodes required for each phase is $(m - 1).(m - 2)$ [27, p. 3]. As an example for a three level NPC, in inverter operation, the switching states are given in table 3.1 [33, p. 144].

Switching state	switching status of devices at phase A S1	S2	S3	S4	Inverter terminal voltage
P	ON	ON	OFF	OFF	+E
O	OFF	ON	ON	OFF	0
N	OFF	OFF	ON	ON	-E

Table 3.1: Switching states for a three level NPC.

When the upper switches for leg phase a are on, the inverter terminal voltage is at positive E which is equal to the voltage with respect to the neutral at the upper capacitor. When the lower two switches conduct, the inverter terminal voltage is at -E and the 0 state represents when the two inner switches are conducting and the inverter terminal voltage is zero. Figure 3.4 shows the switching states, gate signals and inverter terminal voltage.

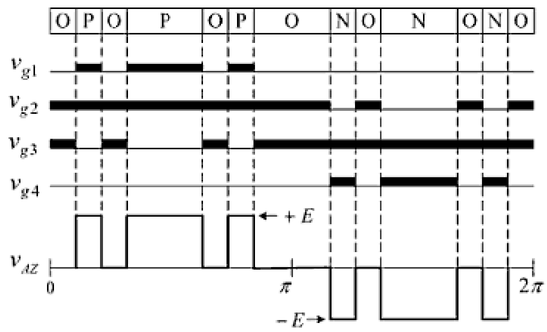

Figure 3.4: Three level diode clamped MPC voltage output.

Flying capacitor clamped

FCC requires isolated DC supplies for the DC bus, and structure of the circuit is similar as NPC, except the clamping diodes are replaced by capacitors. This was done to simplify the neutral point voltage balancing [1, p. 5]. Loss of neutral point voltage balancing can cause unwanted harmonics. The circuit configuration of FCC can be seen in figure 3.5.

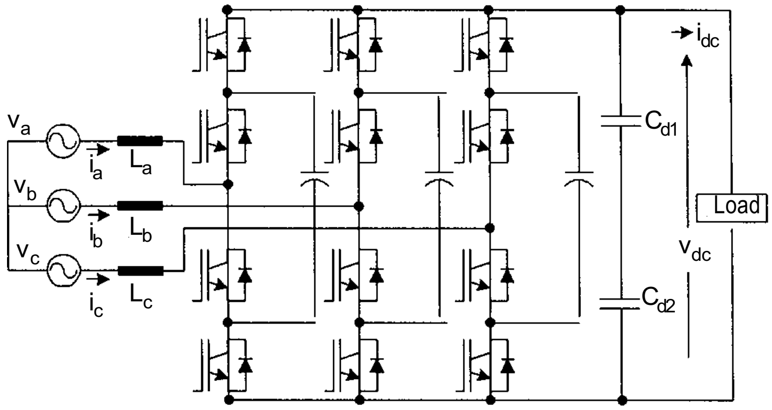

Figure 3.5: Three phase three level flying capacitor MPC.

FCC has the following advantages compared to the NPC and CHB configurations:

- Phase redundancies are available for balancing the voltage levels of the capacitors [17, p. 9]. This implies for a valid switch combination, there is always an equivalent voltage output.
- Real and reactive power flow can be controlled [17, p. 9].
- The large number of capacitors enables the inverter to ride through short duration outages and deep voltage sags. [17, p. 9]

The disadvantages it faces are:

- Control is complicated to track the voltage levels for all of the capacitors. Also, pre charging all of the capacitors to the same voltage level and startup are complex. Moreover for high power applications, its use is limited due to large current stresses on the capacitors [1, p. 5].
- Switching utilization and efficiency are poor for real power transmission.[17, p. 9][27, p. 4]
- The large numbers of capacitors are both more expensive and bulky than clamping diodes in multilevel diode-clamped converters. Packaging is also more difficult in inverters with a high number of levels [1, p. 5].

Cascaded H-bridge

CHB requires isolated DC source for each level. Application area for this type has been in grid interface for photovoltaic generators, wind and other renewable energy sources, where there is a distributed power generation [1, p. 6]. The circuit configuration of this type can be seen in figure 3.6.

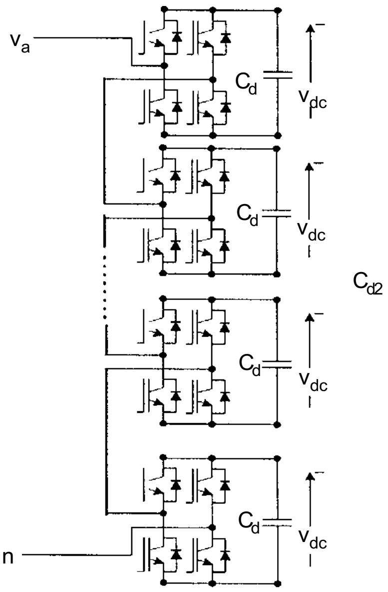

Figure 3.6: n-level H bridge MPC.

CHB has the following advantages compared to NPC and FCC [27, p. 5]:

- requires the least amount of components to produce the same amount of voltage levels

- modularizing and packaging is simple

The main disadvantage it faces is that, it requires separated dc sources which limit its application.

A comparison between the three configuration for a three level converter depending on their physical components is given in table 3.2 [1, p. 5].

Topology	NPC	FCC	CHB
Number of power switches	12	12	8
Switch diodes(free wheeling)	12	12	12
Clamping diodes	6	0	0
Clamping capacitors	0	3	0
Dc link capacitors	2	2	2
Neutral point voltage balance	complex	simple	very simple
Modularity	complex	complex	simple

Table 3.2: Three level converter topologies comparison.

The choice of which topology to use depends on the ac side voltage of the converters, size of the capacitor on the dc side required, and converter complexity [6, p. 3]. The NPC, has lower number of reactive components and is preferred from economical aspect, but the choice for which type of topology will be used in this project has not been made yet.

3.1.3 Modular multilevel converter

With advances in multilevel converters, the type of multilevel converter that is attracting attention is the modular multilevel converter (M2C). The m2c is discussed in chapter four, considering its structure, principle of operation and it modulation technique.

3.2 PWM techniques for MMC

The control mechanism for VSC based converters is based on pulse width modulation (PWM). The PWM techniques which are employed for the two level converter can also be used for MPC's. These techniques are modified to accommodate for the increase in the level of the converters. The most commonly used type of PWM techniques used in MPC are: Carrier based PWM (CPWM), space vector PWM (SVPWM), and selective harmonic elimination PWM (SHEPWM) [17, p. 15]. Other techniques do also exist but the following discussions are on the three main techniques.

3.2.1 Carrier based PWM

Carrier based PWM can be implemented in two ways, sub harmonic PWM and switching frequency optimal PWM.

A. Subharmonic PWM (SHPWM)

SHPWM is the commonly used technique in industrial applications and employs several triangle carrier signals and one reference signal per phase to produce an output [17, p. 15]. For an m level converter, $m-1$ carriers with the same frequency fc and the same amplitude Ac, are used in such a way that they are near each other but without crossing each others bands. The reference waveform has peak to peak amplitude Am, frequency fm and its zero crossing centered around the middle of the carrier set. The reference is continually compared with all the carrier signals. If the reference signal is greater than the carrier signal, then the active device corresponding to that carrier is switched on and if it is less than, then the active device is turned off [20, p. 1].

Figure 3.7 illustrates SHPWM, as such it shows the five set of carriers for a six level diode clamped MPC, the sinusoidal reference waveform and the corresponding output for an inverter operation. The amplitude modulation for the figure is 0.8.

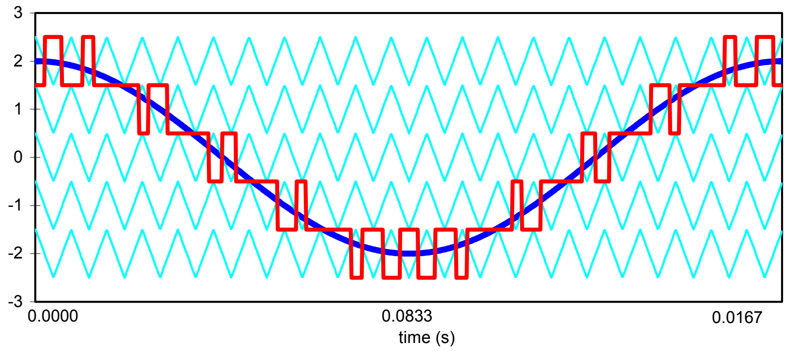

Figure 3.7: Carrier based PWM [17].

B. Switching frequency optimal PWM (SFOPWM)

SFOPWM is similar to SHPWM but extends in a way that, the reference voltages are determined by taking the instantaneous average of the maximum and minimum of the three original reference voltages and subtracts this value from each of the individual reference voltages. This is shown by equations 3.1, 3.2.

$$V_{offset} = \frac{max(V_a^*, V_b^*, V_c^*) + min(V_a^*, V_b^*, V_c^*)}{2} \tag{3.1}$$

$$V_{abcSFO}^* = V_{abc}^* - V_{offset} \tag{3.2}$$

The offset voltage centers all of the three reference waveforms in the carrier band and enables the modulation index to be increased by 15 percent before the overmodulation region is reached [20, p. 2] [17, p. 18].

Amplitude modulation index : For low amplitude modulation indexes, the MPC does not make use of all its levels and at very low values, it operates as a two level converter. When the amplitude modulation index is above 1, over modulation occurs which results in pulse dropping. The amplitude modulation index and the frequency ratio in MPC's are defined by [17, p. 17]:

$$m_a = \frac{A_m}{(m-1).A_c} \tag{3.3}$$

$$m_f = \frac{f_c}{f_m} \tag{3.4}$$

Figure 3.8 shows the output voltage for an inverter operation at modulation indexes of 0.5 and 0.15.

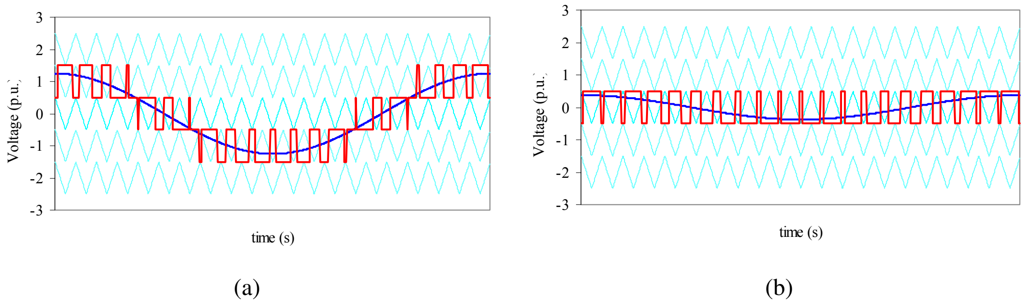

Figure 3.8: Comparison of output at different modulation indexes (a) modulation index 0.5 (b) modulation index 0.15.

The minimum modulation index, that an MPC controlled with CPWM uses all its levels can be determined by:

$$m_{amin} = \frac{m-3}{m-1} \tag{3.5}$$

For the CPWM, the active devices in the top and bottom positions are switched much more often than the ones in the intermediate positions. One method to balance the switching of these active devices so that the switching stress is reduced is by varying the frequency of the carrier signals as shown in figure 3.9 [17, p. 18][20, p. 5]. The figure shows an output using SFOPWM at $m_a = 0.85$, $m_f = 15$ for $band2$ and $m_f = 55$ for $band1$.

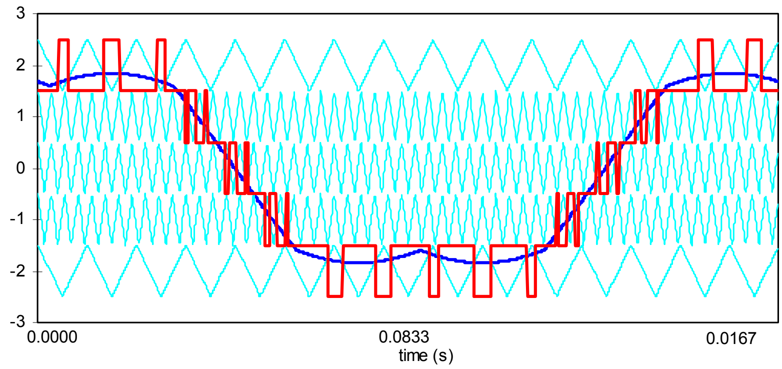

Figure 3.9: Modified Sinusoidal PWM [17].

Moreover to improve the switching stress during low modulation index, the redundant output states of an MPC can be used. For example the diode clamped MPC has line to line redundancy states which can be used to reduce the stress [20, p. 5].

3.2.2 Space Vector PWM (SVPWM)

A MPC can generate output from a number of levels. These output levels are represented in a space vector in SVPWM. Each switching state of the phase legs produces a defined set of three phase voltages, which can be represented in the space vector plane. The points in the space vector represent a particular three phase output voltage of the converter. The vector space for a six level MPC can be seen in figure 3.10 . For example, the point $(3, 2, 0)$ on the space vector plane implies that, phase a is at $3Vdc$, phase b is at $2Vdc$ and phase c is at $OVdc$ with respect to ground [17, p. 26].

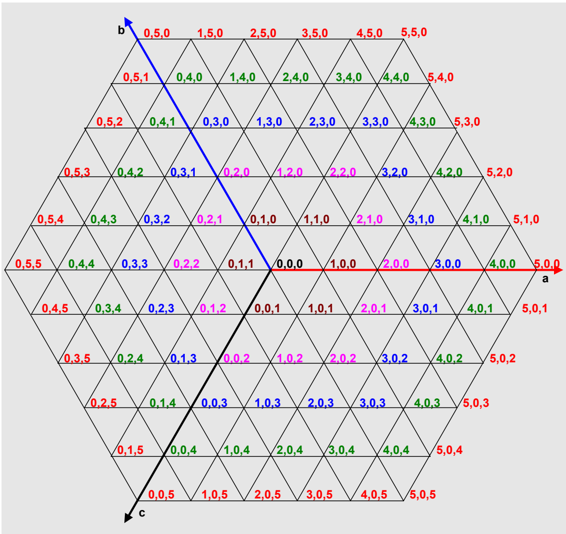

Figure 3.10: Space vector plane for a six level converter.

The operation of the SVPWM can also be illustrated using the model of a multiplexer. Figure 3.11 shows the switching states connected at their specific levels, and that can be extended to other levels also.

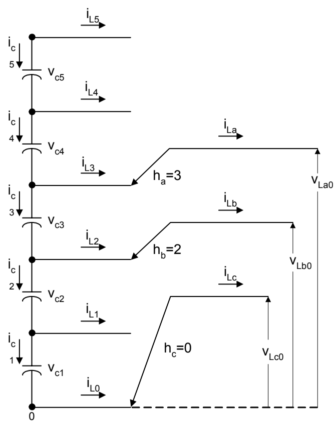

Figure 3.11: Multiplexer model of SVPWM.

An algebraic representation of the output voltage with respect to the switching states and the dc link capacitors is given in [19, p. 3] as:

$$\overline{V_{abc0}} = \mathbf{H_{abc}}\overline{V_c} \tag{3.6}$$

where:

$$V_{abc0} = [V_{a0}V_{b0}V_{c0}]^T \tag{3.7}$$

$$V_c = [V_{c1}V_{c2}V_{c3}...V_{cn}]^T \tag{3.8}$$

$$\mathbf{H} = \begin{bmatrix} h_{a1} & h_{a2} & h_{a3} & ... & h_{an} \\ h_{b1} & h_{b2} & h_{b3} & ... & h_{bn} \\ h_{c1} & h_{c2} & h_{c3} & ... & h_{cn} \end{bmatrix} \tag{3.9}$$

$$h_{aj} = \sum_{j}^{n} \delta(h_a - j) \tag{3.10}$$

where h is the switch state and j is an integer from 0 to n and where $\delta(x) = 1$ if$x > 0$, $\delta(x) = 0$ if $x < 0$.

For an m level converter, the number of possible switching combinations is m^3. The number of unique states is given by $m^3 - (m-1)^3$ and the redundant switching states are $(m-1)^3$. The redundant switching states are the ones where a particular output voltage can be generated by more than one switch combination. As the modulation index decreases, the number of redundant states available increases [20, p. 3].

In tracking the reference voltage, SVPWM, takes the three nearest triangle vertices V_1,V_2, and V_3 to the reference voltage V^*, which are selected to minimize the harmonics content of the output. The time required to be at this vectors so that their sum equals that of the reference is calculated by [11, p. 3]:

$$V^* = \overline{V_1}T_1 + \overline{V_2}T_2 + \overline{V_3}T_3 \tag{3.11}$$

$$T_s = T_1 + T_2 + T_3 \tag{3.12}$$

Where T_s is the switching period.

Equation 3.11 consists of the real and imaginary in the dq reference frame and can be decoupled to its components. Taking these two equations, the time for each of the three vertices can be calculated.

3.2.3 Selective harmonic elimination PWM (SHEPWM)

To produce an output voltages with minimized total harmonics distortion level (THD), selective harmonics elimination PWM is used. The THD is minimized by eliminating the particular harmonic levels by producing an appropriate conducting angles. The fourier series of an output voltage can be expressed as [17, p. 2]:

$$V(\omega t) = \frac{4V_{dc}}{\Pi} \sum_{n} [\cos(n\theta_1) + \cos(n\theta_2) ... + \cos(n\theta_s)] \qquad where n = 1, 3, 5, ... \quad (3.13)$$

When the above equation is normalised with respect to Vdc, the magnitude of the fourier coefficients is given by:

$$H(n) = \frac{4V_{dc}}{n\Pi} [\cos(n\theta_1) + \cos(n\theta_2) ... + \cos(n\theta_s)] \qquad where n = 1, 3, 5, ... \quad (3.14)$$

Then the conducting angles can be chosen such that the THD is minimum. For example for an 11 level converter, the $5th$, $7th$, $11th$ and $13th$ harmonics can be eliminated by selecting an appropriate conducting angles [25, p. 3] . From the fourier series, equation 3.14 can be modified for the harmonics mentioned as such:

$$\cos(5\theta_1) + \cos(5\theta_2) + \cos(5\theta_3) + \cos(5\theta_4) + \cos(5\theta_5) = 0 \quad (3.15)$$

$$\cos(7\theta_1) + \cos(7\theta_2) + \cos(7\theta_3) + \cos(7\theta_4) + \cos(7\theta_5) = 0 \quad (3.16)$$

$$\cos(11\theta_1) + \cos(11\theta_2) + \cos(11\theta_3) + \cos(11\theta_4) + \cos(11\theta_5) = 0 \quad (3.17)$$

$$\cos(13\theta_1) + \cos(13\theta_2) + \cos(13\theta_3) + \cos(13\theta_4) + \cos(13\theta_5) = 0 \quad (3.18)$$

$$\cos(\theta_1) + \cos(\theta_2) + \cos(\theta_3) + \cos(\theta_4) + \cos(\theta_5) = 5m_a \quad (3.19)$$

The above equations are nonlinear and can be solved with iterative methods, such as Newton-Raphson method. By defining the modulation index, the appropriate conducting angles can be determined. The calculated angles can be used so that the $5th$, $7th$, $11th$ and $13th$ harmonics components will not appear in the output.

The SHEPWM can be implemented in two ways, the fundamental switching frequency and virtual stage PWM. For fundamental frequency switching method, the switching angles is equal to the number of dc sources while for the virtual is not. The virtual method is a modified version of the fundamental switching method to increase the range of modulation indexes that can be used [17, p. 30]. A voltage output for the virtual method is shown in figure 3.12.

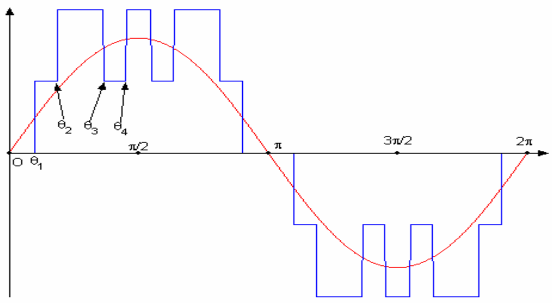

Figure 3.12: SHEPWM for a three level converter.

The next sections deals with the principle of operation of LCC and after that with VSC.

3.3 Principle of operation of LCC

The twelve pulse bridge line commutated converter, is used commonly in industrial applications for rectification, where the power flow is from the AC to the DC and inversion, where power flows from the DC to the AC side. The bridge is made up of twelve thyristors, with four thyristors in each leg. The thyristor valves are used as switching devices in which, when they are forward biased and receive a gate pulse, they start to conduct and turn off when they are reverse biased.

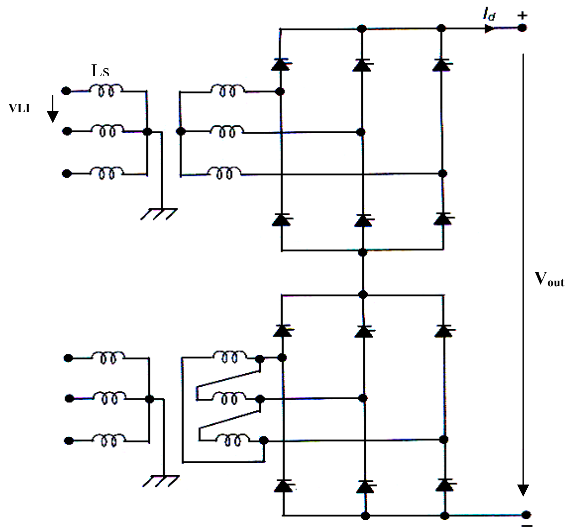

Figure 3.13: 12 pulse LCC.

The converter performs its function as a rectifier or inverter by line commutating. Commutation is the process of transferring of current between two thyristor valves while both of them are conducting current simultaneously [32, p. 13]. The electrical angles which are important in the operation of an LCC are shown in figure 3.14. These angles are measured on the ac side and their values determines the operation of the LCC as an inverter and rectifier [32, p. 14].

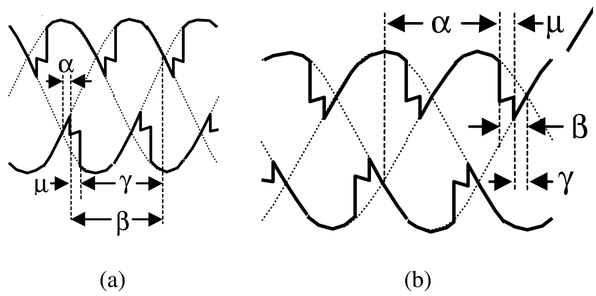

Figure 3.14: Electrical angles (a) rectifier operation (b) inverter operation.

If the Delay angle α (firing angle) is less than 90 degree, then the converter operates as a rectifier and if it is above, the converter operates as an inverter. The advance angle β is the angle between the instant of forward conduction and the next zero crossing of the commutating voltage. The relationship between advance angle and delay angle can be expressed mathematically as [32, p. 14] [22, p. 2]:

$$\beta = 180 - \alpha \tag{3.20}$$

The overlap angle μ is the angle for the duration of the commutation process and is between 15-25 degrees [7, p. 30]. The extinction angle γ is the angle between the instant of the end of current conduction and the next zero crossing of the commutating voltage. The extinction angle depends on the advance and overlap angle and their relation can be expressed as [22, p. 2]:

$$\gamma = \beta - \mu \tag{3.21}$$

During the rectification process, when a thyristor valve receives a gate pulse, and its forward bias voltage is greater than the one conducting, it switches on. However the commutation process does not occur instantaneously as the transfer of current is made through the converter transformer reactance (leakage reactance of the transformer), known as the commutation reactance. The sum of the currents transferred to the DC side is direct current output and it is further filtered by the reactance on the dc side and the dc filters. The average output voltage of the during rectification can be determined by [7, p. 30]:

$$V_{out} = \frac{6\sqrt[n]{2}}{\pi} V_{LL}\cos(\alpha) - \frac{6\omega Ls}{\pi} I_d \tag{3.22}$$

Where :V_{out} is the voltage between the terminal + and terminal -, I_d is the current that goes to the cable, V_{LL} is the line-to-line rms voltage, L_s is per-phase leakage inductance of each transformer, referred to the converter side, and α is the firing angle

During the inversion process, the commutation process takes place when the dc voltage for the forward biasing of the thyristor valves is greater than the AC commutation voltage derived from the AC system. Therefore the AC voltage supplied by the the AC system determines the forward or reverse biase of the thyristor valves. The commutation process is however, the same as that in the rectification process. The output voltage can also be determined by equation , the firing angle α is replaced by the extinction angle γ [7, p. 31].

Reversal of power is achieved by changing the polarity of the dc link. This is accomplished through the firing control of the gate pulses. Change in direction of power is not possible by changing the direction of current [32, p. 14].

Further discussion on how the control for an LCC is implemented is presented in chapter five.

3.4 Principle of operation of VSC

The VSC is made using IGBTs or GTOs. These devices are self commutating switches which can be turned on and off at will. The switching frequency for these devices is up to 2 KHz. Hence the commutation process is a forced one, where commutation may occur many times per cycle and this characteristic enables the VSC to be controlled by PWM. Using PWM, the VSC generates outputs which are close to sinusoidal and reduces the amount of filters required to filter out harmonics [2, p. 1].

The control method using PWM, enables the VSC to operate in the four quadrants as shown in figure 3.15, to operate as an inverter and rectifier [8, p. 29]. When it is operating as an inverter, power is transferred from the DC side to the AC side , and when it operates as a rectifier, power is transferred from the DC to the AC side. In both cases, the VSC can operate by generating, positive reactive power to the AC grid or taking reactive power from the AC grid.

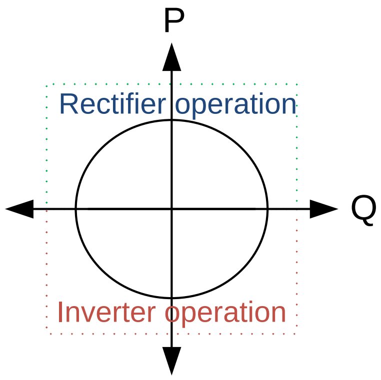

Figure 3.15: VSC four quadrant operation.

The VSC is able to operate at any point in the circle, where the radius of the circle is the MVA rating of the converter [8, p. 29].

Figure 5.8 shows the single line VSC circuit diagram . From the figure, it can be seen that, the exchange of active and reactive power between the converter and the AC grid can be expressed by equations 3.23, 3.24. The voltage on the AC grid (U_g) is taken as a reference and on AC converter side (U_c) at leading phase angle of δ.

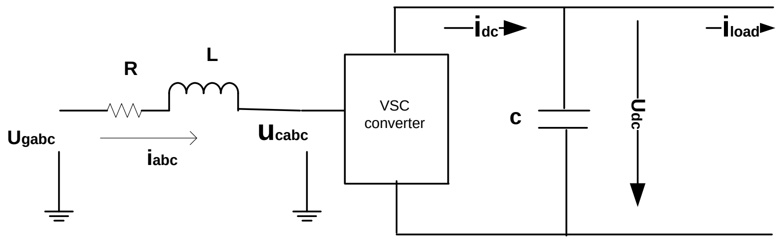

Figure 3.16: Single line diagram of the VSC.

$$P = \frac{U_g U_c \sin \delta}{X_L} \tag{3.23}$$

$$Q = \frac{U_g (U_g - U_c \cos \delta)}{X_L} \tag{3.24}$$

By varying the magnitude of U_c and δ, the active and reactive power can can be adjusted as desired. Changing the δ results in change of the active power exchanged between the converter and the AC network and changing the magnitude of U_c causes changes in the reactive power exchange. The possible exchange of the power between the converter and reactor can be summarized as shown in figure 3.17 [18, p. 53][**?**, p. 29] .

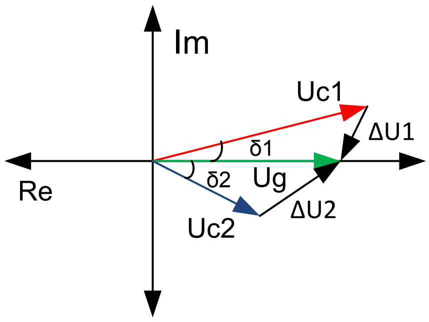

Figure 3.17: VSC exchange of power.

The figure shows the exchange of power depends on the converter voltage magnitude and phase generated. Active power is transferred from AC side to DC (rectifier operation) when the converter voltage is in phase lag to the AC grid voltage while if it is leading, power is transferred in the reverse direction. For the reactive power exchange, if the magnitude of the grid voltage is greater than the converter voltage, reactive power is taken by the converter and if it is less, reactive power is generated to the grid.

Further discussion on how the control for a multilvel VSC is implemented is presented in chapter five.

Chapter 4

Modular Multilevel converters (M2C)

This chapter presents, the modular multilevel converter and discusses on its advantages compared to the multilevel converter, its topology, principle of operation and modulation techniques that are applicable.

4.1 Introduction

With advances in multilevel converters, the type of multilevel converter that is attracting attention is the modular multilevel converter (M2C). The Multilevel converter, as discussed in the previous sections, have the main advantage of handling higher level of voltage and power with lesser harmonic distortions compared to the conventional two level converter. However, as the number of levels increases in MPC, problems occur with the increase in number of diodes for NPC and increase in number of capacitors with FCC, which makes them difficult to assemble and build. Moreover, voltage imbalance occurs in the series connected DC capacitors, which requires an external control circuit to balance them [12, p. 1].

Advantages of M2C compared to the non modular MPC are [21, p. 1] :

- Combining averaging control with balancing control enables the converter to achieve voltage balancing without any external balancing circuit
- Modular realization: it is scalable to different power and voltage levels and is independent of the state of the art of fast developing power devices

- Multilevel waveform: is expandable to any number of voltage steps resulting in low total harmonic distortion and dynamic division of voltage to the power devices
- High availability:
- Failure management: has a fail safe operation on device failures

4.2 classification of M2C

From their topologies, MMCs can be classified into [12, p. 2]:

1. double-star-configured MMCs;

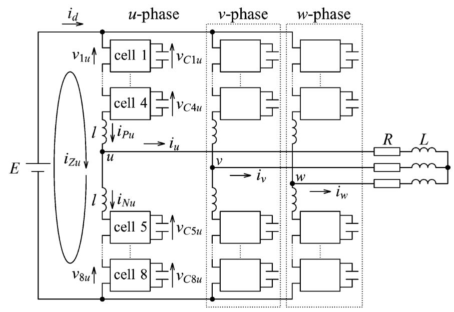

Figure 4.1: Structure of a double-star-configured MMCs.

2. a star-configured MMC
3. a delta-configured MMC

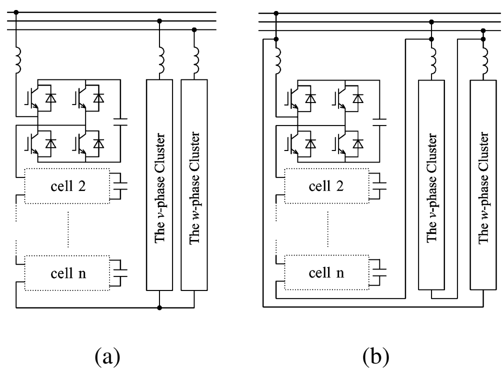

Figure 4.2: (a) Structure of a star-configured MMC (b) Structure of a delta-configured MMC.

4. the dual MMC

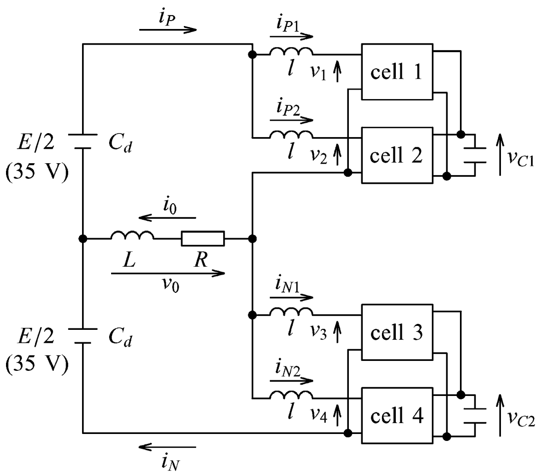

Figure 4.3: Structure of dual MMC.

The above classification of MMCs can also be further categorized based on their use of single-phase half-bridge or full-bridge converter-cells [12, p. 2]. The MMC that is appropriate for this project is the star configured, half-bridge converter type topology and is further discussed in the next sub topic.

4.3 Structure of M2C

To achieve the advantages mentioned in the introduction section, the M2C is made up of submodules, which are made in modular form. The submodules are identical and this is a prerequisite for this kind of system to operate normally. The converter consists of six arms, two per phase (leg). An arm consists of submodules which are connected in series and one reactor. The submodules consist of two switches and a local DC-storage capacitor with two terminal connections. These parts can be seen in figure . This system avoids the central dc link capacitors which exist in the other types of converter.

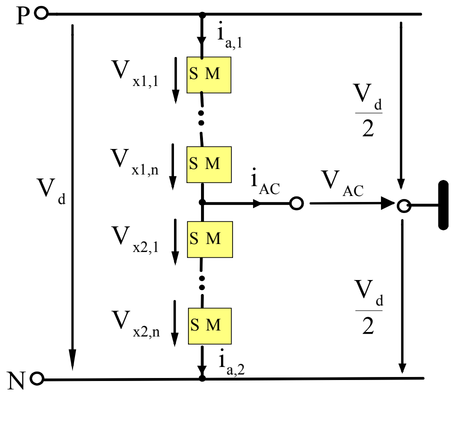

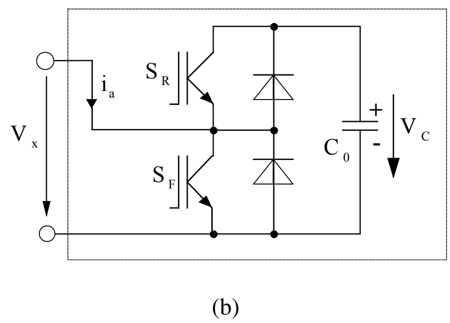

Figure 4.4: M2C (a) structure of M2C (b) structure of a submodule.

The sub module capacitance can be derived from,

$$W_c = \frac{1}{2}.C.U_{c,nom}^2 = \frac{1}{4\varepsilon}.\Delta W_{SM} \tag{4.1}$$

where $U_{c,nom}$ is the nominal voltage across the capacitor,ΔW_{SM} is the energy of the submodule for every half period, and ε is the permittivity.

the capacitor value is determined by,

$$C = \frac{\Delta W_{SM}}{2.\varepsilon.U_{c,nom}^2} \tag{4.2}$$

Depending on the direction of current through them, the capacitors either charge or discharge in their operation. This results in variation of voltages across the submodules. These creates high peak currents, which creates the need to use inductors to limit them. one inductor is included in each arm and is also used to reduce harmonics. The dimensioning of the inductors is made taking in to consideration, those differential currents which resulted due to the unbalanced voltage across the submodules.

$$U_{diff} = U_{dc} - (U_{ua} + U_{la}) = R_{arm}.i_{diff} + L_{arm}.\frac{d}{dt}i_{diff} \tag{4.3}$$

where U_{diff} is differential voltage, i_{diff} is differential current, U_{dc} is the dc voltage, U_{ua} and U_{la} are the voltage across the upper and lower arm.

As the resistive part is negligible, the difference voltage is expressed in terms of the inductor as,

$$U_{diff} = L_{arm} \cdot \frac{d}{dt} i_{diff} \tag{4.4}$$

To keep the differential currents as minimum as possible, and inductance of value 0.15 pu is usually used.

4.4 Principle of operation

The submodules can be considered as a controlled voltage source [21, p. 1]. Regardless of the sign of the current $i_{a,i}$, the terminal voltage $V_{x,i}$ of each submodule can be switched to either $0V$ or to the voltage V_C. By switching a number of submodules in the upper and lower arm, the voltage V_d is adjusted. In a similar manner, the voltage V_{AC} can be adjusted to a desired value.

The relationship of the voltages $Vd(t)$ and $Vac(t)$ with respect to the number of submodules per arm they have can be given by [21, p. 2]:

$$Vd(t) + 2Vac(t) \leq 2nV_c \tag{4.5}$$

Assuming the DC voltage used is constant, then:

$$Vd = nV_c \tag{4.6}$$

and the amplitude of the AC output voltage is:

$$Vac(t) \leq nV_c \tag{4.7}$$

The submodules are made in a way that, their voltage level is controlled independently. The out put from one module is equal to zero or equal to the voltage across the capacitor depending up on the switching state used. The switching states which are relevant for the operation of the submodule are :

- state 1 : Both IGBTs are switched off, during this state, the submodule is on blocked mode, this condition exists during shut down of the system and does not occur during normal operation.
- state 2 : IGBT1 is on and IGBT2 is off, the voltage across the capacitor appears at the submodule terminal and depending on current direction, the capacitor will be charged through the diode or discharge through IGBT1.

- state 3 : IGBT1 is off and IGBT2 is on, zero voltage appears across the terminals and the voltage across the capacitor remains the same.

This states can be observed in figure 4.5.

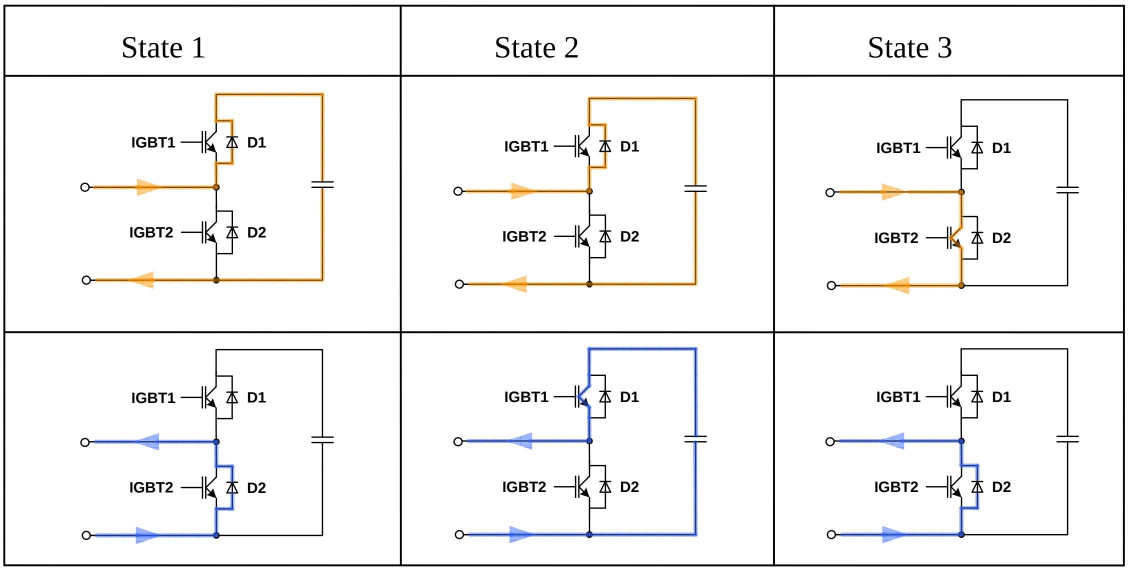

Figure 4.5: switching states of submodule.

For the converter, the total voltage of the two converter arms in one phase equals the DC voltage. A converter arm represents a controllable voltage source, and by adjusting the ratio of the converter arm voltages in one phase module, the desired sinusoidal voltage at the AC terminal can be achieved.

The inductor in the arms is used for damping balancing currents, which may arise due to differences on the dc voltage produced by the three phases which are connected in parallel at the dc buses [21, p. 6]. Moreover, it is used to reduce the effects of fault arising inside or external of the converter and reduce short circuit currents.

Chapter 5

Control

This chapter presents the control methods employed for the control of the LCC and VSC. The control methods that are employed for SK3 are explained and then the control of SK4 based on vector control of VSC is discussed.

5.1 Introduction

HVDC transmission systems transport very large amount of power. In transporting this power, a high coordination of control is required to accomplish this. The DC current and voltage must be precisely controlled to effect the desired power transfer. It is necessary therefore to continuously measure the system quantities. The parameters which are measured and monitored are on both the AC side and DC side and this include the AC currents and voltages, active power and reactive power transferred through the link, and the DC current and voltage. The main purpose of the controls are [18, p. 69]:

- Control power flow between the terminals,
- Protect the equipment against the current/voltage stresses caused by faults, and
- Stabilize the attached ac systems against any operational mode of the dc link.

The controls in general for both the LCC and VSC may be arranged in a hierarchical structure. As such they have a dispatch center, a master controller and local controllers.

The dispatch center is from where the order for level of power transfer is ordered and the master controller is where, the coordination for the terminals is made. The local controller is the controller located at one of the terminals. The coordination between these controllers has to result in a feature which [18, p. 71]:

- limits the maximum dc current, to protect the valves from damage
- maintain maximum dc voltage, to reduce losses
- minimize reactive power consumption for LCC, LCC require reactive power of about 50 percent of the total rating of the converter, hence to reduce cost
- enhance power system stability or control of frequency

For all the above cases the control system has to perform well under steady and dynamic operation of the system.

5.2 SK3 LCC Control

The basic power control is achieved through a system where one of the converters controls its DC voltage and the other converter controls the current through the DC circuit. The control system acts through firing angle adjustments of the thyristor valves [18, p. 71]. The control method that has been implemented in the SK3 system is the current margin method of control. The control is implemented using the ABB MACH2, which uses code generating tool called HiDraw [16, p. 3] . Figure 5.1 shows a typical MACH2 which is used for the control of LCC.

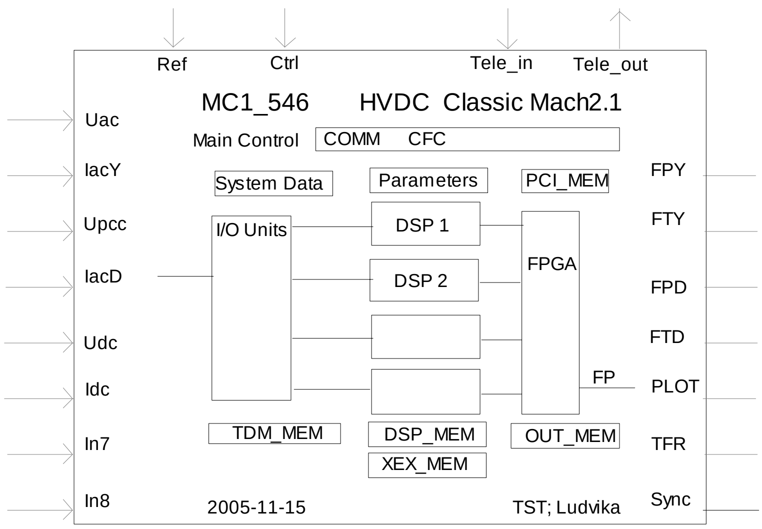

Figure 5.1: Mach2 LCC Control.

The control which are coded in the MACH2 include,

- Voltage dependent current order limit (VDCL)
- Current control amplifier (CCA)
- Rectifier alpha minimum limiter (RAML)
- Inverter gamma 0 function (Gamma0)

The current control margin method is used where there is a defined limit of operation of the dc system. Depending on the levels of the dc voltage and current, the controls which are applicable for a rectifier operation and inverter operation, with their limitations is discussed in the next subsections.

5.2.1 Hierarchy of controls

The control system in the LCC HVDC converter station generally has a hierarchical structure with three layers. These three layers, are referred as bipole control, pole control, and converter unit control. The measurements made for control and protection purposes consist of the 3-phase commutation ac voltages, the ac currents on the primary and secondary sides of the converter transformer, and the dc current and dc voltage [18, p. 100].

The bipole control coordinates the power orders of the poles and distributes the power order to the pole control. The arrangement of the controller can be observed in figure 5.2. The bipolar controller receives a power order Po from the station operator. This is subjected to a controlled rate of increase or decrease in order to protect the system from sudden changes in desired power. Maximum and minimum power limits to the the power controller are imposed. Then, the power order is divided by the DC voltage measured value to derive a current order which is sent to the two Pole Controllers. A bias circuit is required to counteract any problem due to a divide-by-zero function when the dc voltage may be zero or low value. The output of this controller is then limited by Voltage Dependent Current Limit (VDCL) for protection purposes.

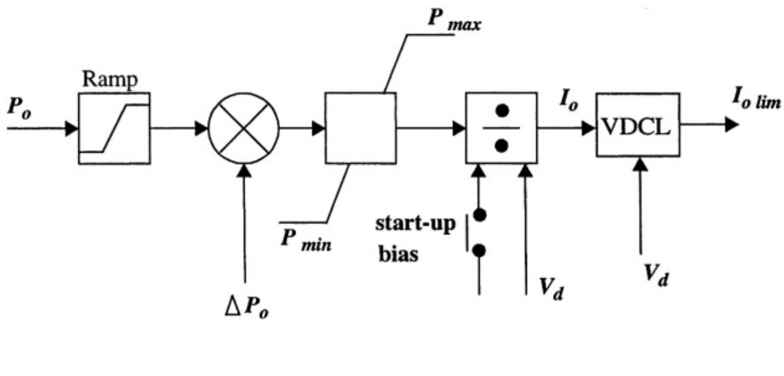

Figure 5.2: Characteristic of bipole control.

For the pole controller, the input is the current order from the Bipole Controller. This can be seen in figure 5.3. The current input is subjected to upper and lower limits for protection purposes. After limitation, the current order is compared to the measured value of dc current to generate an error signal. Another signal which modifies the current order is the current margin which is required only at the inverter end to bias off the current controller so that the gamma angle is within its rated value. The current controller uses the PI regulator to provide dynamic properties to the control loop, and provides the alpha order at its output.

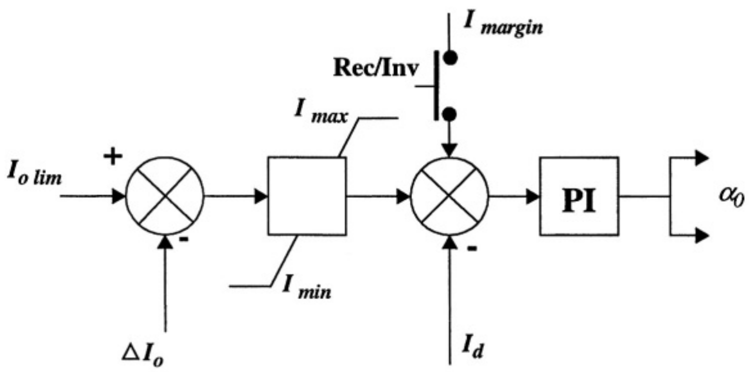

Figure 5.3: Characteristic of pole control.

The alpha order signal from the pole controls is used to generate the firing pulses for the converter in the valve group controller.

Additionally, there is a station controller which looks after the switching of harmonic filters and shunt capacitors depending on operating conditions.

5.2.2 Rectifier mode of operation

Alpha min characteristic at rectifier:

For a rectifier mode of operation, the alpha firing angle with respect to the dc voltage is given by the equation [18, p. 75],

$$V_d = V_{dor}.\cos\alpha - R_{cr}.I_d \tag{5.1}$$

Where R_{cr} is the equivalent commutation resistance, V_{dor} is the equivalent voltage at the rectifier for the equivalent rectifier model in alpha control.

From the equation the maximum limit of the voltage is set when the dc current is zero and alpha has a minimum value of zero. In practice, the minimum value of alpha is 2-5 degrees which ensures the converter valves have a minimum positive voltage for turning on. This characteristic can be seen in the hatched area in figure 5.4.

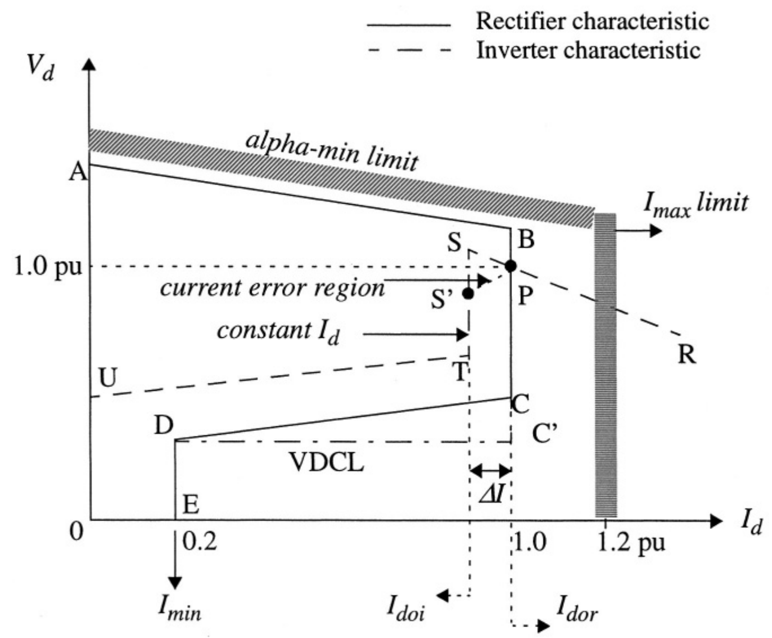

Figure 5.4: Operating characteristic of Id and Vd.

Figure 5.4, shows the operating DC current and voltage characteristics for an inverter and rectifier mode of operation. With respect to this, the regions where the controls are applicable are discussed comparing to the operating charactersic figure.

Constant dc current I_d characteristic:

Depending on the current carrying capacity of the valves, a maximum upper limit of the current is imposed. The I_d constant characteristic is a straight line BC, as shown in the figure 5.4. The zone of operation is also indicated.

Voltage Dependent Current Limit (VDCL) characteristic:

To sustain the dc power flow when the ac voltage at the rectifier bus is reduced due to a fault, a limitation is set by the VDCL. The limit is set depending on the ac system. This is implemented either by utilizing the horizontal portion, as defined by $C'D$, or a sloped portion (as defined by CD) as shown in figure 5.4.

I_{min} **characteristic** :

I_{min} limit is imposed because of two reasons. To maintain enough dc current in the valves and to avoid reaching discontinuous current operation which could lead to dangerous transient dc voltages. Typical minimum values are between 0.2-0.3 pu [18, p. 76].

5.2.3 Inverter Mode of operation

Gamma min characteristic:

To set the gamma minimum characterstic, the relationship between the dc voltage and gamma for an inverter operation can be expressed as [18, p. 77],

$$V_d = V_{doi}.\cos\gamma - R_{ci}.I_d \tag{5.2}$$

Where R_{ci} is the equivalent resistance of commutation, V_{doi} is the equivalent voltage at the inverter for the inverter model in gamma control.

In figure 5.4, The line SR defines this mode of operation and is referred to as the Constant Extinction Angle (CEA) control mode.

Constant current characteristic:

In figure 5.4, the line ST defines the Constant Current characteristic of operation at the inverter. From the figure, it can be seen that, the constant current characterstic for the inverter operation and rectifier operation are not the same. In order to maintain a unique operating point of the dc link, a current margin exists. The current demanded by the inverter is usually less than the current demanded by the rectifier. The difference is the current margin which is typically about 0.1 pu; its magnitude is selected to be large enough so that the rectifier and inverter constant current modes do not interact due to any current harmonics which may be superimposed on the dc current. This is why the control strategy is termed the current margin method [18, p. 77][32, p. 21].

Alpha-min in inverter mode:

The line TU as shown in figure 5.4, defines the alpha minimum in inverter mode characteristic. This value is typically about 100-110 degrees, and is required to limit any inverter from changing into the rectifier mode of operation. Furthermore, the value of 100-110 degrees ensures a minimum dc voltage at the inverter during a fast start-up of the dc link with I_d = 0.

5.2.4 Summary

The control system employed for an LCC in general can be summarized as shown in figure 5.5.

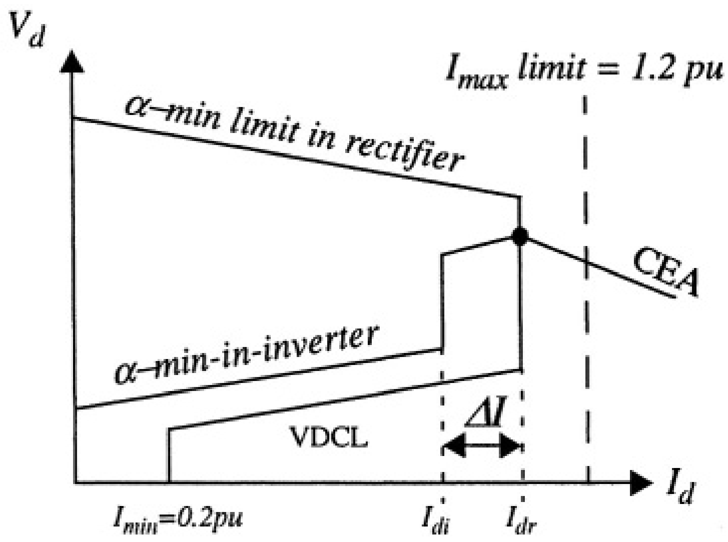

Figure 5.5: Summarized characteristic of Id and Vd.

The main controls which have been implemented for the SK3 LCC as a rectifier and inverter mode of operation are summarised blow. At the rectifier, Voltage Dependent Current Limit, VDCL is made to limit the dc current as a function of either the dc voltage or the ac voltage. The existence of the VDCL, assists the dc link to recover from faults. Id min limit, typically 0.2-0.3 pu is made to ensure that there is a minimum dc current flowing through the valves. This is to avoid the possibility of dc current extinction, caused by the valve current dropping below the hold-on current of the thyristors. If the current goes below the hold on current, the current chopping would cause high overvoltages to appear on the valves.

At the inverter, alpha min limit is used to ensure that power reversal does not occur. The inverter is not permitted to operate in the rectifier region, that is a power reversal may occur due to current margin sign change. To ensure this, an alpha-minimum-limit in inverter mode of about 100-110 degrees is imposed.

The control strategy that is selected is made depending on the criteria that enables a fast and stable operation of the dc link while minimizing the generation of harmonics, reactive power consumption and power transmission losses [18, p. 73][32, p. 22].

5.3 SK4 VSC Control

5.3.1 Introduction

The VSC control mechanism is based on PWM . This gives the VSC an ability to control the active and reactive powers independently. To achieve this ability in the VSC control, the three phase voltages and currents in the ac grid are decoupled to their equivalent dq components and the amplitude and phase of the signal is generated is varied by the PWM. The VSC converters controlling mechanism in general is divided in to two. An inner loop controlling the ac current and an outer loop which consists of an ac voltage controller, dc voltage controller, active power controller, reactive power controller and frequency controller [8, p. 34][24, p. 2]. A general diagram of the controller arrangements is given in Fig.5.6.

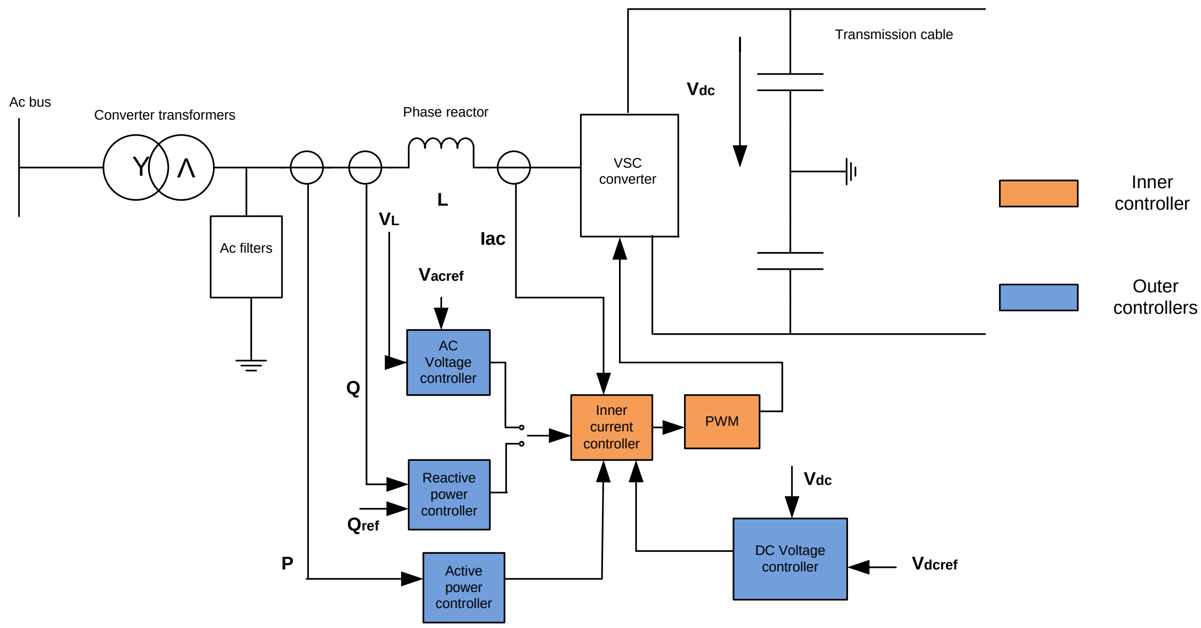

Figure 5.6: VSC general control diagram.

5.3.2 Control method development

The vector control method is widely used for VSC control [24, p. 3]. This method takes the abc to dq rotating reference frame to control the ac current. The phase angle required to transform the abc to the dq is determined by a PLL (phase locked loop).

The inner current loop calculates the voltage drop across the reactor, that is used to establish the exchange of active and reactive power with the ac grid. The outer loop controllers, consisting of dc voltage controller, active power controller and frequency controller are used to generate the i_{qref} reference values and reactive power controller or ac voltage controller can be used to generate the reference values for i_{dref} [24, p. 3][30, p. 4]. A general layout of the control system on the ac side is shown in fig.5.7.

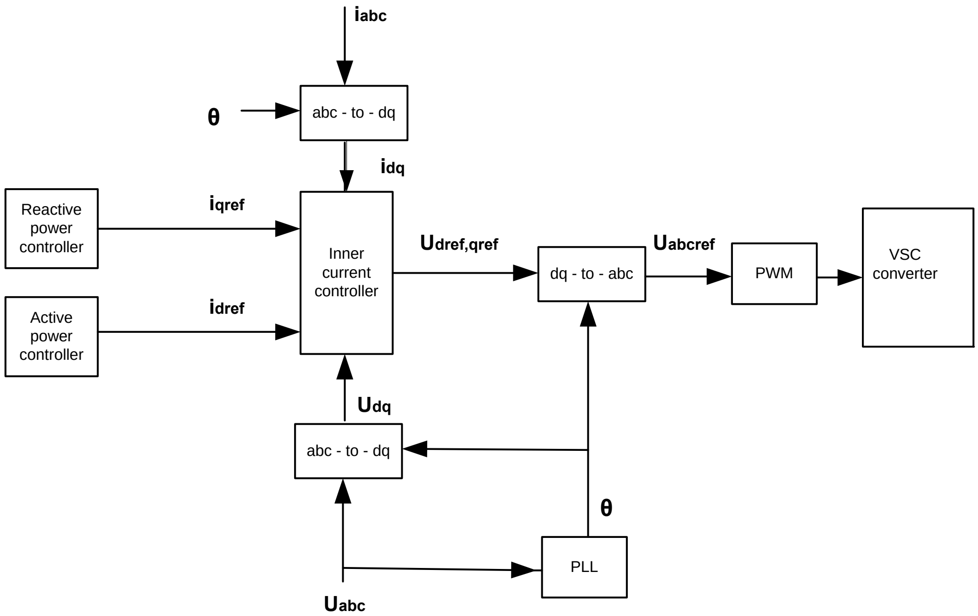

Figure 5.7: VSC ac side control diagram.

To develop the controllers, a model of the VSC on the ac side is developed. The single line diagram of the model is shown in Fig.5.8.

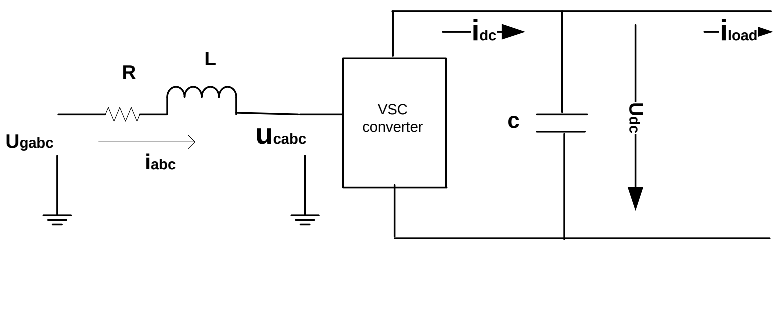

Figure 5.8: Single line diagram of the VSC.

From the model, the three phase voltages can be written as [24, p. 3]:

$$U_{ga} = U_{ca} + i_a R + L\frac{di_a}{dt} \tag{5.3}$$
$$U_{gb} = U_{cb} + i_b R + L\frac{di_b}{dt} \tag{5.4}$$
$$U_{gC} = U_{cc} + i_c R + L\frac{di_c}{dt} \tag{5.5}$$

where : i_a,i_b, i_c are the line currents and R, L are the resistance and inductance of the reactor respectively.

Applying Park transformation on the equations 5.3, 5.4,5.5 and where $\theta = \omega t$, the resulting equations are:

$$U_{g0} = U_{c0} + i_0 R + L\frac{di_0}{dt} \tag{5.6}$$
$$U_{gd} = U_{cd} + i_d R + L\frac{di_d}{dt} + \omega L i_q \tag{5.7}$$
$$U_{gq} = U_{cq} + i_q R + L\frac{di_q}{dt} - \omega L i_d \tag{5.8}$$

Where : U_{g0}, U_{gd}, U_{gq} are the zero, d axis and q axis components of the grid voltage, U_{c0}, U_{cd}, U_{cq} are the zero, d axis and q axis components of the converter voltage, i_0, i_d, i_q are the zero, d axis and q axis components of the ac current.

Assuming the converter to be lossless, the power on both the ac and dc sides is assumed to be equal $(P_{ac} = P_{dc})$. Taking this in to account, and neglecting the zero sequence order, the power at the converter on the ac side can be determined by:

$$P_{ac} = U_{cq} i_q + U_{cd} i_d \tag{5.9}$$

and the current on the dc side can be calculated by:

$$i_{dc} = \frac{U_{cq} i_q + U_{cd} i_d}{U_{dc}} \tag{5.10}$$

where : i_{dc} is the current on the dc side and U_{dc} is the dc voltage. And the current across the load may be determined by:

$$i_{load} = \frac{U_{cq} i_q + U_{cd} i_d}{U_{dc}} - C\frac{dU_{dc}}{dt} \tag{5.11}$$

Considering i_q, i_d and Udc as state variables, the state equations are:

$$\frac{di_q}{dt} = \frac{1}{L}U_{gq} - \frac{R}{L}i_q - \omega i_q - \frac{1}{L}U_{cq} \tag{5.12}$$
$$\frac{di_d}{dt} = \frac{1}{L}U_{gd} - \frac{R}{L}i_d - \omega i_d - \frac{1}{L}U_{cd} \tag{5.13}$$
$$\frac{dU_{dc}}{dt} = \frac{U_q i_q + U_d i_d}{CU_{dc}} - \frac{U_{dc}}{CR_{dc}} - Ci_{load} \tag{5.14}$$

Taking the above discussion in to account, next sections deals on the design of the inner controller and the outer controllers.

Inner Current controller

By decoupling equations 5.12, 5.13 and introducing control input variables, X_d and X_q:

$$X_d = U_{gd} - \omega L i_q - U_{cd} \tag{5.15}$$
$$X_q = U_{gq} - \omega L i_d - U_{cq} \tag{5.16}$$

and :

$$X_d = (sL + R)i_d \tag{5.17}$$
$$X_q = (sL + R)i_q \tag{5.18}$$

Where : s is the laplace operator and using equations 5.15 and 5.17, the inner current controller can be developed.

Dc voltage controller

The DC voltage controller for a single VSC is implemented as a PI controller.

$$i_{qref} = K_{pdc}(U_{dcref} - U_{dc}) + \frac{P}{U_{gq}} \tag{5.19}$$

where: i_{qref} is the q component of the ac reference current, K_{pdc} is the proportional dc gain, and U_{dcref} is the dc reference voltage.

Active power controller

In most applications, the active power controller is implemented as an open loop controller. The equation used is given by:

$$i_{qref} = \frac{P_{acref}}{U_{gq}} \tag{5.20}$$

For more accuracy, the controller can be modified to closed loop system.

Reactive power controller

The reactive power controller is controlled in the same manner as the active power, as such it uses an open loop control. The equation implemented in the controller is:

$$i_{dref} = \frac{Q_{acref}}{U_{gd}} \tag{5.21}$$

where : i_{dref} is the d component of the ac reference current, and Q_{acref} is the reactive power reference.

Ac voltage controller

From figure 5.8, it can be seen that, the voltage drop across the reactor is given by [8]:

$$\Delta U = U_g - U_c \tag{5.22}$$

$$\Delta U = \Delta U_p + j\Delta U_q \tag{5.23}$$

$$\Delta U = \frac{RP + X_l Q}{U_c} + j\frac{X_l P + RQ}{U_c} \tag{5.24}$$

Where : ΔU_p and ΔU_q are drops due to the active and reactive parts respectively.

If the reactive part drop is less than the real:

$$\Delta U_q \ll \Delta U_p \tag{5.25}$$

Then the voltage drop across the reactor can be approximated by:

$$\Delta U = \frac{RP + X_l Q}{U_g} \tag{5.26}$$

In ac networks, the inductive reactance is much higher than the resistive part, hence the voltage drop across the reactor will depend mainly on the reactive power flow. Therefore the grid voltage level will vary depending on the reactive power flow.

Frequency controller

Frequency deviations in the AC system indicate an imbalance in the active power flow. The VSC has the capacity to adjust the frequency by controlling the active power transfer in the system. The imbalance can be approximated by :

$$\frac{\Delta P}{\Delta f} = K \tag{5.27}$$

Where : ΔP is the power unbalance, Δf is the frequency variation and K is a constant.

PLL

The phase locked loop is used to generate a synchronizing θ depending on the measured ac source voltage. The θ is used for the transformation of the abc quantities to dq quantities and vice versa. When θ is phase locked with the ac voltage source, then the dq reference is synchronized with the three phase abc reference frame.

5.3.3 conclusion

The controller methods implemented for the VSC link is: for the converter found in Kristian sand, active and reactive power control has been used and for Tjele active power and dc voltage control method was used. An example of the active and reactive power control (PQ control) structure implemented is shown in fig.5.9.

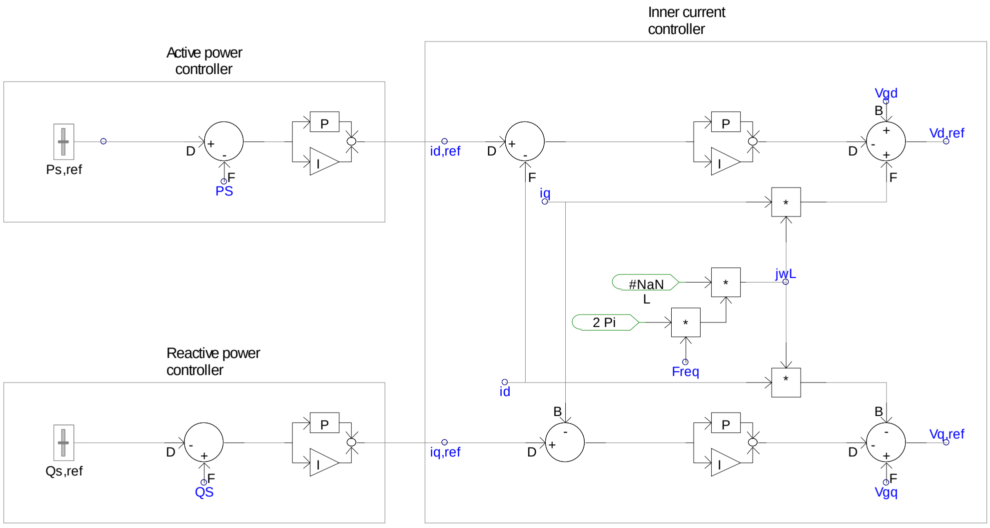

Figure 5.9: Active and reactive power controller.

Figure.5.9 illustrates the active power part control and the reactive power part control. The output id,ref and iq,ref is further used by the inner current controller to produce the Vd, ref and Vq, ref. These are converted to abc reference frame and then used by the PWM to generate the firing pulses required for the VSC.

Chapter 6

Description of SK3 and SK4 model

In this chapter, the models used in the simulation of the bipole HVDC link SK3 and SK4 are described. For SK3, the electrical LCC station components used are described and the control part is further explained in the control chapter. For the SK4, the electrical models and the control models used is described.

6.1 SK3 model Introduction

The SK3 model is an LCC based link. The link has been modeled by including all the components that have been implemented in the real station and are identical to the system used in the real station.

The model's main electrical circuit representation of the HVDC link includes the following:

- AC network
- AC filters and DC filters
- Converter transformers
- LCC converter
- DC smoothing reactors
- DC line

These components of the station and the DC line are discussed in the following sections.

6.1.1 The AC network

At Tjele, the AC network is at 400kV, having a minimum short circuit capacity of 1700MVA. At Kristiansand, the AC network is 300KV, with a minimum short capacity of 2500MVA. The AC network for both of them is modeled with a three phase voltage source terminated with an equivalent R-R/L impedance as shown in figure 6.1.

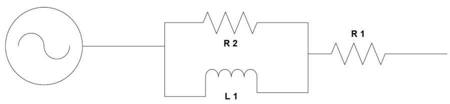

Figure 6.1: AC network model

The values used for the equivalent R-R//L impedance for Tjele and Kristiansand AC networks are given in tables 6.1, and 6.2.

Component	value
R1	1.265 [ohm]
R2	10000000 [ohm]
L1	0.029 [H]

Table 6.1: Tjele R1, R2 and L1 values.

Component	value
R1	5.94 [ohm]
R2	10000000 [ohm]
L1	0.191 [H]

Table 6.2: Kristiansand R1, R2 and L1 values.

6.1.2 Filters

The LCC converter that is used produces harmonics. The converter used at both ends is a twelve pulse converter which generates harmonics on the AC and DC side. The harmonics on the AC side are of the order, $12n+/-1$ and on the DC side are of the order, 12n, where n is 1,2,3 .... Depending on the requirements of the system operators, these harmonics have to be reduced to an acceptable level. These level in denmark is a THD level of 3 percent. The filters are implemented on the AC side of the converter and on the DC side. These filters also are used to contribute to the supply of reactive power needed by the converter.

AC filters

At Tjele, there are two 11th and 13th harmonic filters each 20 MVAr. Furthermore one shunt capacitor bank of 80 MVAr is used. For Pole SK3, four 11th, 24th harmonic filters are used. At Kristiansand, two 11th and 13th. harmonic filters each with 83 MVAr, and two HP (high pass) filters, of 90 MVAr are used. The filters arrangement used for SK3 can be seen in figures 6.2 for (a) is an 11th/13th filter with 83 MVAr and (b) HP24 filter of 90 MVArs located at kristiansand and (c) HP 12/24 filter located at Tjele.

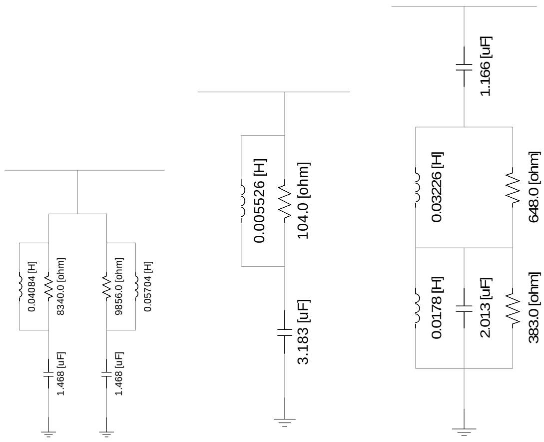

(a) (b) (c)

Figure 6.2: (a) 11th and 13th harmonic filter (b) 24th harmonic filter (c) 12/24 Hp filters.

These filters are brought online depending on the steady and and dynamic conditions of the system for a stable operation.

DC filters

At Tjele, there is a filter between the neutral bus and ground, made up by four 1 F capacitors. There is also an active filter. The principles of the active filter is that harmonics in the DC-lines of 3 is measured. A controller reproduces an equal current in counter phase. This signal is then amplified in a high power amplifier and fed into the neutral bus end of the passive DC-filter by a transformer, thereby removing the disturbances. The active dc filter arrangement is shown in figure 6.3.

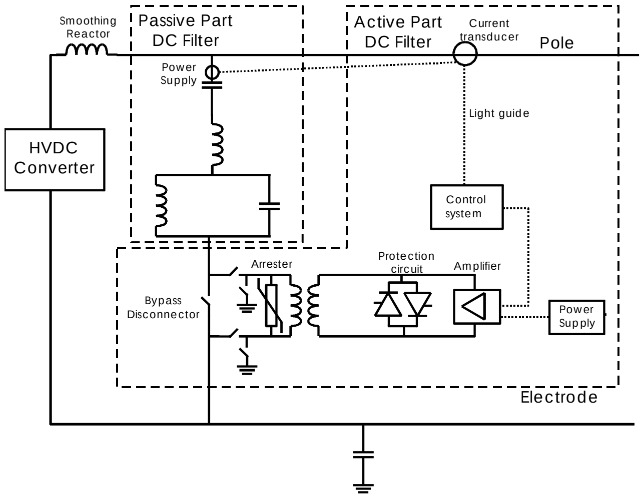

Figure 6.3: Arrangement of active Dc filter for SK3

At Kristiansand, the DC-filters of conventional passive filters are also used. The filters used at Kristiansand and Tjele for SK3 is shown in figures 6.4.

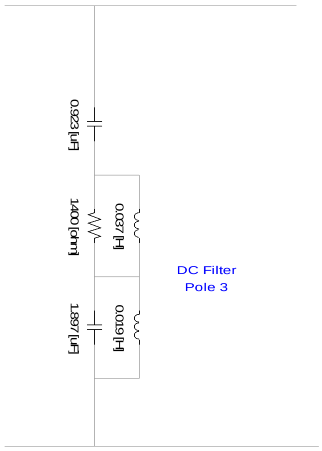

Figure 6.4: Dc filter for SK3

Smoothing reactors: for Pole SK1 and pole SK2, the smoothing reactors which are equal in both terminals are placed on the neutral side and is designed for 0.5 H at 1000 A. For Pole SK3, the reactors are placed on the high voltage side and are designed for 225 mH at 1260 A.

6.1.3 LCC Converter

A 12-pulse converter unit, is used at both ends of the link. The model implemented for the converter can be seen in figure 6.5.

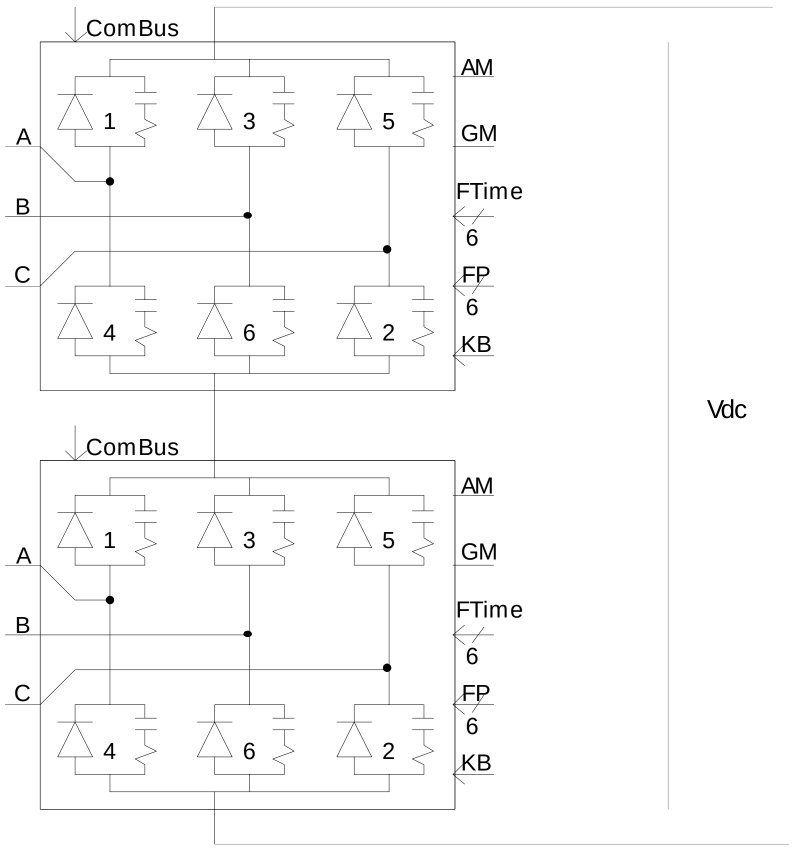

Figure 6.5: LCC converter

The converter is made up of two 6-pulse Graetz converter connected in series. The converter has in built phase locked loop (PLL) and the combus input node is used as an input for the PLL. AO is alpha order (firing angle) input for the converter, KB is block/deblock input control signal, AM is Measured alpha (firing angle) output and GM is Measured gamma (extinction angle) output. All these signals are transferred between the converter and the control circuit.

6.1.4 Converter transformers

At all terminals two 3-phase converter transformers are used per pole. At Tjele, the converter transformers rating are given as in table 6.3. For the converter transformers at Kristiansand, the rating are given in table 6.4.

Pole	Primary[kV]	Secondary[kV]	S[MVA]
SK1	150	109	154
SK2	150	109	154
SK3	400	143	256

Table 6.3: Converter transformer ratings at Tjele.

Pole	Primary[kV]	Secondary[kV]	S[MVA]
SK1	275	109	154
SK2	275	109	154
SK3	300	143	256

Table 6.4: Converter transformer ratings at Kristiansand.

The modeling of the transformers have been done taking in to consideration their connection type, transformer tapping, and transformer reactance. All the poles have two transformers with YNy0- and YNd11-couplings. The transformer reactance was 0.22 pu. This is considered as typical for transformers used in HVDC links.

6.1.5 DC line

The route length of the link between Tjele and Kristiansand is 240 km. There is one cable per pole, each with a single Copper conductor. The route consists of submarine underground cables and overhead lines at both ends of the link. Therefore the model includes cable and overhead lines to get an accurate response as possible. The cable is modeled as a Bergeron model which can be seen in figure 6.6 for one of the distributed parameters with the DC cable values from the manufacturer, values obtained from Energinet.dk. The overhead lines moreover are modeled as Pi type on the Kristiansand and Tjele side. The models can be seen in figure 6.6 for a) overhead line model on kristiansand side, b) cable model c) overhead line model on Tjele side.

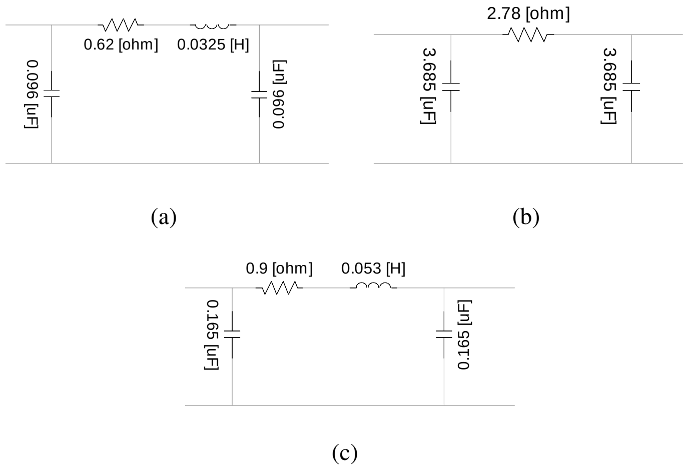

Figure 6.6: (a) Model for overhead line (b) cable model (c) model overhead line.

The electrode stations, which are used to ground the links, are located on the shore at Tjele and Kristiansand.

6.1.6 Modeling of HVDC Control

The controls implemented in the model for the converter firing include:

- Voltage dependent current order limit (VDCOL)
- Current control amplifier (CCA)
- Rectifier alpha minimum limiter (RAML)
- Inverter gamma 0 function (Gamma0)

These controls, how they are implemented and their use is discussed in the control chapter. The next section describes the SK4 model used in the simulations.

6.2 SK4 model Introduction

The SK4 model consists of an electrical part and a control part. In the electrical part of the SK4 model, AC network at Tjele and Kristiansand, the converter transformers, AC and DC filters, the VSC converter, and DC line were modeled respectively. The following section discusses the implemented models for each part.

6.2.1 AC grid

The AC network used for SK4 is the same as for SK3. The AC network is modeled as a source voltage of 400KV at Tjele with a short circuit rating of 1700MVA. At Kristiansand, 300KV, and short capacity of 2500MVA. The source voltage is terminated by an R-R/L impedance which is also equal to the ones used at Tjele and Kristiansand. This values are give in tables 6.1, and 6.2. These values are obtained from the transmission operator, Energinet.dk.

6.2.2 Converter transformer

The converter transformers used are of the rating 400/150 KV, 500MVA at Tjele and 300/150 KV, 500MVA at Kristiansand. The transformer models used are an ideal ones and have a leakage reactance of 0.22pu [22, p. 4]. The transformer is in a Y/Y arrangement.

6.2.3 Filter

The filters used on the AC side are of second order passive filters. The filter's are tuned at the switching frequency and multiple of the switching frequency to remove higher harmonics. There are three filters tuned at the switching frequency of 8Mvars and three tuned at the multiple frequency of 4Mvars both at Tjele and Kristiansand. A model of the filter used to remove higher harmonics is shown in figure 6.7.

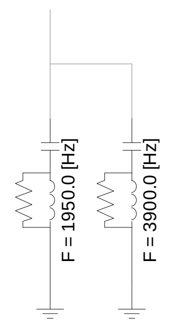

Figure 6.7: Second order ac filter.

6.2.4 Reactor size

The reactor size between the converter transformer and the converter is assumed to be $0.15pu$ impedance of the system. To determine the size of the reactor, the short circuit power rating of the grids is taken in to account. Typical values used from other systems has been adopted, which is equal to 0.019H.

6.2.5 Dc line

The dc cable that has been used is assumed to be similar to that of the one used by SK3 dc link. The dc line is modeled taking in to consideration the cable and the overhead lines. This has been modeled as distributed Pi model with the values used for the model given in figure 6.6.

6.2.6 VSC converter

The VSC model used is a three level multilevel converter type. The converter is made of twelve IGBT's. This type is chosen for simplicity's sake and has been applied in many projects at different power levels. A figure of the model used is shown in fig.6.8.

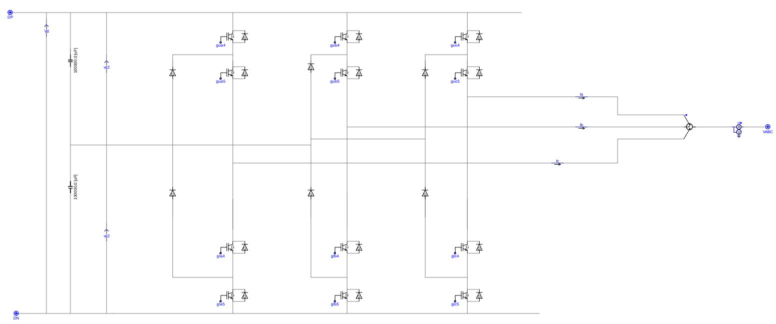

Figure 6.8: three level multilevel converter.

The VSC has also been implemented using a two level converter and the same control method is applicable.

6.2.7 Control Models

The control method implemented in the system is a vector control as discussed in the control chapter. The possible control methods that can be used for the converter are the outer controllers: active power,reactive power, dc voltage, ac voltage and frequency control and the inner current control. The control method used determines the mode of operation of the converter and the models implemented in PSCAD are discussed in the following section.

Conversion of abc to DQ frame and vice versa

In the vector control method, the control is implemented in the DQ reference frame, hence the measured voltage and current parameters at the ac side are required to be converted to DQ reference frame for control purposes and in the end converted to abc reference frame to be the input to the PWM. The model used is the abc-to-DQ and vice versa conversion model in the PSCAD library.

PLL

The PLL is required to determine the θ of ac measured parameters which is used in the conversion of abc-to-dq and vice versa. This block is also available in the PSCAD library and has been used in the model.

PWM

The PWM used to generate the firing pulses for the converter is the carrier based PWM type. The principle of operation of this type has been discussed in section 3.2 PWM Techniques for MMC. The SHPWM has been implemented for the modulation technique. The switching frequency is at 1.5KHz resulting in a frequency in a frequency ratio of 30. The amplitude modulation index is at 0.8.

Outer loop controllers

The outer loop controllers which provide the id,ref and iq,ref can be arranged in different configurations. For example the active power controller can be made to provide the id,ref and the dc voltage controller to provide for the iq,ref. Similar arrangements can be implemented using the other outer controllers so that the desirable mode of operation is achieved. The following section shows the models implemented for each controller.

Active power controller

The active power controller is implemented as a feed forward as shown in fig. 6.9. The measured active power and the target value are compared and the PI controller is used to generate the current reference values required for the inner current controller.

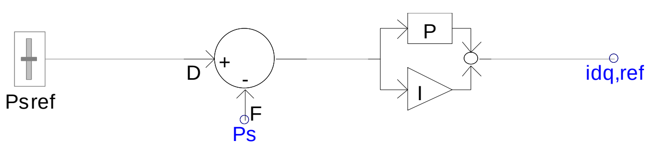

Figure 6.9: Active power controller.

Reactive power controller

The reactive power controller in a similar manner is modeled as a feed forward and can be seen in fig. 6.10.

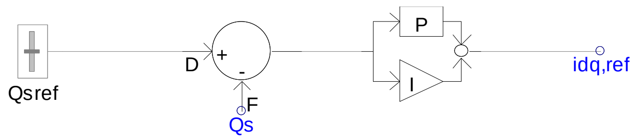

Figure 6.10: Reactive power controller.

DC voltage controller

The purpose of the Dc voltage controller is to keep the DC voltage in the system at a constant value. The target dc voltage level in this case is at 500 KV. The controller implemented is shown in fig.6.11.

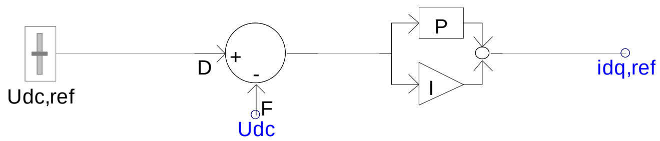

Figure 6.11: Dc voltage controller.

Inner current controller

The inner current controller determines the voltage dq inputs that are converted to abc to be an input to the PWM. The control arrangement is shown in figure6.12.

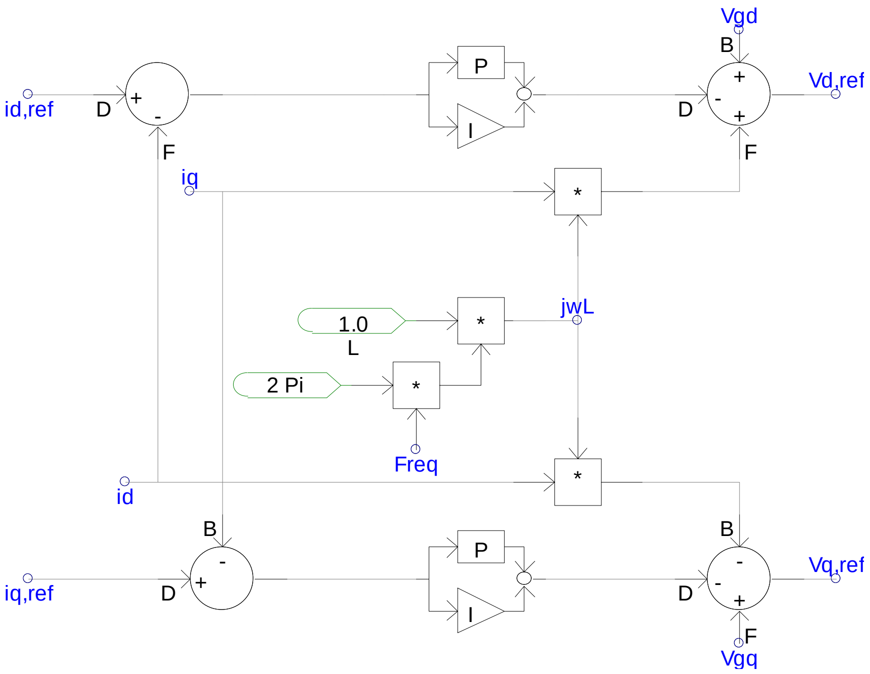

Figure 6.12: Inner current controller.

The id,ref and iq,ref are provided by the outer loop controllers and id and iq are dq equivalent of the ac currents measured.

The next chapter presents, commutation failure in SK3 for model verification.

Chapter 7

Commutation Failure in SK3 for model verification

Commutation failure for a converter can occur due to faults on the DC and AC side as discussed in section 3.3. In this chapter simulations of commutation failure of the SK3 model due to drop in the voltage has been made to validate the model with measurement values.

7.1 Introduction

When using LCC , a problem that may occur is commutation failure. All thyristor valves, to block their forward bias require removal of the internal charges accumulated during their conducting mode period. For example for an inverter, the period is defined by $\alpha + \mu$. Hence the valves require a minimum extinction angle for the forward blocking to be successful. If forward blocking fails, then the valve will conduct without firing gate pulse and commutation failure occurs. This results in the commutation process failure. The current will not be able to transfer to the other thyristor valves and the line current return to the thyristor which was conducting previously and had failed to block its forward bais [22, p. 1][29, p. 2].

Commutation failure for a converter operating as an inverter can occur due to faults on the DC and AC side.

Causes from the AC side may be due to:

- due to the decrease in magnitude of one or more of the phases or distortions, causes the extinction angle to be inadequate for commutation [22, p. 2]

- a phase shift in the commutating voltage
- the value of the extinction angle prior to the commutation also determines the possibility of commutation failure. The higher the extinction angle is, the less is the possibility of commutation failure. Typical steady state operating value of extinction angle is 18 degrees, and increasing this angle reduces the possibility of commutation failure [32, p. 18].

Causes from the DC side which result in commutation failure are related with the rapid increase of the DC current. When the DC current increases in magnitude, it results in the increase of the overlapping angle. Increasing the overlapping angle, reduces the extinction angle and the decrease in the extinction angle may reach a point, where the valves can no longer sustain their forward blocking [32, p. 18].

7.2 Measurement preconditions

The commutation failure measurements were made for a reduction in the voltage level at Tjele for SK3 pole, which was the cause for the commutation failure. This drop in the voltage has been emulated in the PSCAD model by adding line inductances between the Tjele 400kV bus and the converter transformers as shown in figure 7.1. A 1H inductor was used which resulted in the same average reduction of voltage as that of SK3 Tjele, 29 percent of the rated voltage during the real measurements.

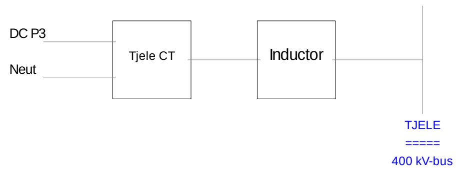

Figure 7.1: Inductor insertion to simulate voltage drop

The voltage drops from the measurement are not balanced type, in that the voltage drop on the three phase lines is not the same. The 29 percent is the average value which has been used.

7.3 Results from real Measurement

To verify the model used, real measurement data's of a commutation failure at Tjele SK3 has been provided by the network owner, energinet.dk. The measurement data's were provided in comtrade format which is a standardized file format used in power system monitoring. The comtrade format consists of a configuration file and a data file. The data has been simulated with Wavewin Bitronics ProE6 [34], which is a commercial software that can diplay the wave form of the files in comtrade format. Moreover, PSCAD has also been used to display the comtrade file waveforms for a better comparison with the model which has been built in PSCAD. However, the PSCAD generated waveforms for the measured values, the scaling has been done manually as PSCAD doesn't have an option to consider the configuration file. The results obtained using PSCAD and then with Wavewin Bitronics ProE6 are presented. For all the displayed wave forms, the time scale used is in seconds.

AC side voltage and DC voltage and current:

The AC side voltage is observed to be at maximum peak of 330kV. During the commutation failure, the voltage drops down by 29 percent. This can be seen in figure 7.2.

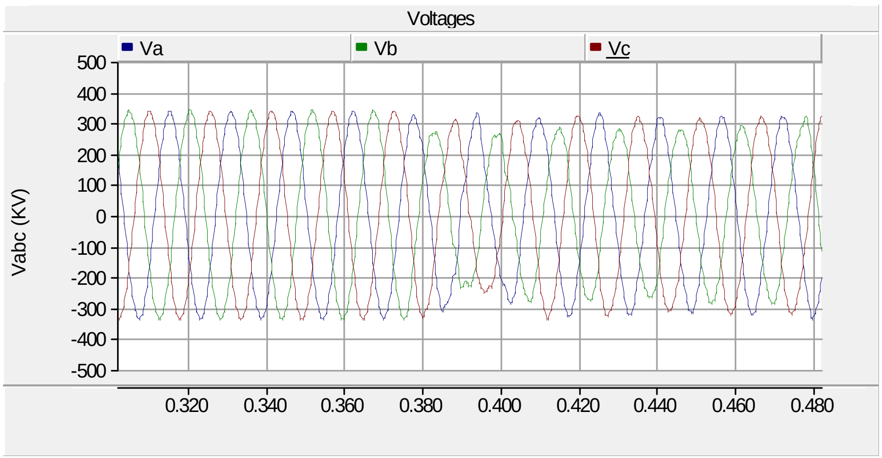

Figure 7.2: Ac side voltages

The DC side voltage during the commutation failure decreased from 345kV to 0kV, and the current also from 1420A goes to 0A. This can be seen in figure 7.3.

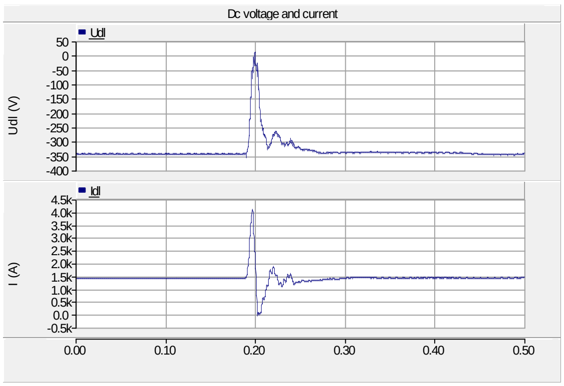

Figure 7.3: DC side voltage and current

Thyristor firing angle and current order:

The thyristor firing angles before and during the fault were observed to vary. The maximum value of the angle γ reaches 80 degree during the commutation failure and during normal operation the value is 18 degrees. The current order which was at 1430A, during commutation failure goes down to 452A. This may be observed in figure 7.4

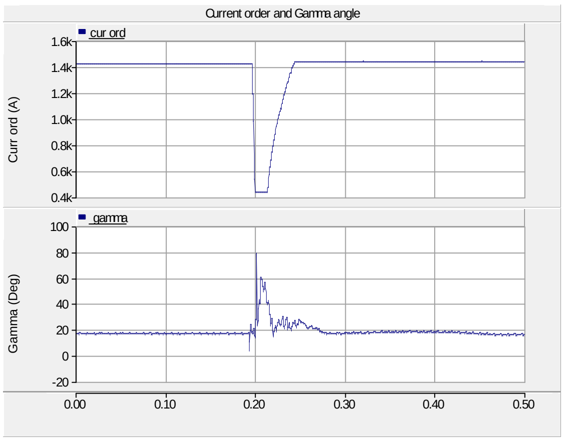

Figure 7.4: Current order and Firing angle gamma

For an inverter operation, the extinction angle is usually the control parameter used as is in this case, and a value of 18 degrees for extinction γ is a commonly used value during normal operation.

Waveforms obtained by the Wavewin Bitronics

The waveforms obtained for the measurement datas by the Wavewin Bitronics can be seen in figure 7.5. The results are presented in a way that all the measured waveforms are displayed in one window and then a summary of the waveform parameters, such as the rms value, instantaneous peak, maximum and minimum peak values and so on are given in another window. The measurements are made for the line voltages, the currents across the Y/D and Y/Y configured converter transformers for the three lines, the DC line voltages and currents, firing angles alpha-gamma, and the current ordered by the control system. This are shown in figure 7.6.

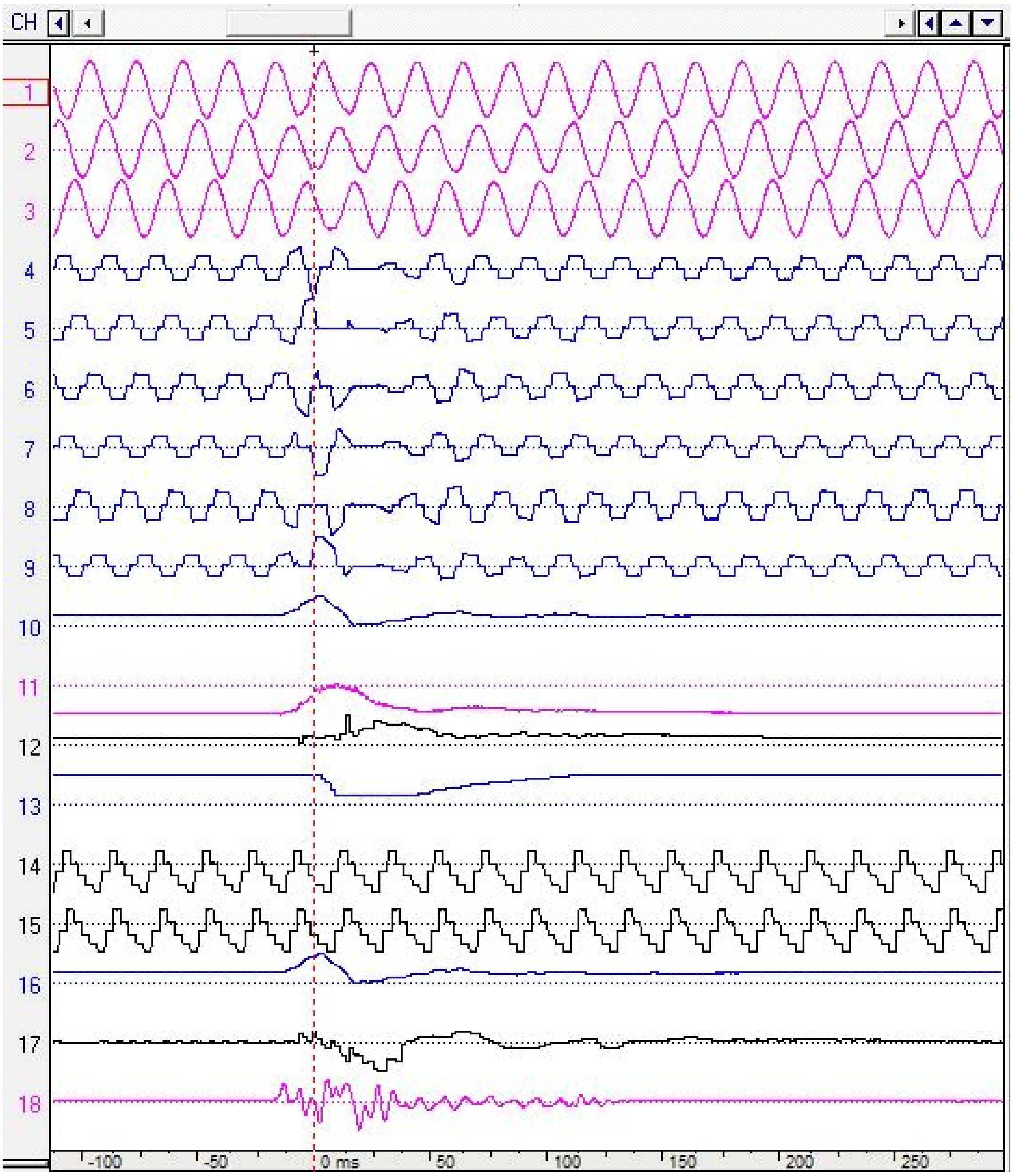

Figure 7.5: Waveforms obtained from Wavewin Bitronics

CH	Title	RMS	InstPeak	Phase	InstVal	RefVal	MaxPeak	MinPeak	
1	UAC_L1	238.501	-337.258	293.549°	135.562	90.254	338.250	-337.912	K
2	UAC_L2	236.526	338.262	173.369°	-337.245	-226.502	338.917	-338.917	K
3	UAC_L3	237.075	338.901	53.753°	200.991	161.038	340.261	-339.944	K
4	IVY_L1	1133.689	1445.295	140.789°	-1414.085	-3610.304	2653.268	-3630.203	A
5	IVY_L2	1124.487	1473.359	20.874°	1396.588	3474.048	3585.664	-2004.044	A
6	IVY_L3	1126.187	34.679	261.527°	34.679	163.790	2021.318	-3313.496	A
7	IVD_L1	1137.219	1455.811	110.982°	-20.967	-2786.251	2422.893	-4061.355	A
8	IVD_L2	1125.907	-1438.542	350.574°	1410.415	34.718	1951.596	-2870.013	A
9	IVD_L3	1126.490	-1456.034	231.387°	-1382.739	2754.605	4168.957	-1871.440	A
10	IDL	1419.623	1431.965	121.824°	1411.635	3574.899	4130.892	-46.089	A
11	UDL	343.061	-345.090	357.391°	-341.684	-146.883	19.159	-353.781	K
12	ALPHA_GAMMA	17.135	17.980	166.480°	17.007	17.980	79.427	3.809	D
13	CUR_ORD	1422.741	1424.285	332.092°	1422.569	1422.569	1443.092	433.806	A
14	CPR_Y	3.475	-0.013	93.843°	-2.574	-4.139	2.624	-6.158	
15	CPR_D	3.422	2.713	63.972°	0.083	-2.569	2.719	-6.113	
16	IDNE	1401.763	1412.269	175.698°	1395.197	3555.637	4172.393	-131.270	A
17	DFREQ	0.021	-0.045	N/A	-0.039	0.633	0.726	-2.003	H
18	UDN	0.413	0.659	17.077°	0.550	1.041	20.361	-25.700	K

Figure 7.6: Values for waveforms obtained from Wavewin Bitronics

For the above measured values, their corresponding simulation results for the PSCAD model of SK3 is presented in the next section.

7.4 Results from PSCAD simulation

To validate the model of SK3, for the normal operation of the link during power transfer from Norway to Denmark, the simulation was made with the parameters specified in table 7.1. For commutation failure to occur, an inductor of value 1H was inserted in the lines to reduce the voltage by an average 29 percent for 340kV line to ground voltage.

Power direction	P/I ref [max = 2]	Time to deblock [sec]	U_{dcref} [KV]
Kristiansand to Tjele	1	1	360

Table 7.1: Sk1 simulation parameter settings.

The results obtained are presented for the inverter side (Tjele).

AC side voltages and DC voltage and current:

AC side voltages during normal operation are, 350KV. At time t = 1.95 sec, the voltages drops down by 29 percent and then recovers at t = 2.05. This may be observed in figure 7.10.

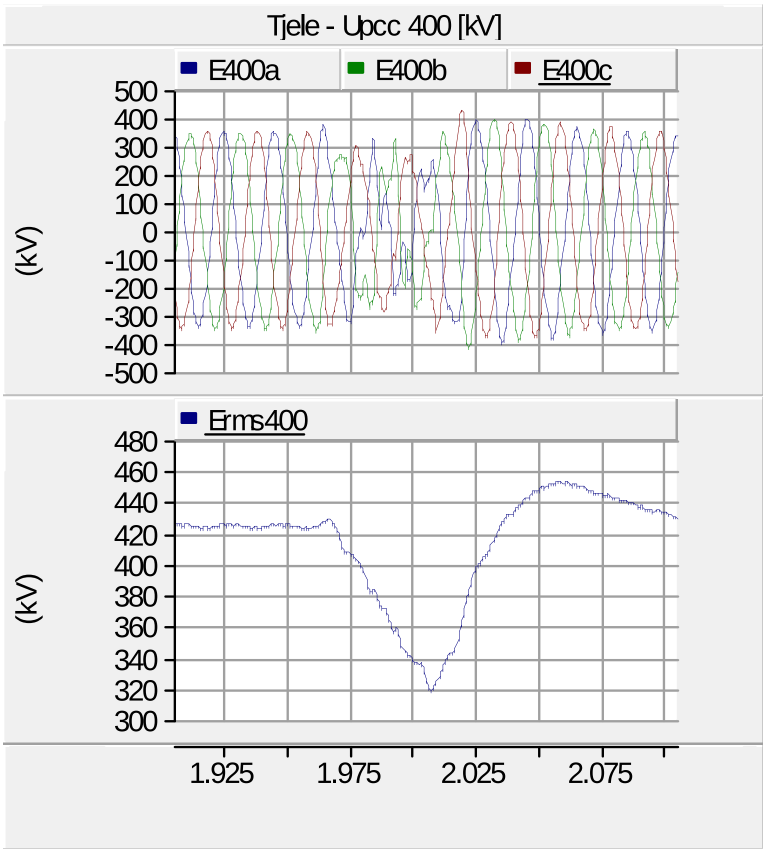

Figure 7.7: AC voltages and equivalent rms value

DC side ratings of SK3 for voltage is 350 kV and current of 1430A. These values have been expressed in per unit value and are shown in figure 7.12. The dc voltage as well as the dc current are observed to drop to zero during the commutation failure.

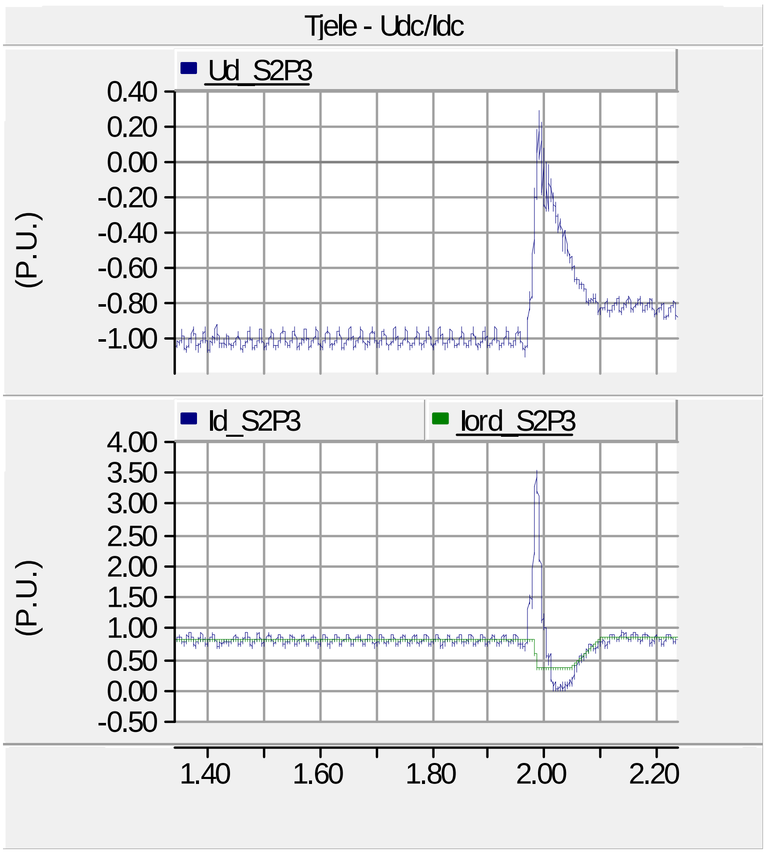

Figure 7.8: DC voltage, current and current order

Thyristor firing angles :

The values of the thyristor firing angles determine the operation of the converter, depending on their values, the converter will act as a rectifier or inverter. The firing angles (α (, extinction angle (γ) and overlap angle (μ), have been measured for this simulation and the values obtained at instants during normal operation and commutation are presented in table 8.3 for the rectifier operation and the simulation results are shown in figure 7.9.

Rectifier	α	γ	μ
During normal operation	148	18	14
During commutation failure	78	80	50

Table 7.2: Firing angles values.

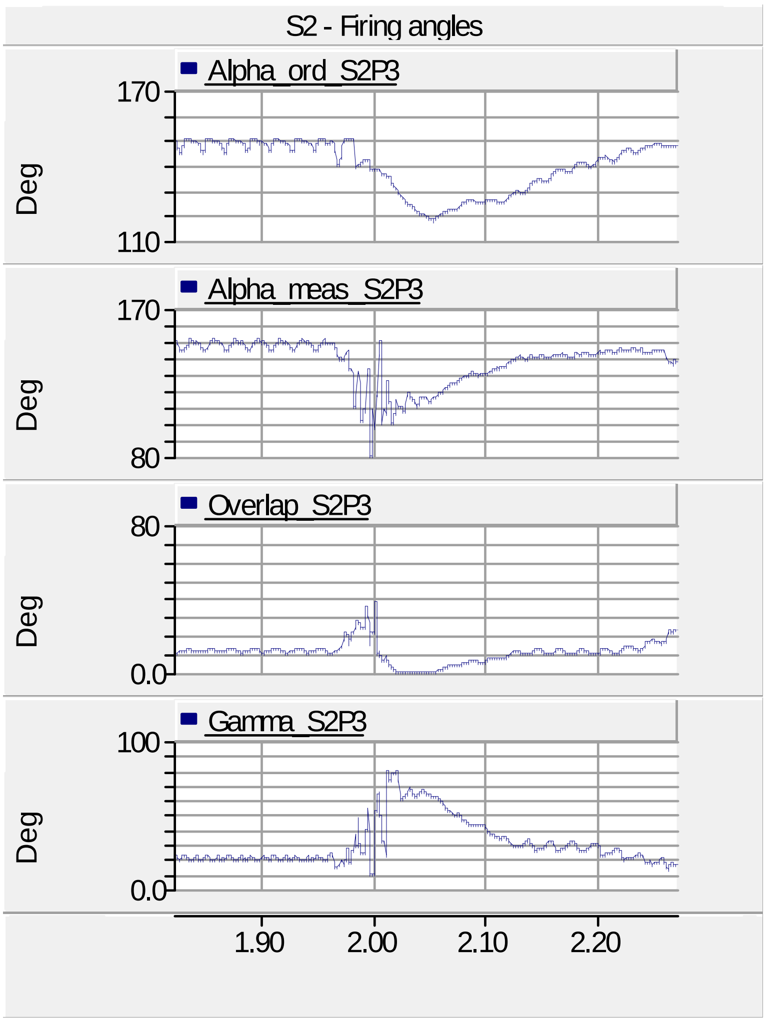

Figure 7.9: Firing angles

The thyristor firing angles during normal operation are typically in the range given in table 7.3 for an inverter and rectifier operation.

For	α	γ	μ
rectifier	< 90	> 90	$\mu = 180 - \alpha - \gamma$
inverter	> 90	> 18	$\mu = 180 - \alpha - \gamma$

Table 7.3: Firing angle values for normal operation.

It can be observed that, the angles obtained from the simulation are within the rating during normal operation and during commutation failures, the angle values are out of the range of normal operation.

7.5 Comparison between simulation results and measurement

AC voltage comparison : The voltages from the measurement are shown in figure 7.10 (a). The voltage from the model simulation (b), have been made to have a value close to the measured values by the insertion of an inductor in the line between the 400kV bus and the converter transformer at Tjele as mentioned before. The voltage drop in both cases can be seen to vary at different level in the three lines at different times.

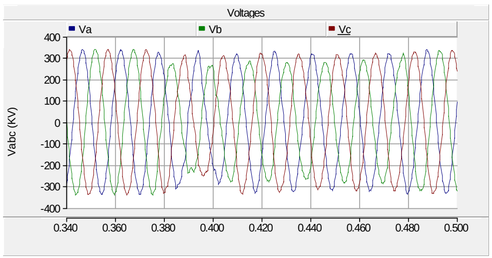

(a)

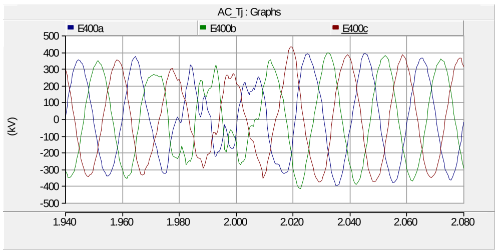

(b)

Figure 7.10: Ac voltages (a) measurement (b) simulated

From the figures, it can be observed that the voltages between the two have a maximum amplitudes during normal operation and maximum voltage drop from the normal, as given in table 7.4.

For	Normal operation [KV]	Voltage drop to [KV]	Difference in drop [percent]
Real Measurement values	340	210	38
Simulated model values	340	200	41

Table 7.4: AC voltages comparison for measured and simulated values.

The voltages from the simulated model have a maximum deviation of 3 percent from the measurement values. The comparison is made taking this deviation in to consideration.

DC current comparison: The dc measured value and the simulated values can be seen in figure 7.11. The simulation values are expressed in per unit values with a base of the rated value 1430kA.

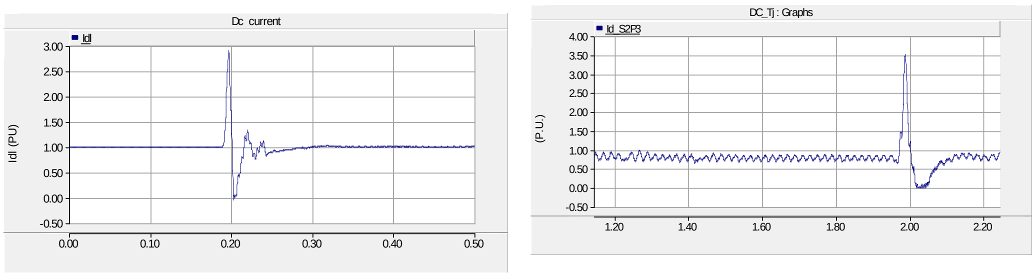

(a) (b)

Figure 7.11: Dc currents (a) measurement (b) simulated

The magnitude of the currents for both the measured and simulated values during normal operation and during commutation are given in table 7.5.

For	Normal [PU]	commutation [PU]
Real Measurement values	0.97	0
Simulated model values	0.91	0

Table 7.5: DC current comparison for measured and simulated values.

The measured dc current has a higher value by 0.06 PU and for both cases, during commutation failure, the current goes down to zero.

DC voltage comparison: The measured dc voltage value and the simulated one may be seen in figure 7.12.

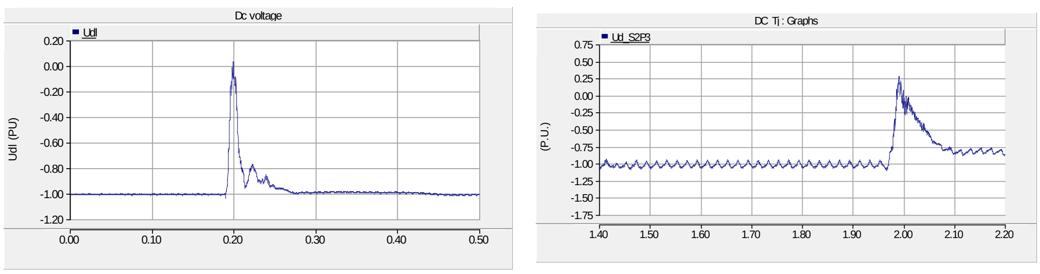

(a) (b)

Figure 7.12: Dc voltages (a) measurement (b) simulated

The values are given in PU values with a base voltage of 350kV. The comparison between the two for normal operation and during commutation failure is given in table 7.6.

For	Normal [PU]	commutation [PU]
Real Measurement values	1	0.05
Simulated model values	1.05	0.25

Table 7.6: DC voltage comparison for measured and simulated values.

The DC voltage measured is less than the simulated by 0.05 pu and during commuatation both go to 0 PU.

DC current order comparison: The measured and simulated values of the ordered DC current from the control system are shown in figure 7.13.

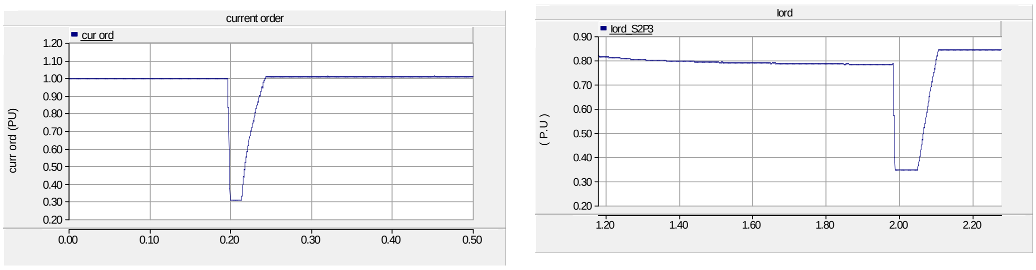

(a) (b)

Figure 7.13: DC Current order (a) measurement (b) simulated

The values are given in PU values with a base current of 1430A. The comparison between the two for normal operation and during commutation failure is given in table 7.7.

For	Normal [PU]	commutation [PU]
Real Measurement values	0.97	0.32
Simulated model values	0.81	0.35

Table 7.7: DC current comparison for measured and simulated values.

Angle gamma comparison: The firing angle control for an inverter operation is the gamma angle. A comparison between the measured and simulated value of the gamma angle is given in figure 7.14.

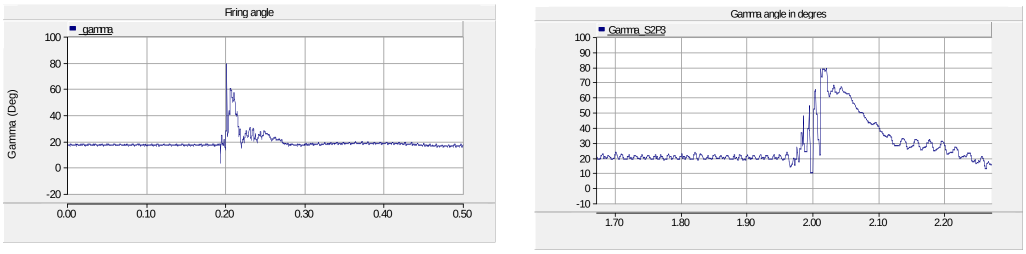

(a) (b)

Figure 7.14: Firing angle gamma (a) measurement (b) simulated

From the figure it can be observed that, the gamma angle in both cases during normal operation is above the minimum value of 18 degree. The measured gamma angle is 19 and the simulated one has a 20 degree gamma angle. During commutation the gamma angle in both cases increases to 80 degrees.

7.6 Conclusion

In conclusion, by observing the waveforms of the measurement voltage, the voltage in the PSCAD simulation has been made to closely behave as the waveform from the measurements. This was accomplished by inserting an inductor of value 1H between the 400kV bus and the converter transformers at Tjele. This was done to reduce the voltage of the simulated model, by a percentage that is close to that of the measured values. Different values of the inductor were tried and the one that gave a reduction of voltage close to the measured one was taken. The results show that during normal operation, in both cases , for the measured as well as the PSCAD simulation, the extinction angle is above 18 degrees. Considering the AC voltage deviation of 3 percent between the measured and simulated, the dc voltage and current have been observed to behave similarly. A commutation failure occurs in those instants where the voltage drops down, the extinction angle was up to 80 degrees and the dc voltage and current went down to zero. This kind of problem, that is drop of voltage or distortions in the waveforms is a common cause for commutation failures in power networks.

Chapter 8

Performance of SK4 in bipole to SK3

In this chapter, the performance of the bipole SK3,SK4 link is presented. The results for the performance of the link simulated during normal operation and then during AC and DC faults on the link is presented and discussed.

8.1 Introduction

Commutation failure for a converter can occur due to faults on the DC and AC side as discussed in previous sections. In this chapter different simulation cases to observe the performance of the bipole link SK3 and SK4 model has been made. The simulation cases that have been simulated deal with faults on the AC side and DC side. The faults that can occur on the AC side may be balanced faults and unbalanced faults. The unbalanced type single phase to ground, reduction in the voltage at the end of the link and balanced three phase to ground fault have been selected for the simulation. The single phase to ground fault and reductions or distortions in the voltages are common faults that appear on the power network, and the three phase to ground fault rarely occurs but is the worst fault that may appear on the power network.

For DC side fault, rapid increase in the DC current which can result due to transient phenomena has been made. This is because, for the normal operation of a DC link, the DC voltage is always kept constant at the rated value by the voltage controller assigned for it, however the DC current is variable depending on the amount of power transferred.

In order to compare and evaluate the performance of the bipole link under these different scenarios, the chapter starts with the normal operation of the bipole SK3,SK4 link and then the results obtained with the different type of fault cases is presented.

8.2 During Normal operation

To observe the performance of the bipole link SK3 and SK4 during normal operation, for power transfer from Denmark to Norway, the simulation was made with the parameters specified in table 8.1 and 8.2. The setting for the P/I reference, which is the current order controller at SK3, was adjusted at 0.25sec from 1 to 0.7 and then at t = 0.4 changed to 1, to observe the performance of the link. For the SK4 link, the power ordered after deblocking was 100MW and then at t = 0.9 sec, the order was changed to 250MW.

Power direction	P/I ref	Time to deblock SK3 [sec]	$U_{dcref}SK3$ [KV]
Tjele to Kristiansand	1	0.2	380

Table 8.1: SK3 simulation parameter settings.

Power direction	P ref[MW]	Time to deblock SK4 [sec]	$U_{dcref}SK4$ [KV]
Tjele to Kristiansand	100	0.15	500

Table 8.2: SK4 simulation parameter settings.

The results obtained are presented for both the rectifier side (Tjele) and inverter side (Kristiansand). The time scale is in seconds for all the simulation results.

AC side voltages during normal operation are, at the rectifier side 400kV at a THD level of 0.135 percent and inverter side 300kV at a THD level of 0.263 percent values. This may be observed in figure 8.1.

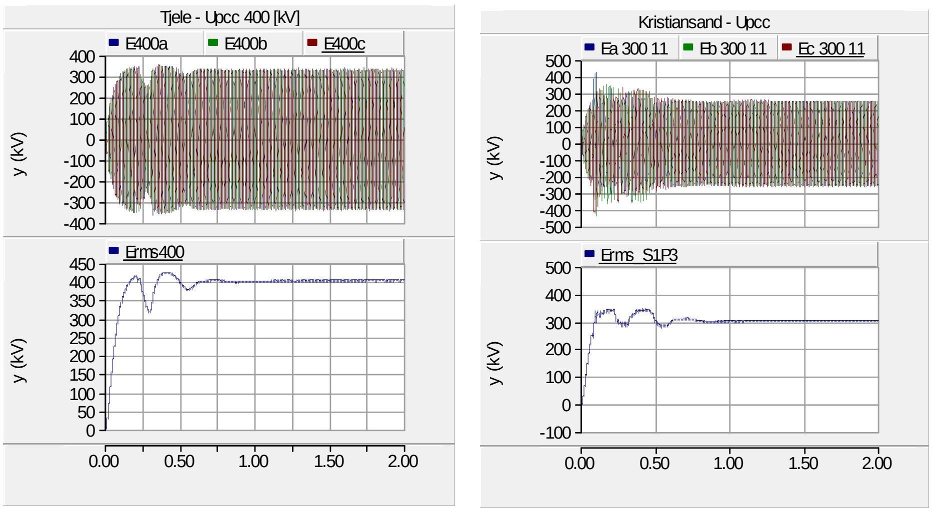

(a) (b)

Figure 8.1: AC Voltages at (a) SK3 Tjele (b) SK3 Kristiansand.

The DC side voltage for SK3 link during normal operation is 350kV and a rated DC current of 1300A. This values have been expressed in per unit value and are shown in figure 8.2 for both Tjele and Kristiansand. The DC current ordered and the actual DC current flowing are also illustrated in figure 8.2. The current ordered can be observed to vary through the simulation time. The current ordered is at 1 pu value at the beginning and then it was adjusted to 0.7 pu to observe the behavior of the link. The actual DC current flowing is observed to follow the current ordered.

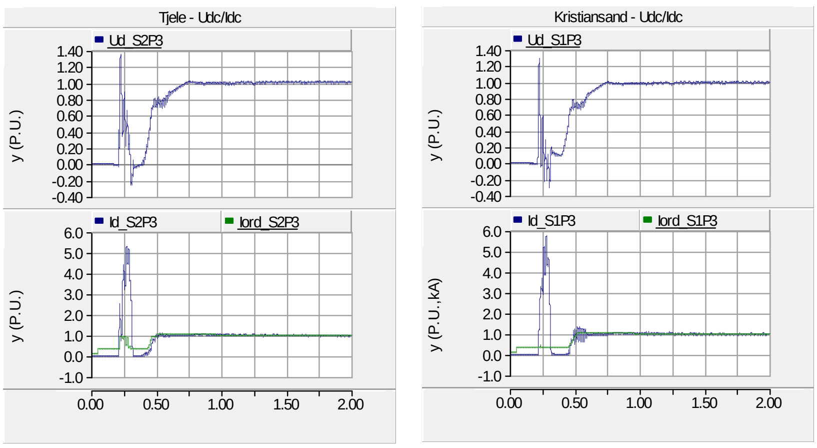

(a) (b)

Figure 8.2: DC Voltage and Current at (a) SK3 Tjele (b) SK3 Kristiansand.

At SK4 link, the AC voltages and DC voltages are shown in figures 8.3, and 8.4 respectively. The AC voltage at Tjele SK4 is similar to SK3 at 400kV. Moreover for the AC voltage at Kristiansand SK4 is similar to SK3, which is 300kV. This is because at both ends, the links are connected to the same bus. The DC voltage at SK4 is 500kV during normal operation and this value is illustrated in figure 8.4 in pu value for Kristiansand and Tjele.

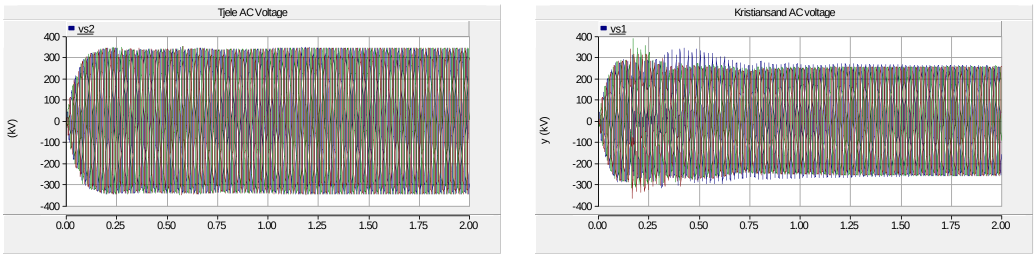

(a) (b)

Figure 8.3: AC voltage at (a) SK4 Tjele (b) SK4 Kristiansand.

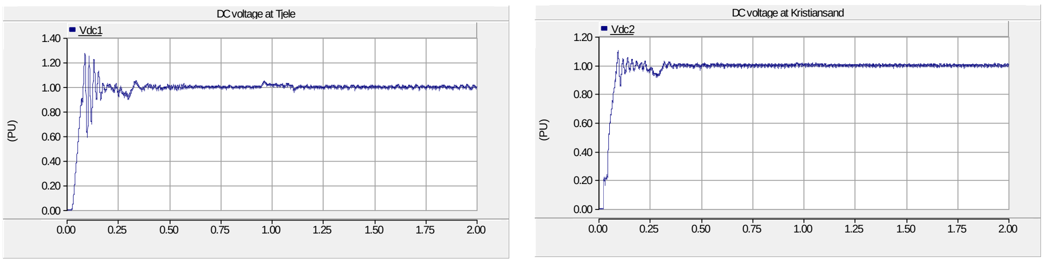

(a) (b)

Figure 8.4: DC voltage at (a) SK4 Tjele (b) SK4 Kristiansand.

The maximum Power transfer through the SK3 link is 500MW, and for SK4, a maximum of 750MW. To observe the firing angles at different rated power transfer, the power level was varied within its rating during the simulation time, at 0.25 sec by changing the current ordered by the controller of SK3. The power transfer variation can be observed for SK3 in figure 8.5. The active power transfer through SK3 link after deblocking starts at 300MW and then at t = 0.4sec, the power increases to 450MW. This is caused due to the increase in the current ordered at the SK3 current order controller. The reactive power can be observed to vary also at both ends where at Tjele, the reactive power consumed by the converter is at 153Mvar and on Kristiansand, the reactive power is at 190Mvar.

The active power transfer through the SK4 link can also be observed in figure 8.6. The power can be seen to start at 100MW which is the ordered power after deblocking. At t = 0.9sec, the power order is changed to 250MW by the power reference controller at SK4 link. At t = 0.9sec, the power can be observed to increase to 250MW.

The power transfer across the links is controlled by the controller part of each link respectively.

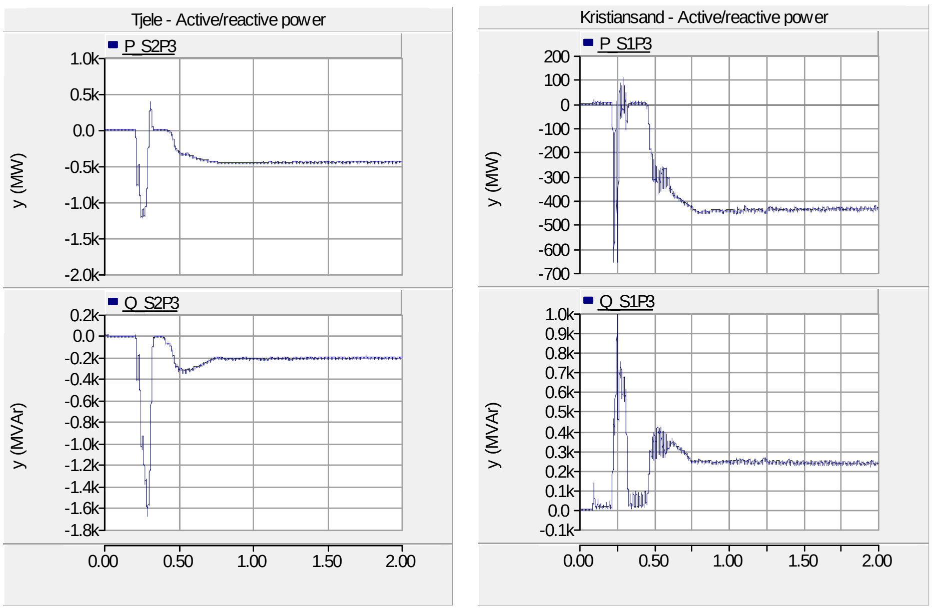

(a) (b)

Figure 8.5: Active and reactive power SK3 at (a) Tjele (b) Kristiansand.

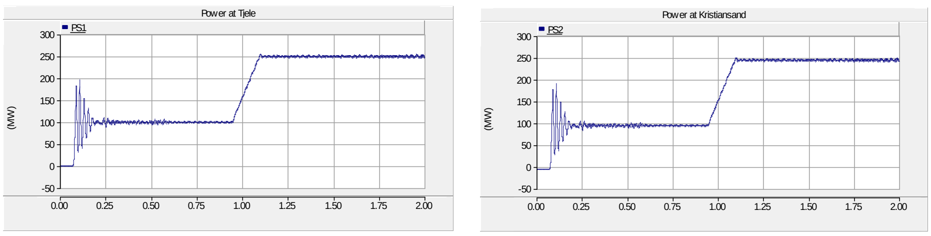

(a) (b)

Figure 8.6: Active and reactive power SK4 at (a) Tjele (b) Kristiansand.

The thyristor angles, such as firing angle α , extinction angle γ and overlap angle μ , during the simulation are given in table 8.3 for an inverter and rectifier operation.

For	α [Deg]	γ [Deg]	μ [Deg]
rectifier	24	150	10
inverter	150	22	15

Table 8.3: Firing angles values during normal operation.

Comparing the above thyristor angle values obtained with the permitted values of thyristor angle values discussed in chapter seven section 7.4 PSCAD simulations, the range of value of the thyristor angles obtained in the simulation shown in figure 8.7, are within the normal operating rating.

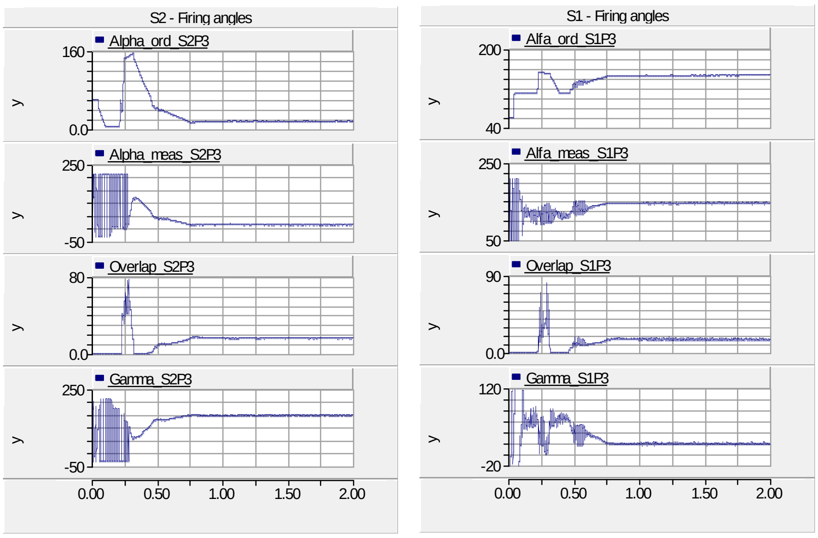

(a) (b)

Figure 8.7: Thyristor firing angles at (a) Tjele (b) Kristiansand.

The results overall indicate that the power transfer across the bipole link can be controlled independently. Depending on the transmission system operator needs, the bipole link can be operated at different power level and the power transfer through each link may be at different level also.

Next section presents the performance of the bipole link during AC side faults.

8.3 AC side faults

8.3.1 Single phase to ground

To observe the performance of the bipole link SK3, SK4 during a single phase to ground, a single phase to ground fault was applied at SK3 link on the inverter side (Kristiansand) at time, t = 0.8sec for a duration of 0.2sec. The simulation was made with the parameters specified in table 8.4 and 8.5.

Power direction	P/I ref	Time to deblock SK3 [sec]	$U_{dcref}SK3$ [KV]
Tjele to Kristiansand	1	0.2	380

Table 8.4: SK3 simulation parameter settings.

Power direction	P ref[MW]	Time to deblock SK4 [sec]	$U_{dcref}SK4$ [KV]
Tjele to Kristiansand	400	0.15	500

Table 8.5: SK4 simulation parameter settings.

AC side voltage is observed to be within its rating at both ends of the link until the fault. During the fault, the voltage decreased to 250KV on the inverter side and at the voltage remained constant at 420kV except for a transient perturbation at t = 0.8sec, when the fault was applied. This can be seen in figure 8.8. The AC voltage at SK4 link can also be seen in figure 8.9. The voltages are 420kV at Tjele and at Kristiansand, the voltage is 310kV but from t = 0.8sec to t = 1sec, it can be observed one of the phases, has gone down to ground.

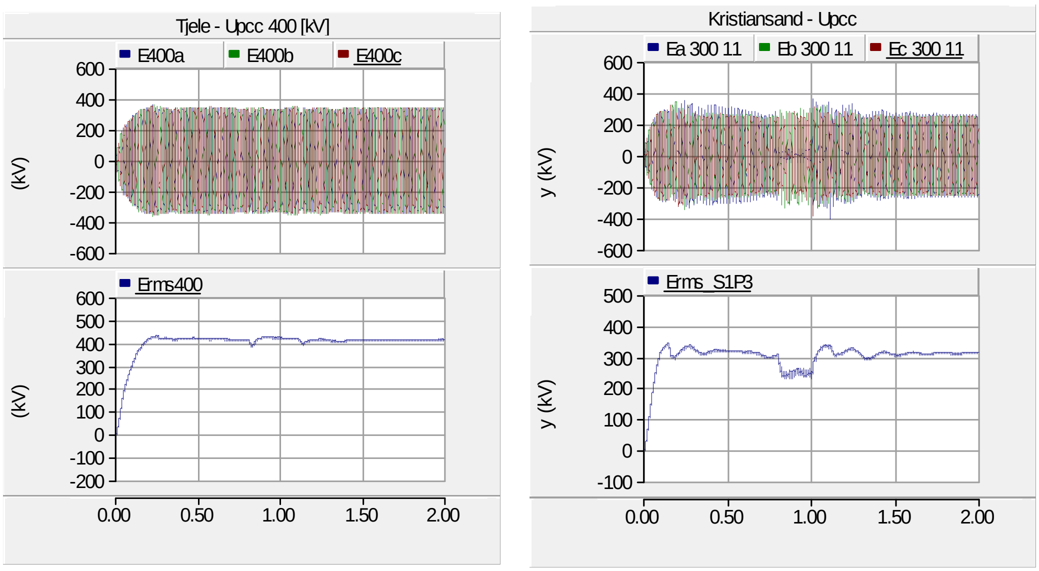

(a) (b)

Figure 8.8: AC voltage at (a) SK3 Tjele (b) SK3 Kristiansand.

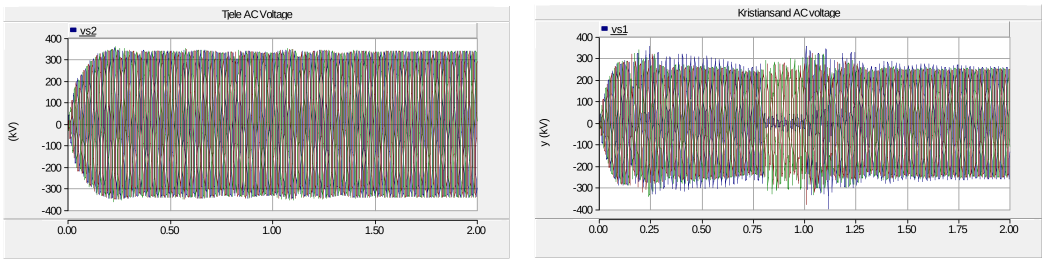

(a) (b)

Figure 8.9: AC voltage at (a) SK4 Tjele (b) SK4 Kristiansand.

The DC side voltage for the SK3 link is observed to be at 1 pu after SK3 has been deblocked. At t = 0.8, when the single phase to ground occur, the voltage goes down to 0 pu. Then it recovers at t = 1sec and stabilizes at its previous operating level. This is observed at both ends of the link and can be seen in figure 8.10. The DC current ordered can also be seen to be at its rated level, 1pu after deblocking and then goes down to 0.4pu during the fault and recovers also at t = 1sec. The DC voltage at SK4 link can also be seen in figure 8.11. The DC voltage is at its rated value 1pu and then at t = 0.8 sec decreases to 0.9pu and then recovers to its previous operating level 1pu.

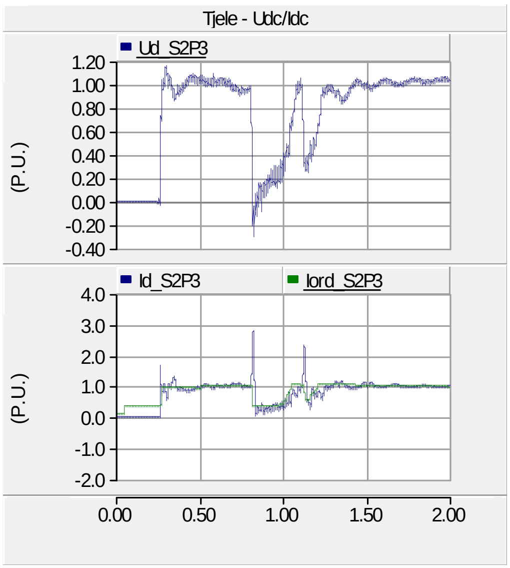

(a)

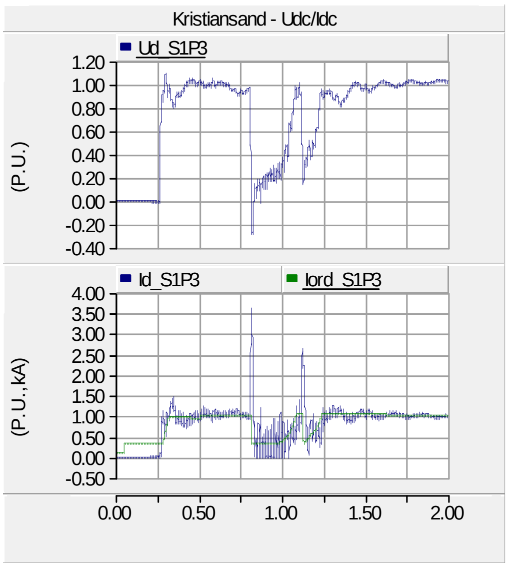

(b)

Figure 8.10: DC voltage and current at (a) SK3 Tjele (b) SK3 Kristiansand.

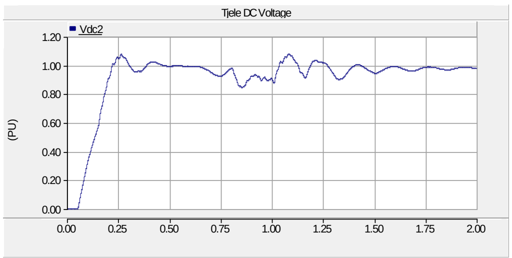

(a)

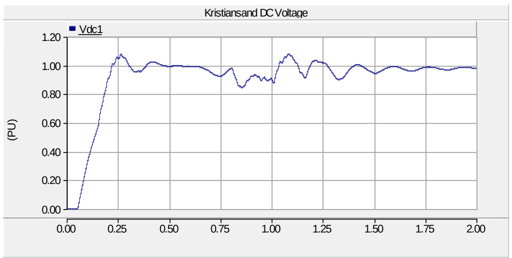

(b)

Figure 8.11: DC voltage at (a) SK4 Tjele (b) SK4 Kristiansand.

The power transfer through the SK3 link can be observed to be at 450MW after deblocking. During the application of the fault, the power transfer goes to 0MW and then recovers at t = 1sec. This can be observed in figure 8.12. For the SK4 link, the power transfer can be observed in figure 8.13 where the power transfer is also affected by the fault and decreases to 250MW minimum during the fault and recovers at t = 1sec.

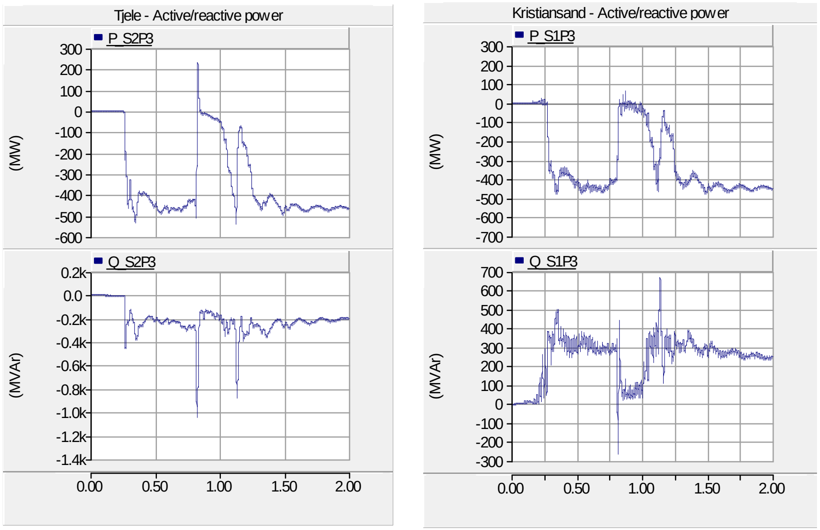

(a) (b)

Figure 8.12: Active and reactive power at (a) SK3 Tjele (b) SK3 Kristiansand.

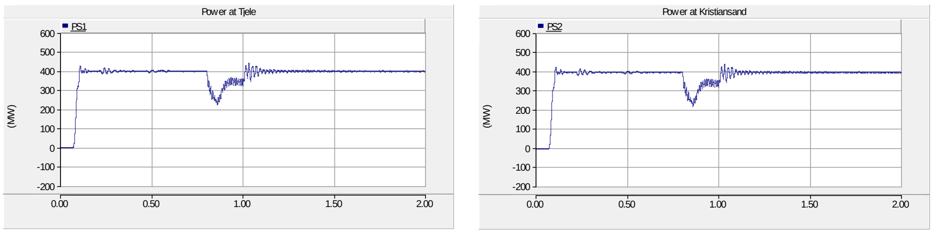

(a) (b)

Figure 8.13: Power at SK4 (a) Tjele (b) Kristiansand.

The thyristor angles before and during the fault were observed to vary. The maximum and minimum values obtained during the duration of the fault are presented in table 8.6, which are out of the normal operating range and result in commutation failure at SK3. During normal operation the angles are observed to be within the allowed range of the rectifier and inverter operation.

For	α [Deg]	γ [Deg]	μ [Deg]
rectifier	100	50	2.5
inverter	80	120	0

Table 8.6: Firing angles values during single phase to ground fault.

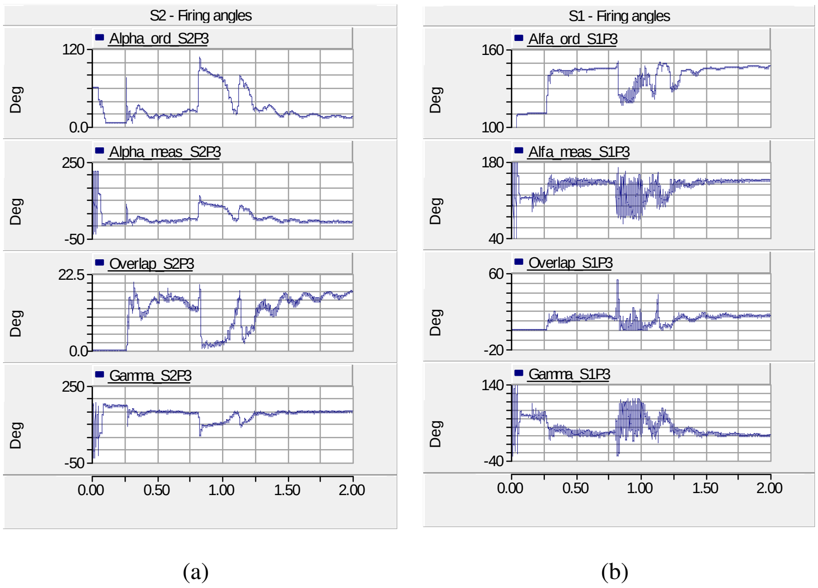

Figure 8.14: Thyristor firing angles at (a) Tjele (b) Kristiansand.

During this type of fault, it may be concluded that commutation failure occurs at SK3 link and the transfer of power is interrupted during the fault. However for the VSC, the transfer of power is not interrupted but continues at a lower level decreasing by an average of 25 percent.

The next subsection presents the performance of the link during reductions in the AC voltage at the end terminals of the link.

8.3.2 Reduction in the AC voltage

To observe the performance of the bipole link SK3, SK4 during a reduction in the AC voltage at one end of the terminals, Kristiansand, an inductor of 0.75H was used to drop the voltage by 23 percent of the rated value. Similar simulation has been done previously for the validation of the SK3 model during commutation failure. However the simulation was made for the SK3 link only. In this case, the SK3 and SK4 are simulated in bipole mode. The inductor was placed between the converter transformer and the AC bus at Kristiansand. The parameter settings used are similar to that stated in tables 8.4 and 8.5. The results obtained are presented below.

AC side voltage is observed to be within its rating at both ends of the link until the fault. During the fault, the voltage decreased from 310kV to 240kV on the rectifier side and at inverter the voltage decreased from 400kV to 370kV. This can be seen in figure 8.15. The

AC voltage at SK4 link can also be seen in figure 8.16. The voltages are similar to that of SK3.

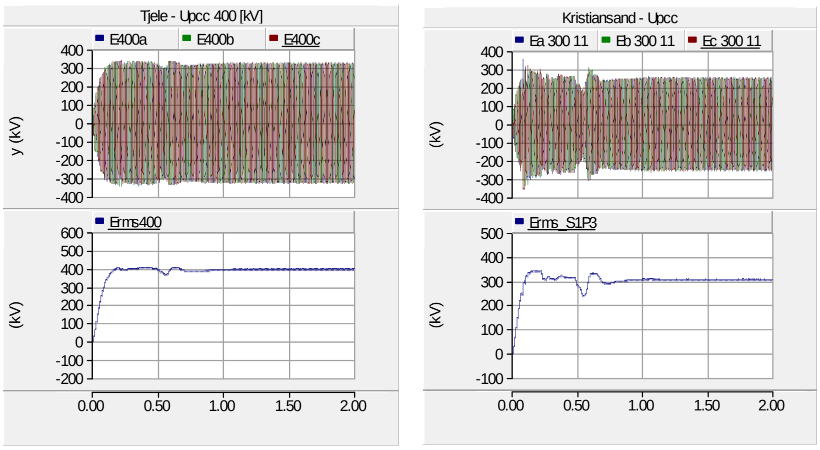

(a) (b)

Figure 8.15: AC voltage at (a) SK3 Tjele (b) SK3 Kristiansand.

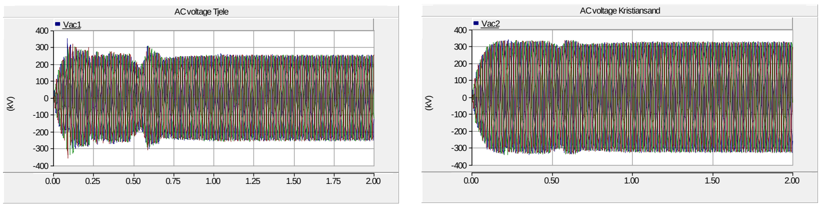

(a) (b)

Figure 8.16: AC voltage at (a) SK4 Tjele (b) SK4 Kristiansand.

The DC side voltage for the SK3 link is observed to be at 1 pu after SK3 has been deblocked. At t = 0.5, when the reduction in the AC voltage at Kristiansand occurs, the voltage goes down to 0.4 pu at Kristiansand. Then it recovers at t = 0.6sec and stabilizes at its previous operating level. This is observed at both ends of the link and can be seen in figure 8.17. The DC current ordered can also be seen to be at its rated level, 1pu after deblocking and then initially increases to 2.7 pu and then decreases down to 0 pu and recovers also at t = 0.6sec. The DC voltage at SK4 link can also be seen in figure 8.18. The DC voltage is at its rated value 1pu throughout the simulation time.

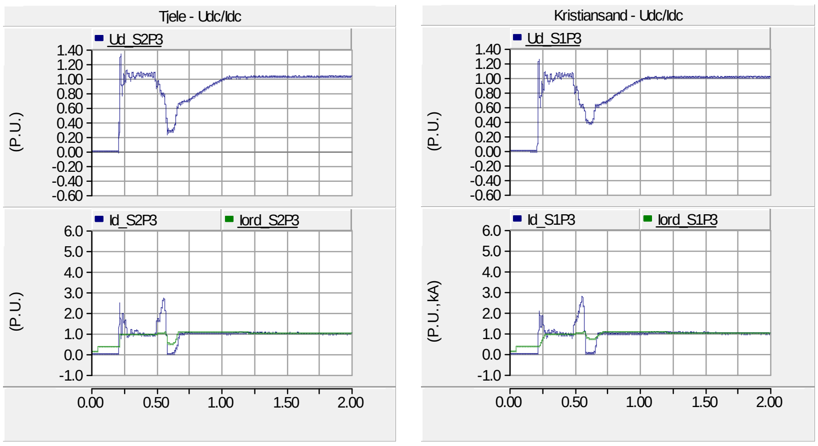

(a) (b)

Figure 8.17: DC voltage and current at (a) SK3 Tjele (b) SK3 Kristiansand.

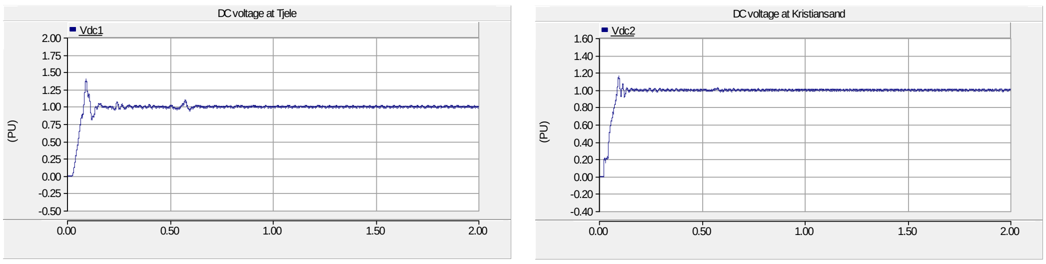

(a) (b)

Figure 8.18: DC voltage at (a) SK4 Tjele (b) SK4 Kristiansand.

The power transfer through the SK3 link can be observed to be at 450MW after deblocking. During the application of the fault, the power transfer goes to 0MW and then recovers at t = 0.6sec. This can be observed in figure 8.19. For the SK4 link, the power transfer can be observed in figure 8.20 where the power transfer ordered is 400MW. This power transfer is sustained throughout the simulation time.

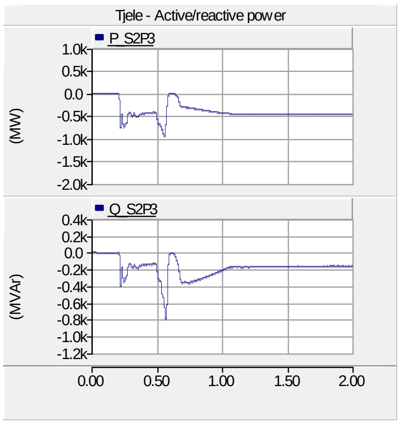

(a)

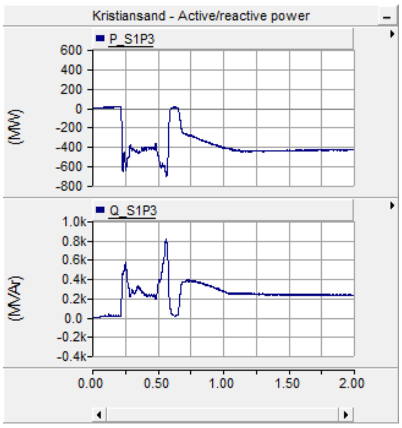

(b)

Figure 8.19: Active and reactive power at (a) SK3 Tjele (b) SK3 Kristiansand.

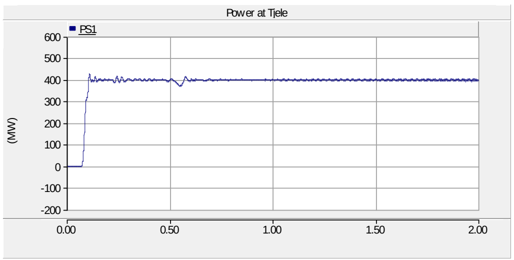

(a)

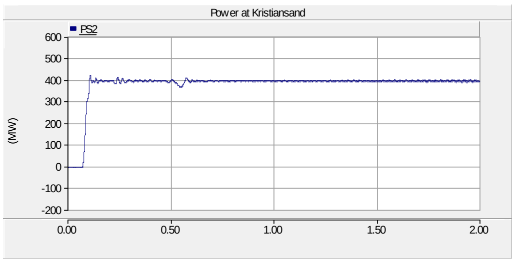

(b)

Figure 8.20: Power at SK4 (a) Tjele (b) Kristiansand.

The thyristor angles before and during the fault were observed to vary. The maximum and minimum values obtained during the duration of the fault are presented in table 8.7. During normal operation the angles are observed to be within the allowed range of the rectifier and inverter operation.

For	α [Deg]	γ [Deg]	μ [Deg]
rectifier	91	88	0
inverter	108	67	0

Table 8.7: Firing angles values during single phase to ground fault.

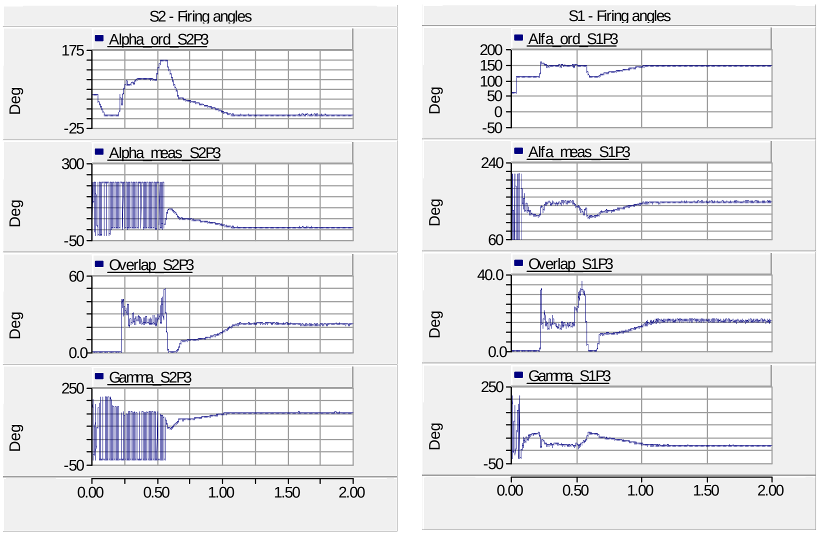

(a) (b)

Figure 8.21: Thyristor firing angles at (a) Tjele (b) Kristiansand.

The results for AC voltage reductions at one end of the link shows that the SK3 link falls under commutation failure and the transfer of power is interrupted while the SK4 is able to sustain the transfer of power.

Next section presents the performance of the link during the worst type of fault, three phase to ground.

8.3.3 Three phase to ground fault

To observe the performance of the bipole link SK3, SK4 during a three phase to ground fault, a three phase to ground fault was applied at the inverter side (Kristiansand) at time, t = 0.8sec for a duration of 0.2sec. The simulations are made with the same parameter setting as in tables 8.4 and 8.5. The results obtained are presented below.

For the AC side voltages at SK3, on the inverter side when the fault is applied, the voltage goes down to 25kV rms, whereas the voltage at the rectifier side (Tjele) remains at 400kV, through out the simulation time. This may be observed in figure 8.22. The DC voltage is also observed to be at its rated value 1 pu and then during the fault, the dc voltage goes down to 0 pu. At the same time, the DC current from 1 pu goes to 0.4 pu during the fault. This can be seen in figure 8.23.

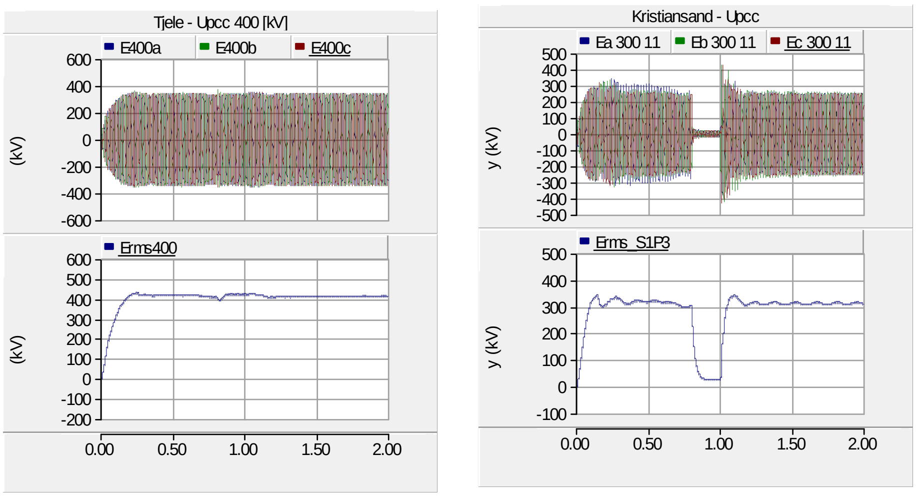

(a) (b)

Figure 8.22: AC voltages at SK3 (a) Tjele (b) Kristiansand.

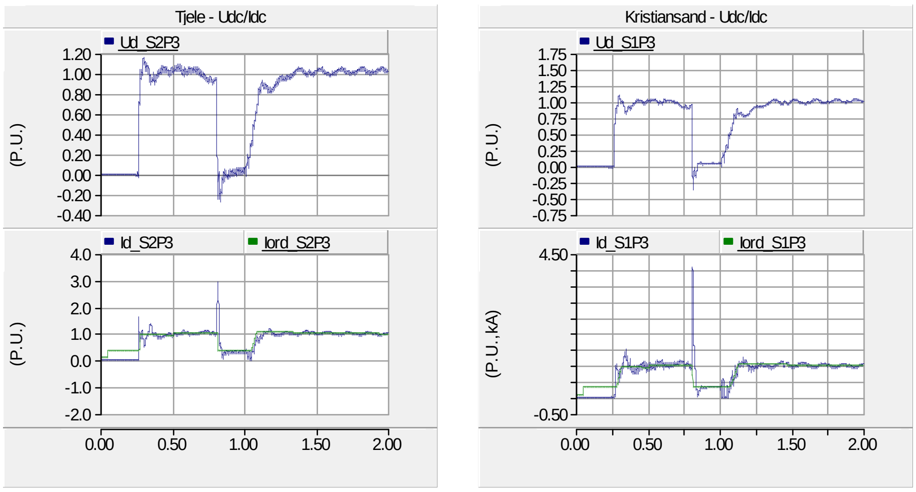

(a) (b)

Figure 8.23: Dc voltage and current at SK3 (a) Tjele (b) Kristiansand.

At the SK4 link, the AC and DC voltages can be seen in figure 8.24 and 8.25 respectively. The AC voltages are observed to be at 400kV at Tjele through out the simulation time but for Kristiansand, the voltage goes down to 25kV during the fault. The DC voltage at the link is observed to be at 1 pu.

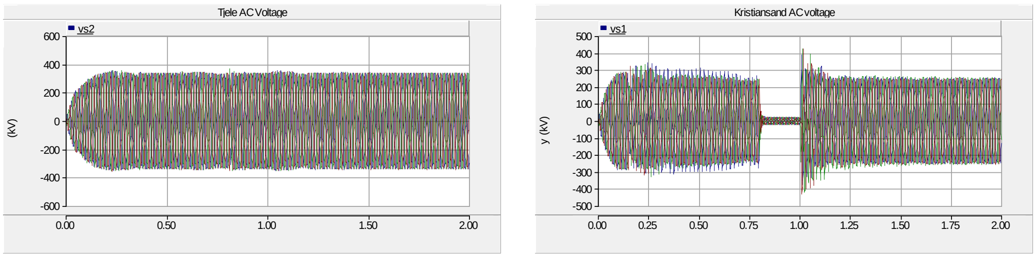

(a) (b)

Figure 8.24: AC voltage at SK4 (a) Tjele (b) Kristiansand.

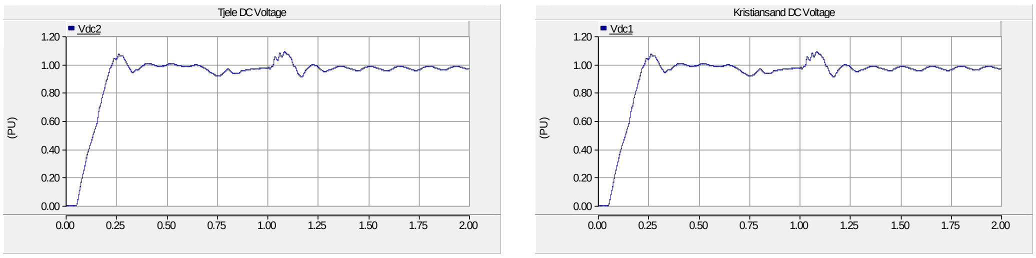

(a) (b)

Figure 8.25: DC voltage at SK4 (a) Tjele (b) Kristiansand.

The power transfer across the SK3 link can be seen in figure 8.26. The power goes down to zero for the duration of the fault and then recovers to its rated value at 450MW. Figure 8.27 shows the variation of power transfer across the SK4 link, where the power transfer was made at a power order of 330MW.

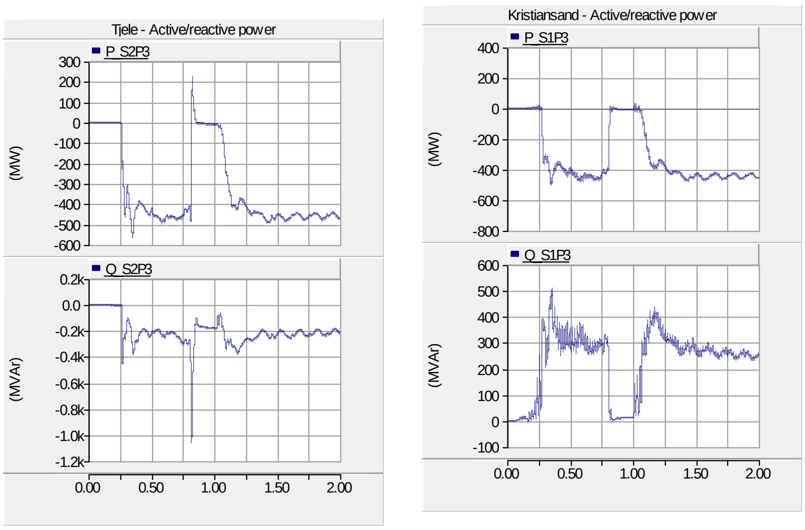

(a) (b)

Figure 8.26: Active and reactive power (a) SK3 Tjele (b) SK3 Kristiansand.

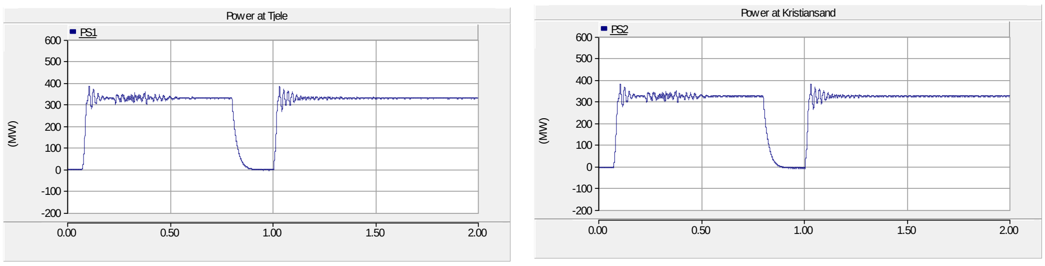

(a) (b)

Figure 8.27: Power at (a) SK4 Tjele (b) SK4 Kristiansand.

The firing angles for the SK3 converter during the simulation time can be observed in figure 8.28. The maximum and minimum values of the firing angles during the fault are also presented in table 8.8 which result in commutation failure.

For	α [Deg]	γ [Deg]	μ [Deg]
rectifier	80	80	0
inverter	100	50	2.25

Table 8.8: Firing angles values during three phase to ground fault.

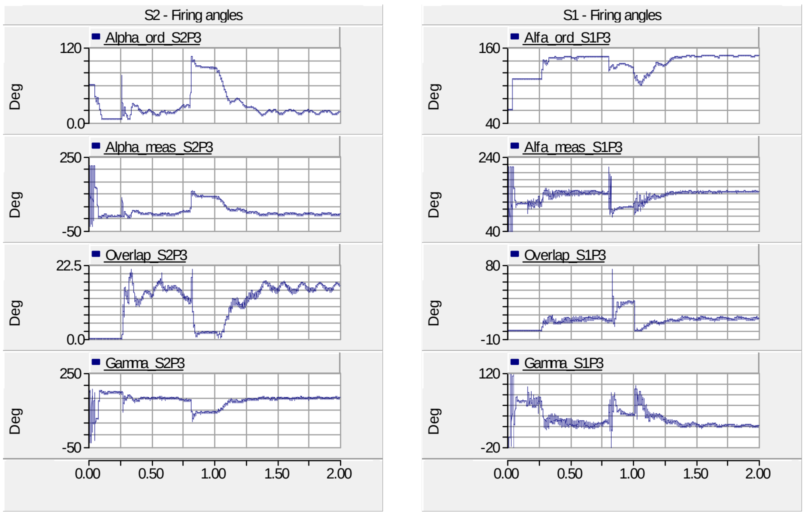

(a) (b)

Figure 8.28: Thyristor firing angles (a) Tjele (b) Kristiansand.

During this type of fault it has been observed that, the whole bipole link will go down and the transfer of power through the bipole link is not possible.

The next section presents results obtained for DC side fault on the bipole link.

8.4 DC side faults

8.4.1 Sk3 line to ground fault

To observe the performance of the bipole link SK3, SK4 during a line to ground fault, a line to ground fault was applied at the DC line at Tjele at time, t = 0.8sec. The simulations are made with the same parameter setting as in tables 8.4 and 8.5. The results obtained are presented below.

For the AC side voltages at SK3, on the rectifier side, the voltage is observed to be at 420kV throughout the simulation time except for a transient perturbtion when the fault is applied. The voltage at Kristiansand is observed to be at 310kV but after the application of the fault, the voltage increases to 340kV. This may be observed in figure 8.29. The DC voltage is also observed to be at its rated value 1 pu during normal operation and then during the fault starting at t = 0.8 sec, goes down to 0 pu. At the same time, at the application of the fault, the actual flowing DC current from 1 pu goes initially to 2.6 pu at Tjele. This high rise in current is limited by the current order limiter and the refernce current is reduced to 0.38 pu and the actual current eventually follows the ordered current. At Kristiansand, the current ordered is similar to that of Tjele, however the actual current after the application of the fault is zero. This can be seen in figure 8.30.

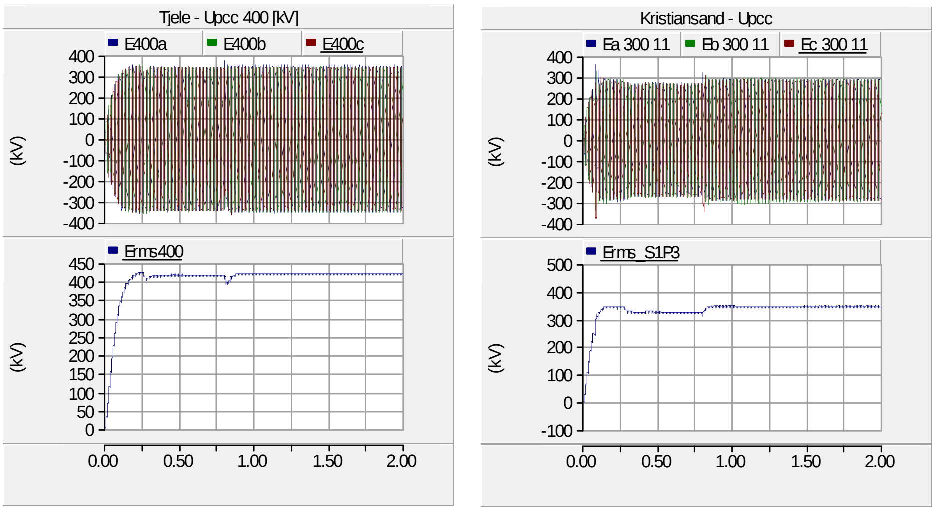

(a) (b)

Figure 8.29: AC voltages at SK3 (a) Tjele (b) Kristiansand.

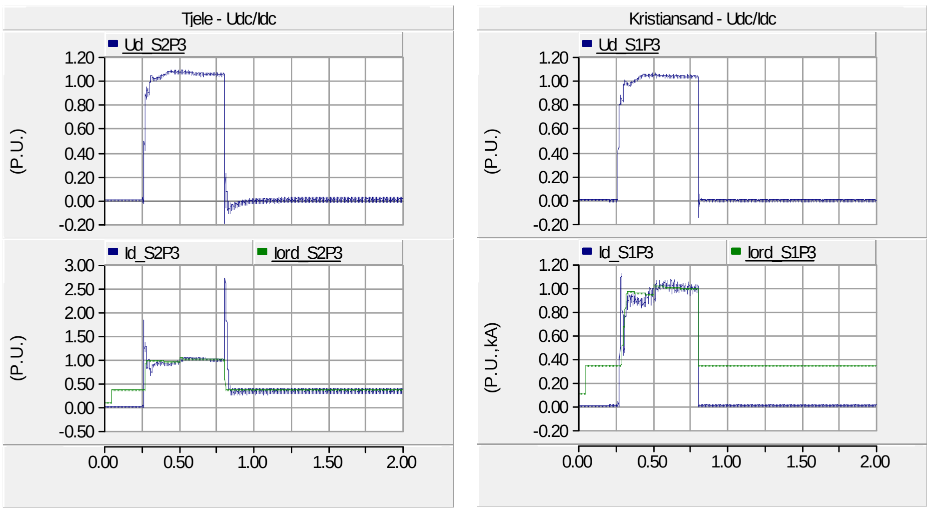

(a) (b)

Figure 8.30: Dc voltage and current at SK3 (a) Tjele (b) Kristiansand.

At the SK4 link, the AC and DC voltages can be seen in figure 8.31 and 8.32 respectively. The AC voltages are observed to be at 420kV at Tjele through out the simulation time but for Kristiansand, the voltage in similar manner as that of SK3 from 310 goes up to 340kV after the application of the fault. However the DC voltage at the link is observed to be at 1 pu during the simulation time.

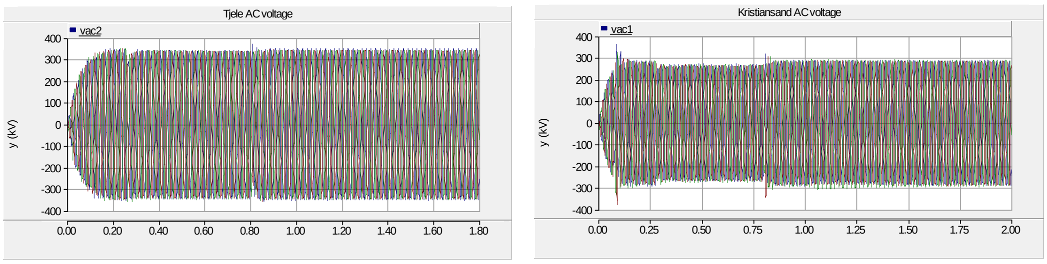

(a) (b)

Figure 8.31: AC voltage at SK4 (a) Tjele (b) Kristiansand.

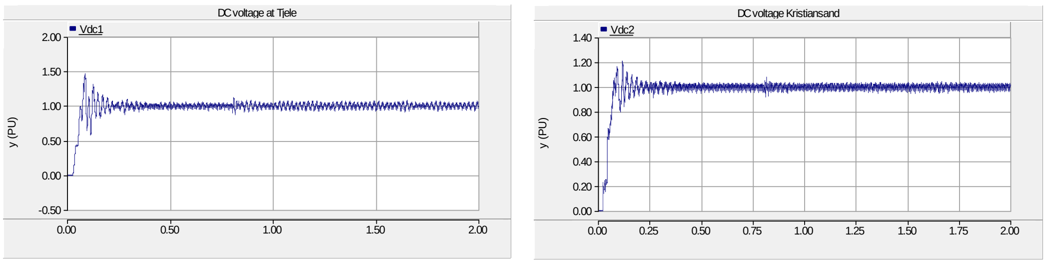

(a) (b)

Figure 8.32: DC voltage at SK4 (a) Tjele (b) Kristiansand.

The power transfer across the SK3 link can be seen in figure 8.33. The power transfer after deblocking of SK3 is observed to be at 450MW. However the power goes down to zero at time t = 0.8sec after the line to ground fault occurs. Figure 8.34 shows the variation of power transfer across the SK4 link, where the power transfer was made at a power order of 200MW, in this case, the power transfer through the SK4 link is not interrupted.

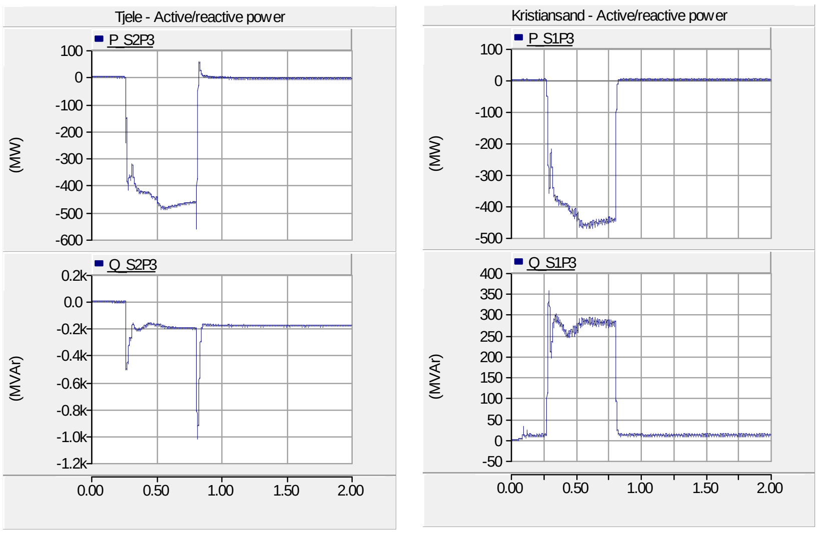

(a) (b)

Figure 8.33: Active and reactive power (a) SK3 Tjele (b) SK3 Kristiansand.

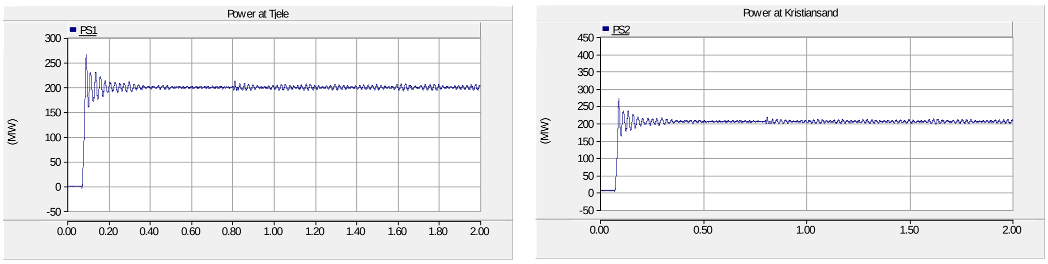

(a) (b)

Figure 8.34: Power at (a) SK4 Tjele (b) SK4 Kristiansand.

The firing angles for the SK3 converter during the simulation time can be observed in figure 8.35. The maximum and minimum values of the firing angles during the fault are also presented in table 8.9. The values obtained are out of the range of normal operation and result in commutation failure.

For	α [Deg]	γ [Deg]	μ [Deg]
rectifier	98	97	2
inverter	110	60	0

Table 8.9: Firing angles values during three phase to ground fault.

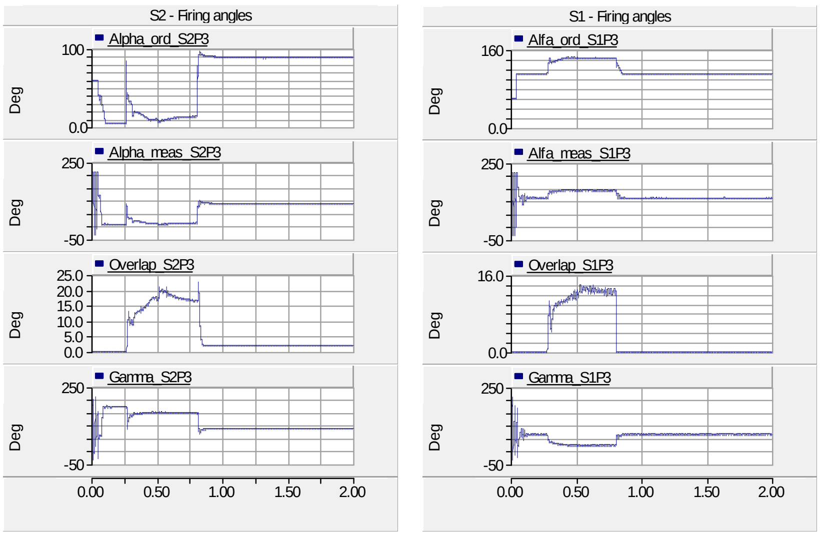

(a) (b)

Figure 8.35: Thyristor firing angles (a) Tjele (b) Kristiansand.

In conclusion, during this type of fault, the results show that, the SK3 DC link is not able to sustain the transfer of power while the SK4 is able to continue transferring power. This is one advantage of implementing HVDC links in bipole fashion, so that when one of the DC lines is under fault, power can still be transferred through the other line. This is not possible with a monopolar HVDC link.

In the next section, abnormal operation in the SK3 HVDC link due to rapid increase in the DC current through the link is presented.

8.4.2 Rapid increase in the DC current

To observe the performance of the bipole link SK3, SK4 during a rapid increase in the DC current which may be caused due to transient phenomenons, the DC current order was made to rapidly increase from its 1pu value to double at SK3 controller. This order was applied at the DC current controller at time, 1.6sec for a duration of 0.1sec. The results obtained are presented below.

The AC side voltages for the SK3 are observed to be within their rating. During the increase in current ordered, the voltage on the rectifier side goes down from 420kV to 400kV, this is shown in figure 8.36. The DC side voltage also decreases from 1 pu to 0.2 pu. The DC current ordered and actual one, at t = 1.6sec increase to 2 pu and 3.5 pu respectively and then decrease to 0.4 pu and 0 pu respectively at kristiansand. This may be observed in figure 8.37.

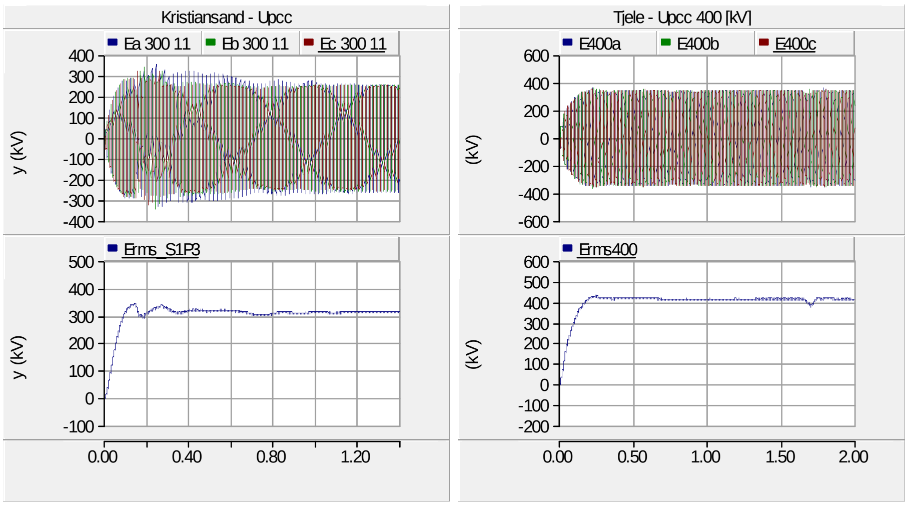

Figure 8.36: AC voltages at SK3 Tjele SK3 Kristiansand.

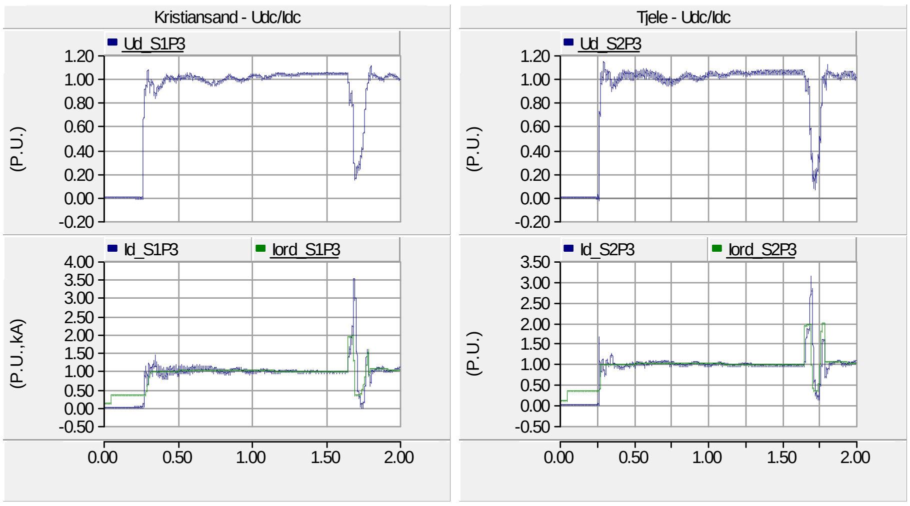

Figure 8.37: (a) DC Tjele (b) DC Kristiansand.

For SK4, the AC and DC voltages may be observed in figures 8.38 and 8.39. The AC voltages are observed to be within their rating during normal rated operation but decrease when the current order increase is applied. The voltage at Tjele decreases from 420kV to 400kV and at Kritiansand from 320kV to 290kV.

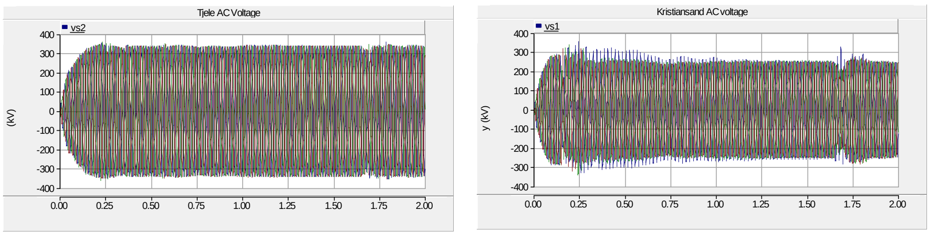

(a) (b)

Figure 8.38: AC voltage at (a) SK4 Tjele (b) SK4 Kristiansand.

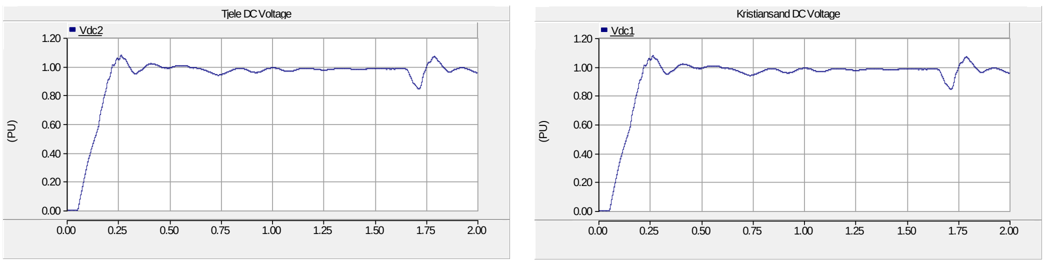

(a) (b)

Figure 8.39: DC voltage at (a) SK4 Tjele (b) SK4 Kristiansand.

The power transfer across the SK3 link is observed to increase from 400MW to 800MW at Tjele for a duration of 0.01sec and then commutation failure occurs resulting in the loss of power at time t = 1.62 sec. This may be observed in figure 8.40. For SK4, the power reference was made at 200MW. The power transfer may be observed to be stable at 200MW and during the current order increase there is a slight perturbation but power transfer is not interrupted. This can be seen in figure 8.41.

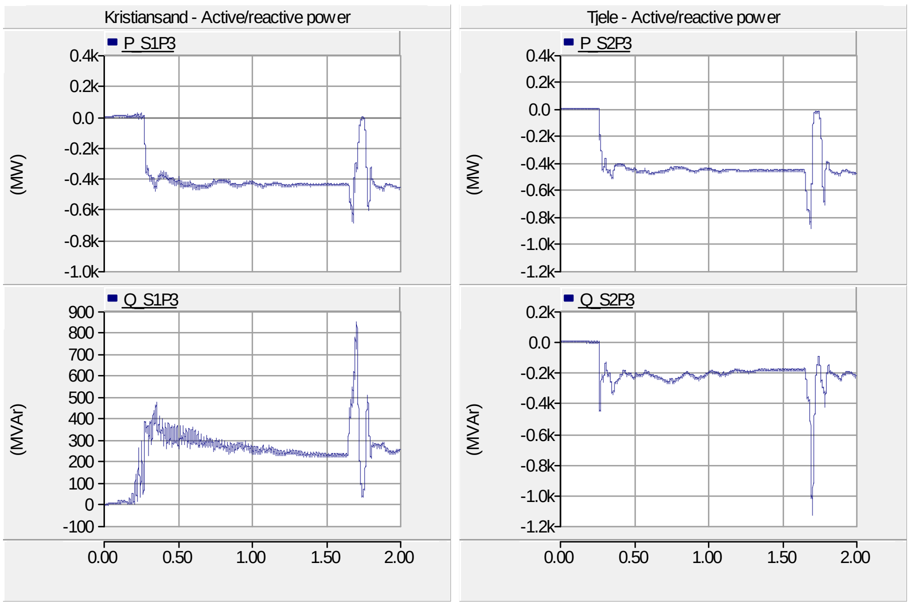

Figure 8.40: Power transfer SK3 link

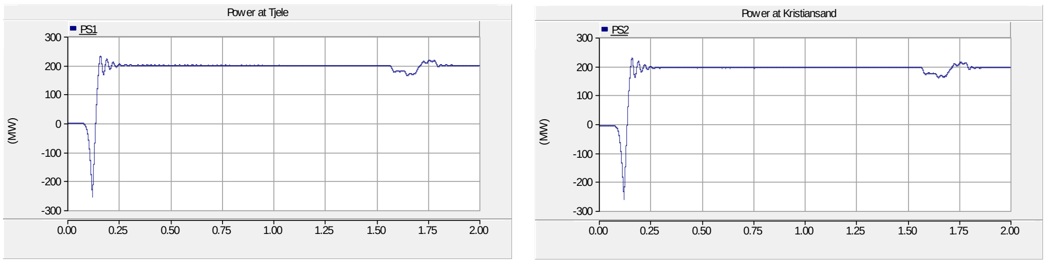

(a)

(b)

Figure 8.41: Power transfer (a) SK4 Tjele (b) SK4 Kristiansand.

The thyristor firing angles values variation during the simulation is shown in figure 8.42. The maximum and minimum values for them are given in table 8.10. The values obtained during the fault, are out of the range for a normal operation of the inverter and rectifier and result in commutation failure.

For	α [Deg]	γ [Deg]	μ [Deg]
rectifier	≤ 120	≥ 25	≤ 50
inverter	≥ 80	≤ 80	≤ 60

Table 8.10: Firing angles values during rapid increase in the dc current.

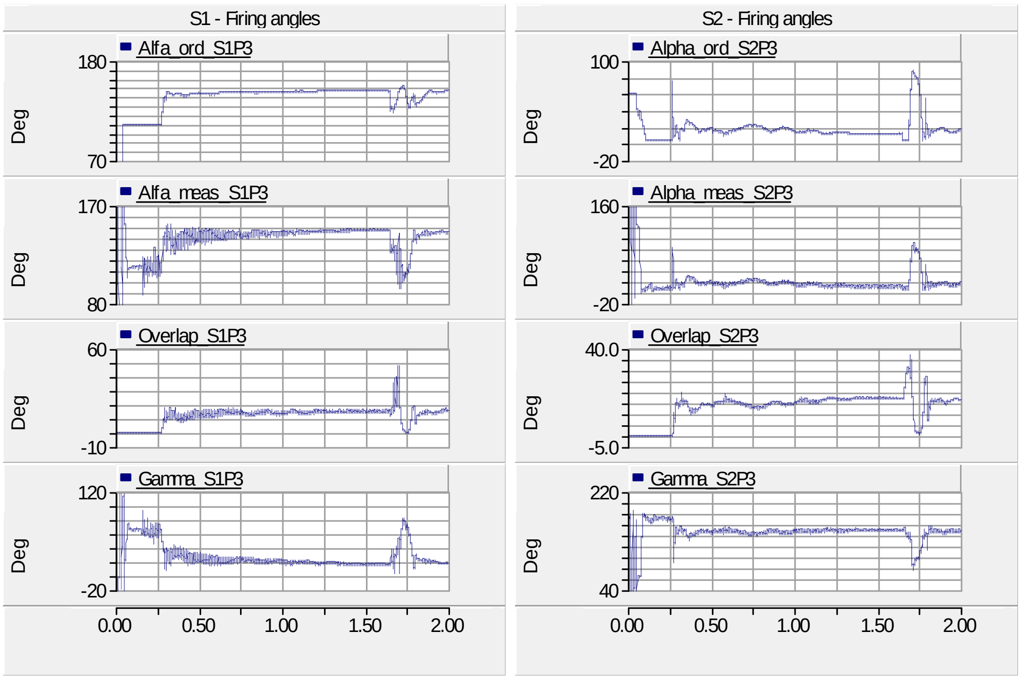

Figure 8.42: Thyristor firing angles

The results show that from such kind of abnormal operation where there is a rapid increase in the dc current through the SK3 link, the SK3 can not sustain the transfer of power through it and falls under commutation failure. However as the DC side of the SK4 link is not affected, that link is able to continue transferring power.

The performance of the bipole link under AC and DC side faults has been simulated and depending on the results obtained, the next chapter presents the conclusions and further work.

Chapter 9

Conclusion

9.1 Conclusion

The project has tried to evaluate the performance of an LCC based HVDC link in bipole fashion with VSC HVDC based link. These evaluation has been based on the new SK4 HVDC link project which is being by energinet.dk and statnet and an existing HVDC link SK3. The SK4 HVDC link is assumed to be VSC based and is to be operated in bipole mode with the SK3 which is LCC based.

The attempt to evaluate the performance of the bipole link has been made by considering different operating conditions. The conditions which were considered are, normal operational condition and during faulty conditions. The faults simulated were both AC and DC side faults. For the AC side faults, faults such as single phase to ground, three phase to ground and reduction of the voltage at the AC buses has been made. For the DC side, a line to ground fault and a rapid increase in DC current which may be caused due to transient phenomenas resulting in commutation failure of the SK3 link converters, has been simulated.

The results obtained from these different cases show that:

During normal operating time, the power transfer through each line of the bipole link can be controlled independently. The power through the SK3 link can be controlled by adjusting the current order controller of the link within its rated range. Moreover for the transfer of power through the SK4 link, the power also can be adjusted within its rating by the power reference controllers at SK4. The direction of the power flow may also be altered by the use of the controls assigned for each line of the link.

The THD levels measured during the simulations times on both sides of the link were within the rated standards. The use of an appropriate filter mechanism ensures the fulfilment of the requirements set by the power system operators. The harmonics which are may be generated by the SK3 link is of the order 12n+/-1 on the AC side and 12n on the DC side. For the reduction of these harmonics, appropriate filters have been provided which have enabled the systems THD level to be within the power system operators requirements on both the AC and DC side.

During the AC side fault simulations, the results obtained for a three phase to ground faults, show that a commutation failure occurs on the SK3 link and also the power transfer through the SK4 link goes down to zero. If this fault occurs on one of the AC side of the bipole HVDC link, the power transfer through the link inevitably goes down to zero. For the simulation cases where there is an AC voltage drop and a single phase to ground fault at either end of the bipole link, the results obtained were that, the SK3 link is affected and results in commutation failure. However the SK4 link is able to continue transferring power. Hence for AC side faults, the conclusion can be made that, three phase to ground fault affects the whole bipole link whereas distortions and reduction of the AC voltage and single phase to ground fault affect the LCC based link SK3 and result in commutation failure while SK4 is able to sustain the transfer of power through the link.

For DC side faults, the faults that were simulated were a line to ground fault and a rapid increase in the DC current through the SK3 link. To simulate the rapid increase in DC current through the SK3 link, the current ordered was increased from 1 pu to 2 pu value by the current order controller in SK3 and a line to ground fault was applied at Sk3 to see the performance under line to ground fault. For both cases, the results obtained show that, the SK3 link undergoes a commutation failure and the power transferred through the link goes down to zero. However, the power transfer through the SK4 link was not affected by the disturbances in the DC SK3 link.

9.2 Further work

The project focuses on the performance of the link under different AC side and DC side faults. However, the protection of the system on both the AC and DC side has not been studied. For AC side protection, the conventional relays and circuit breakers may be used however on the dc side, the protection system is more challenging as there doesn't exist commercial dc breakers hence further work can be made with this regard.

Moreover, the filters used for the VSC based SK4 link have not been optimized. These could be further optimized which could result in an improved quality of the voltages and currents.

The power losses in the system have not been covered. The power losses may be evaluated by making the components used as close to the reality as possible. The models which have been used for the SK4 such as the converter transformer and the converter IGBTS are ideal ones and this could be improved by using the manufacturers datas for the modeling of these components. Then evaluations can be made for the whole system to determine the power loss at different operating conditions. This could result in improved operation and implementation of the system.

The control implemented for the SK4 is the vector method and performance of the link may further be evaluated by using other control methods.

The SK4 link as previously mentioned can be made using a multilevel VSC converter or with the recent advanced modular multilevel converter which has been discussed theoretically. This project can further be advanced by implementing the modular type of the VSC converter.

Bibliography

[1] B Singh A Pandey and K Al Haddad. *A review of multilevel power converters*. 2006. IE Journal.

[2] ABB Power Systems AB. *DC transmission based on voltage source converters*. 2007.

[3] ABB. *http://www.abb.com/cawp/gad02181/c1256d71001e0037c1256c7900298ff1.aspx*. accessed 10/03/2010.

[4] Jos Arrillaga. *High Voltage Direct Current Transmission*. IEEE, 2.ed edition, 1998. ISBN 0-85296-941-4.

[5] Urban Axelsson and Christer Liljegren. *Gotland HVDC light transmission*. 1999. CIRED Conference.

[6] P. Boonchiam and N. Mithulananthan. *Diode-clamped Multilevel Voltage Source Converter Based on Medium Voltage DVR*. 2008. IEEE.

[7] Filipe Miguel Faria da Silva. *Offshore wind parks electrical connection*. 2008.

[8] Cuiqing Du. *The control of VSC-HVDC and its use for large industrial power systems*. 2003.

[9] Leopoldo G. Franquelo, Jose I. Leon, and Eugenio Dominguez. *New Trends and Topologies for High Power Industrial Applications: the Multilevel Converters Solution*. 2009. POWERENG.

[10] Turan Gonen. *Modern Power System Analysis*. John Wiley and Sons, 1988. ISBN - 0-471-62802-6.

[11] N. S. Choiand G. Ho. Cho H. L. Liu. *DSP Based Space Vector PWM for Three- Level Inverter with DC-Link Voltage Balancing*. 2003. IECON.

[12] Makoto Hagiwara and Hirofumi Akagi. *Control and Experiment of Pulsewidth-Modulated Modular Multilevel Converters*. 2009. IEEE Power Electronics.

[13] Mika Ikonen and Ossi Laakkonen. *Two-level and three-level converter comparison in wind power application*. 1999.

[14] Ying Jiang and Hugo Duchen. *HVDC with Voltage Source Converters, A powerful standby blackstart facility*. 2008. IEEE Power and Energy Society.

[15] Sadrul Ula Kala Meah. *Comparative Evaluation of HVDC and HVAC Transmission Systems*. 2007. IEEE PES.

[16] Torbjörn Karlsson. *modern control and protection system for hvdc*. 2005. ABB Power Systems.

[17] Surin Khomfoi and Leon M. Tolbert. *Multilevel Power Converters*. 2009. The University of Tennessee.

[18] Vijay K.Sood. *HVDC and FACTS controllers*. kluwer academic publishers, 6.ed edition, 2004. 1-4020-7890-0.

[19] Fang Zheng Peng Leon M. Tolbert and Thomas G. Habetler. *Multilevel PWM Methods at Low Modulation Indices*. 2000. IEEE.

[20] Thomas G. Habetler Leon M. Tolbert. *Novel Multilevel Inverter Carrier-Based PWM Methods*. 1998. IEEE.

[21] R. Marquardt and A. Lesnicar. *An Innovative Modular Multilevel Converter Topology Suitable for a Wide Power Range*. 2004. PESC 2004 Conference in Aachen, Germany.

[22] Sid Ahmed Mohammed Khatir. *Analysis of recovery from commutation failures in an HVDC inverter connected to a weak receiving as system*. 2008.

[23] K. R. Padiyar. *HVDC power transmission systems: technology and system interactions*. New Age International, 1990. ISBN 8122401023, 9788122401028.

[24] W. L. Kling R. L. Hendriks, G. C. Paap. *Control of a multi-terminal VSC transmission scheme for connecting offshore wind farms*. 2008. IEEE ,.

[25] Y. Zhuang R. W. Menzies. *Advanced Static Compensation Using a Multilevel GTO Thyristor Inverter*. 1995. IEEE.

[26] Roberto Rudervall and J.P. Charpentier. *High Voltage Direct Current (HVDC)Transmission Systems Technology Review Paper*.

[27] Jih Sheng and Fang Zheng Peng. *Multilevel converters, A new breed of power converters*. 1996. IEEE Transactions.

[28] IEEE Power Engineering Society. *The ABCs of HVDC Transmission Technology*. 2007. IEEE Power and Energy Magazine Vol5 No2.

[29] S. Upadhyay S.O.Faried. *Impact of HVDC commutation failure on turbine-generator shaft torsional torques*. 2007.

[30] Tore Undeland Temesgen M. Haileselassie, Marta Molinas. *Multi-Terminal VSC-HVDC System for Integration of Offshore Wind Farms and Green Electrification of Platforms in the North Sea*. 2008. Nordic Workshop on Power and Industrial Electronics ,.

[31] Its time to connect.

[32] Dennis A. Woodford. *HVDC transmission*. 1998. Manitoba HVDC Research Centre.

[33] Bin Wu. *High-power converters and AC drives*. IEEE press, 2006. ISBN 10-0471-73171-4.

[34] www.wavewinbitronics.com. *wavewinbitronics viewer*. 2010. Commercial software.

Part I

Appendix

Appendix A

Detailed model of SK1, SK2, and SK3

Skagerak 1,2,and 3 detailed layout

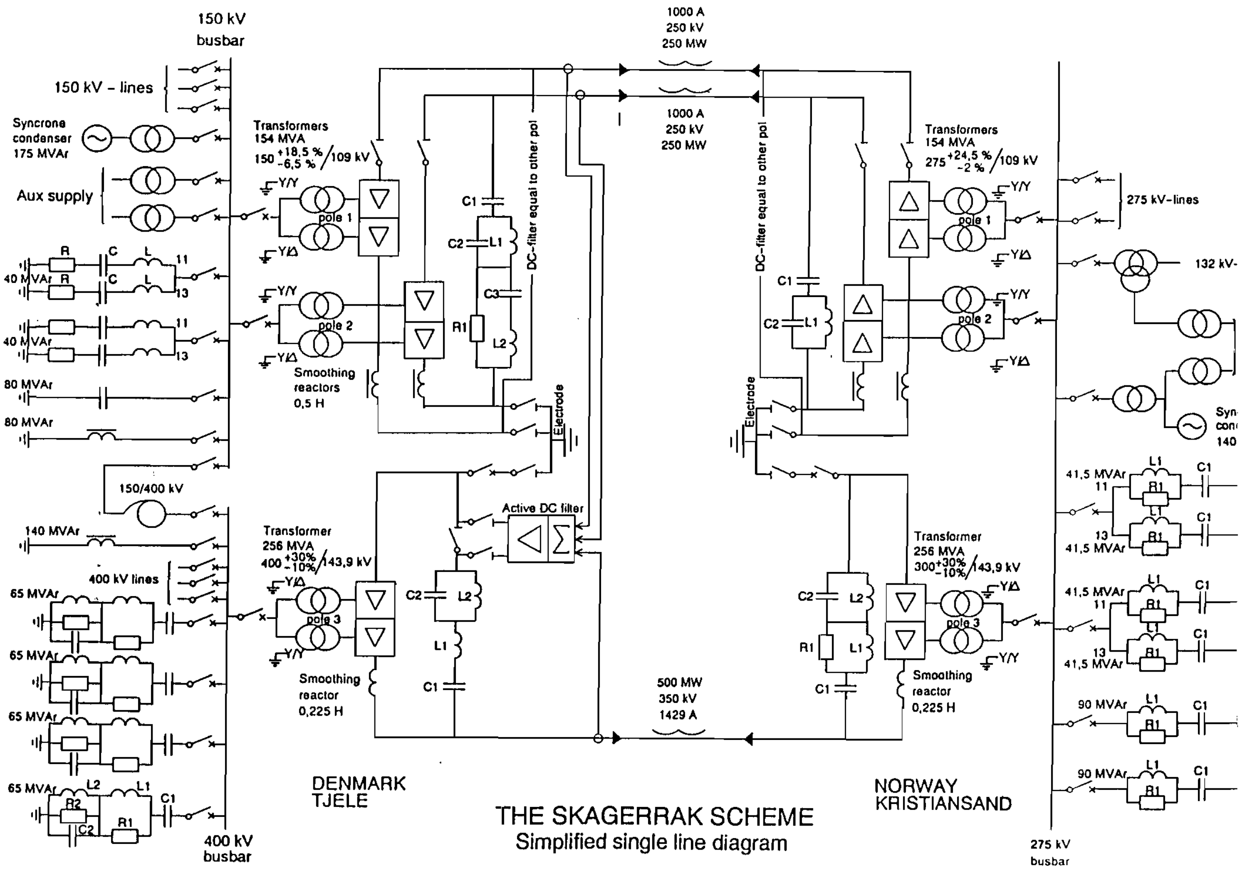

Figure A.1: Sk1, Sk2 and SK3 layout used for simulation

Appendix B

PSCAD Comtrade file view

PSCAD has a component that reads comtrade format but does not consider the configuration part of the comtrade file. The configuration file has been included as shown in figure B.1.

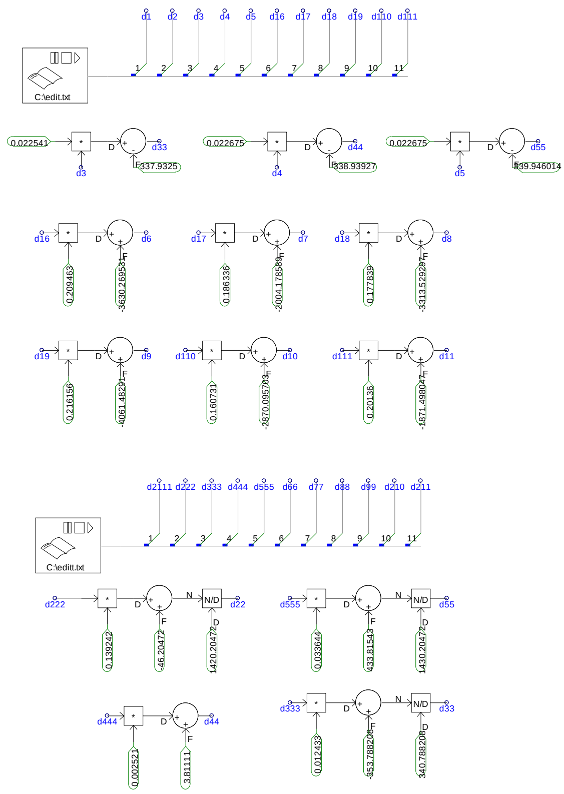

Figure B.1: PSCAD comtrade reader.

Appendix C

SK3 converter transformer, filters and converter models

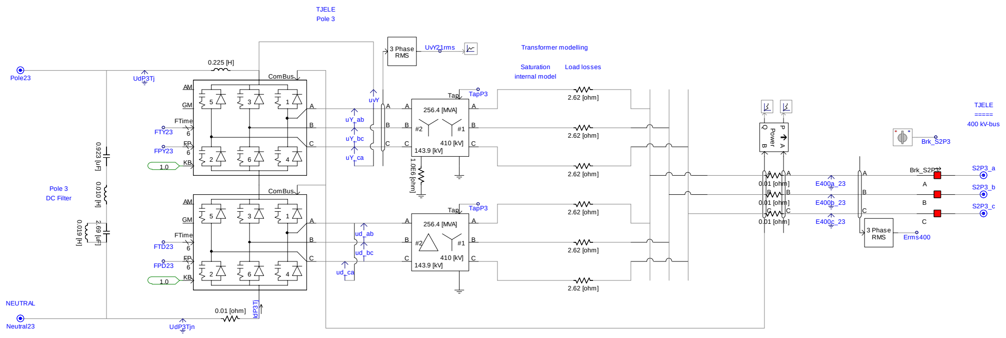

Figure C.1: Converter and Converter transformer of SK3 model.

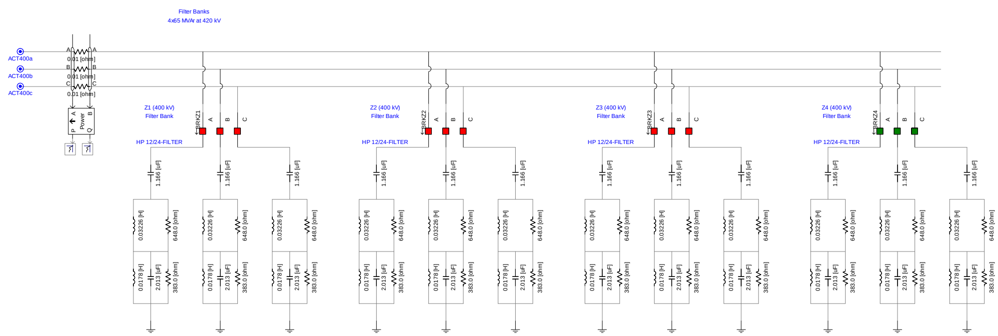

Figure C.2: Filter banks of SK3 model.

Appendix D

SK4 PLL, abc to dq and control models

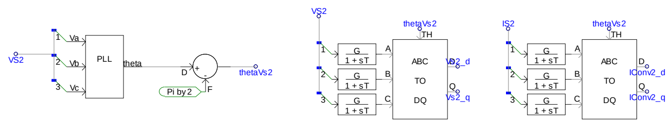

Figure D.1: PLL and abc to dq converters at SK4.

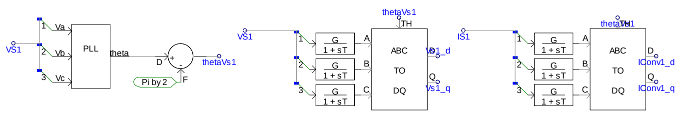

Figure D.2: PLL and abc to dq converters at SK4.

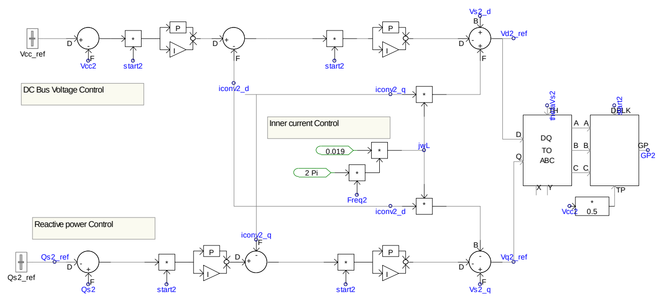

Figure D.3: Outer and inner controller of one VSC converter.